常温時と低温時における高減衰ゴム支承の耐震設計用レオロジーモデル

A RHEOLOGY MODEL OF HIGH DAMPING RUBBER BEARINGS FOR SEISMIC ANALYSIS AT ROOM AND LOW TEMPERATURES

２０１６年３月

埼玉大学大学院理工学研究科（博士後期課程）

理工学専攻（主指導教員　奥井義昭）

NGUYEN ANH DUNG

A RHEOLOGY MODEL OF HIGH DAMPING RUBBER BEARINGS FOR SEISMIC ANALYSIS AT ROOM AND LOW TEMPERATURES

常温時と低温時における高減衰ゴム支承の耐震設計用レオロジーモデル

A DISSERTATION

SUBMITTED TO THE COMMITTEE ON GRADUATE STUDIES IN PARTIAL FULFILLMENT OF THE REQUIREMENTS FOR THE DEGREE OF

DOCTOR OF PHILOSOPHY

NGUYEN ANH DUNG

DEPARTMENT OF CIVIL AND ENVIRONMENTAL ENGINEERING
GRADUATE SCHOOL OF SCIENCE AND ENGINEERING
SAITAMA UNIVERSITY
SAITAMA, JAPAN

2016

ACKNOWLEDGEMENTS

First of all, I would like to express my gratitude to all those who have helped me to complete this research.

First and foremost, I am greatly indebted to Prof. Yoshiaki Okui for everything he has done for me over the last five years. He guided me from the beginning of this research, and taught me how to conduct a profound academic research. He also supported for my living expense. I would like to thank Prof. Okui for his professional guidance, constructive comments and great encouragement during my study. I will not forget his endless of corrections and critical questions.

I am indeed grateful to the members of my dissertation committee for their valuable comments and suggestions at various stages of my study: Prof. Matsumoto, Prof. Masato Saitoh, Associate Professor Takeshi Maki.

I would like to highly appreciate the valuable questions of Prof. Hiroki Yamaguchi at the Lab, Meetings. I would like to express my appreciation to Prof. A.F.M. Saiful, BUET for his enlightening discussion, suggestions regarding this work. It is also a pleasure for me to express my gratefulness to Assistant Prof. Dang Ji for giving me useful suggestions for the progress of this research.

My thanks are special to all the members of Japan Rubber Bearing Association for their kind cooperation by providing a lot of supports for conducting all the experiments required to carry out this research work.

Sincere thanks are addressed to all the members of the Structural Mechanics and Dynamics Laboratory, especially Dr. Duc, Dr Hung, Dr Dammika, Mr. Ishijima, Mr. Hagiwara, Mr. Ito, Mr. Hasan, Miss Takahashi, Mr. Matsumoto for their good teamwork spirit, sharing valuable experience, and their friendship with many unforgettable memories in study as well as in life.

I would also like to send special thanks and appreciation to my parents, parents-in-law and my beloved wife and two little sons who have created aspiration and sacrificed for me to fulfill my study.

ABSTRACT

High damping rubber bearings (HDRBs) are seismic isolating devices used widely in Japan, especially after Kobe earthquake in 1995. They provide a cost effective and reliable technology for earthquake protection of the bridge structure. In some guide specifications for the seismic design of bridges with HDRBs, the nonlinear characteristics of HDRBs are expressed in terms of a bilinear model. However, the mechanical behavior of HDRBs is characterized by strong strain-rate dependency. The current bilinear model cannot represent this behavior.

Rate-dependent behavior of high damping rubber bearing (HDRBs) is investigated at subzero temperatures (-30^{o}C and -10^{o}C) and also at room temperature (23^{o}C) under horizontal cyclic shear deformations with a constant vertical compression load. On the basis of experimental observations, an improved elasto-viscoplastic rheology model has been proposed where the total stress has been decomposed into rate independent elasto-plastic stress, nonlinear elastic stress and the nonlinear visco-elastoplastic overstress. To represent the nonlinear viscosity behavior at both subzero and room temperatures, the overstress branch of an existing elasto-viscoplastic rheology model has been modified by replacing the linear elastic spring of the branch with two parallel branches that include a linear elastic spring and a nonlinear elasto-plastic model (spring-slider). This part is connected in series with the dashpot. To identify constitutive relations of each element in the resultant rheology model, an experimental scheme comprised of three types of tests, namely cyclic shear (CS) tests, multi-step relaxation (MSR) tests, and simple relaxation (SR) tests, are carried out at constant strain rates for the three reference temperatures. An optimum calculation approach is developed to determine a unique set of overstress parameters capable of representing CS, MSR, SR tests and also the sinusoidal loading tests with variable input strain rates. Finally, the ability of the proposed model and parameter identification procedure are verified by comparing numerical simulation results with experimental data.

The final objective is to enhance the capability of the proposed model by incorporating self-heating effect into the model. As the first step, an experimental program is conducted to investigate the self-heating effect on the mechanical characteristics of HDRBs under sinusoidal loading at room and low temperatures. Experimental results show that the inside

temperatures of HDRBs increases by cyclic loading, especially at low temperatures. Moreover, it is shown that the stress-strain relationships of HDRBs are governed by the inside temperatures. Therefore, a seismic model for HDRBs at low temperatures should be based on the inside temperatures.

Keywords: *High damping rubber bearings, rate dependence, low temperature, rheology model, parameter identification, self-heating effect.*

TABLE OF CONTENTS

LIST OF FIGURES

LIST OF TABLES

CHAPTER 1
INTRODUCTION

1.1 General

In order to mitigate the hazardous effects of earthquakes on bridges and buildings, from the last few years, engineers and researchers have studied and proposed solutions to improve the earthquake resistance of these structures. The objective of these solutions is to ensure the safety of the structures without damage or within limited damage. However, the conventional approaches showed that in spite of expensive cost, structures were still suffered severe damage by earthquakes, such as Loma Prieta earthquake in 1989, Northridge earthquake in 1994, and Kobe earthquake in 1995. These conventional approaches must be replaced by a better approach.

On the basis of the observations from nature, leaves connected with branches by soft joins can resist winds and earthquakes very well. People would like to make soft joins for structures that could absorb the energy introduced by earthquakes and could lengthen the natural period of structures to avoid the resonance with excitations. Following this approach, a technology called seismic isolation has emerged as a practical and economical alternative to the conventional approach. The main concept of seismic isolation is to decouple a structure from the horizontal components of the ground motion by inserting structural elements (e.g. isolation bearings) between the structure and its foundation. The technique of seismic isolation is characterized by flexibility and damping capability. Isolation bearings with flexibility can shift the natural periods of structures to reduce the acceleration response, while its damping capability can diminish the displacement response. These characteristics are illustrated in Fig 1.1 and 1.2. Numerous experimental studies on isolation bearings (Abe et al., 2000; Igarshi and Iemura, 1996; Koo and Ohtori, 1998; Tsopelas and Constantinou, 1997; Wei et al., 1992) and numerical analyses (Hwang, 1996; Hwang et al., 1996; Hwang and Chiou, 1996; Jangid, 2004; Wang et al., 1998) were conducted to investigate the effect of the isolation technology on reducing the acceleration responses of structures, and they indicated the advantaged of isolation technique in the earthquake resistant design. Until now, this technology is being applied to a wide range of civil engineering structures.

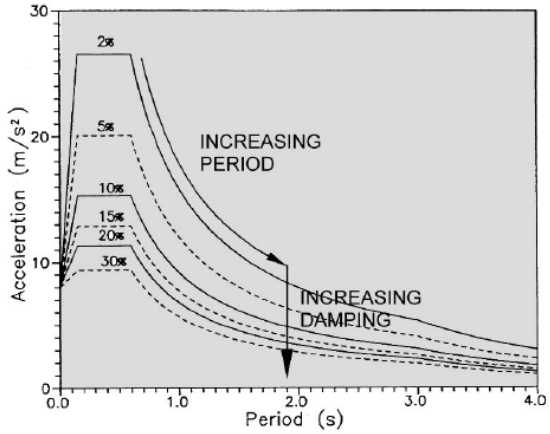

Fig.1.1. Acceleration response spectrum in function of the damping (as defined by EC8 for ground acceleration 0,8g, medium soil)

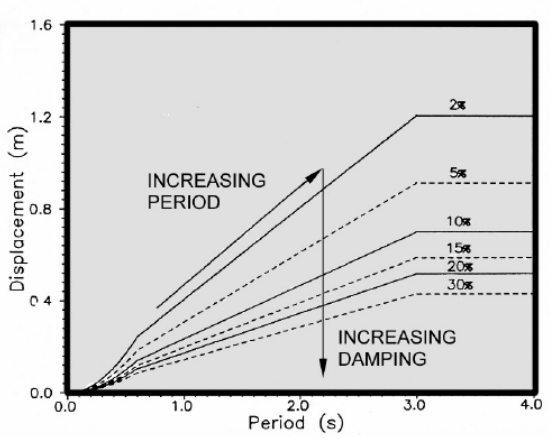

Fig.1.2. Displacement response spectrum in function of the damping (as defined by EC8 for ground acceleration 0,8g, medium soil)

1.2 High damping rubber bearings

Various isolators have been manufactured with a similar objective to provide a natural period shift and additional energy dissipation to structures. The laminated rubber bearings have been widely applied in recent years as seismic isolation devices in bridges, especially after Kobe earthquake in 1995, when good behavior of structures with rubber bearings was recorded. There are three types of laminated rubber bearings: natural rubber bearings (RB), lead rubber bearings (LRB), and high damping rubber bearings (HDRBs). More recently, high damping rubber bearings have been widely used in Japan due to their high flexibility and high damping capability.

In the manufacture process of high damping rubber material, a large amount of fillers (about 30%) including carbon black, silica, oils and some other particles is added during the vulcanization process (Kelly, 1997; Yoshida et al., 2004) in order to improve the desirable material properties, such as the strength and damping capabilities. HDRBs consist of alternative layers of high damping rubber and steel plates bonded by vulcanization. They have some similar behavior to other elastomeric bearings, such as being able to support vertical loads with limited or negligible deflection and horizontal loads with large deflections. However, HDRBs are characterized by some special properties that are very different from standard elastomeric bearings. They present high damping capability, and bearings defined as HDRBs should provide an equivalent viscous damping of at least 10% (Mariori, 1998). HDRBs also present a very useful property for the application in the base isolation of structures. They are very stiff for small deformation and soft for large deformation. This property allows the structure to respond rigidly to small excitations like braking forces and provides high flexibility for large excitations like earthquakes. Moreover, high damping rubber material is very durable. Gu and Itoh (2006) estimated that the change of the equivalent horizontal stiffness of HDRBs is about 10-25% after 100 years. Therefore, there is little or no maintenance requirement for HDRBs.

1.3 Review on previous work for high damping rubber bearings

High damping rubber (HDR) later emerged as a novel material for bearing devices not only due to its high flexibility but also to its high damping capability. However, some of the very important mechanical behavior of HDR, such as the rate and temperature dependent behavior are still difficult and less understood issues in engineering practice (Yoshida et al., 2004).

Fundamental nonlinear elastic and nonlinear viscosity behaviors of HDR at room temperature are known from the observations reported in Amin et al. (2002, 2006a,b). Contemporary experimental observations (Dall'Asta and Ragni 2006; Hwang et al., 2002) on laminated rubber bearings further show that restoring force-displacement loops of HDRBs depend prominently on loading history and strain level. Hysteresis loops of HDRBs were also observed to strongly depend on loading rate, ambient temperature and even time interval between two loading tests. Bhuiyan et al. (2009) reviewed well-known

constitutive behaviors of HDR and their effects on the mechanical behavior of HDRB. Past efforts on developing analytical representation of the room temperature mechanical behaviors in rate dependent and rate independent rheology models were also summarized there. Subsequently, Bhuiyan et al. (2009) extended the Maxwell model by adding a nonlinear elastic spring and an elasto-plastic model (spring-slider) in parallel to represent a set of phenomena observed in full scale tests on HDRB. The overstress branch was modeled with a linear spring added in series with a nonlinear dashpot. In order to identify constitutive relations of each element in the rheology model, in line with the concepts followed in Lion (1996), Amin et al. (2002, 2006a) on NR and HDR, an experimental scheme comprised of three types of tests at constant strain rates, namely cyclic shear (CS) tests, multi-step relaxation (MSR) tests and simple relaxation (SR) tests were carried out at room temperature on HDRB specimens with the standard ISO geometry. To observe the fundamental viscosity behaviors during loading and unloading, MSR tests contained multiple hold times while SR tests contained a single hold time during loading and unloading. More recently, Yamamato et al. (2012) investigated the nonlinear behavior of HDRBs under horizontal bidirectional loading at room temperature and propose an analytical model. However, no effort is known either to investigate the applicability of the existing rheology models or to propose a new model for simulating the low temperature behavior of HDRB.

Effect of temperature on visco-elasto-plastic phenomena in rubber is a much less investigated topic reported in current literatures. The effect of ambient temperature and the exposure history on mechanical behavior of rubber is addressed in Lion (1997) and Fuller et al. (2004). A recent comprehensive review of literature together with experimental observations on natural rubber-polybutadiene rubber (NR/BR) blend is provided in Amin et al. (2010). In these studies, rate dependence, hysteresis and well-known Mullins effect (Mullins 1969) were critically addressed for temperature dependence. Depending on the type and composition of the rubber, the mechanical behavior was found to be affected strongly by ambient temperature. Generally, rubbers tested at lower temperatures have shown larger rate dependence and hysteresis whereas these effects got gradually diminished at room temperature. Furthermore, Fuller et al. (2004) reports temperature history dependence of HDR due to crystallization effect on prolonged exposure to low temperature and associated increase in shear modulus. Amin et al. (2010) emphasizes on the role of loading history dependence due to fundamental Gough-Joule effect. The later

notion emphasizes the importance of thermal boundary defined mostly by the specimen size on the response of bearings. Yet, no effort in this respect is known where the fundamental mechanical behavior observed either in HDR or HDRBs at low temperatures is investigated. This obviously restricted not only the development of a rheology model for HDRBs in seismically active cold regions such as Hokkaido of Japan (1968 Tokachi Earthquake) and Alaska of USA (1964 Alaska Earthquake) but also the performance prediction of existing structures in those regions.

Traditional design guidelines generally assume uniform temperature distribution, and the value of design temperature is chosen to be the ambient temperature under which the rubber bearing is intended to operate. However, when HDRBs are subjected to cyclic loads, the energy dissipated by the bearings is converted into heat and this heat may cause significant temperature increase in the rubber bearings. This phenomenon is known as self-heating. Takaoka et al. (2008) indicated that sinusoidal loading causes the stiffness to drop to about 80% and the inside temperature of rubber bearings increases by about 30^{o}C. The rise of temperature in rubber material specimens under cyclic loads is reported to be larger at lower ambient temperatures by Cardone et al., (2011). Therefore, the relationship between the inside temperature rise and the mechanical characteristics of HDRBs is a serious concern. Self-heating effect should be considered in the development of seismic models for HDRBs, especially at low ambient temperatures.

The feat of a rheology model developed to represent a device in structural analysis is frequently judged by its ability to simulate not only the fundamental behavior but also in simulating some practical loading histories that a designer would use at the design desk. Few works have been reported in the development of the rate-dependent models of HDRBs. Hwang et al. (2002) proposed an analytical model to describe the damping force and restoring force of rubber bearings separately as functions of the relative displacement and velocity of the bearing. The model proposed by Tsai et al. (2003) also considered the effect of the rate dependence by modifying the Wen's model to include the rate-dependent effects. These models assumed that the total force is approximated as the superposition of rate-independent spring force and the rate-dependent dashpot damping force. In resemblance with Kelvin model, such models are very straightforward and effective for a few specific loading conditions, even though the relaxation tests have already identified relaxation behavior that is more complicated to represent in Kelvin model. This limitation is improved

by the model proposed in Dall'Asta and Ragni (2006), where the rate-dependent behavior is described by two generalized Maxwell elements. Although HDRBs absorb energy also in a very slow loading rate, the rate-independent part presented by a nonlinear elastic spring in this model cannot represent energy dissipated by hysteresis behavior. Bhuiyan et al. (2009) overcome this limitation by combining a nonlinear spring and an ideal elasto-plastic model (spring-slider) in parallel for the rate-independent part. However, the model had to use two different sets of parameters to represent cyclic shear tests under constant strain rate and sinusoidal loading tests under variable strain rate. Furthermore, most of the previous models were developed from the observations of room temperature tests. Verifications based on low temperature tests are insufficient. All these shortcomings obviously indicate the necessity of addressing not only the low temperature behavior but also proposing a scheme to identify optimal parameters at least to hold for both constant strain rate loading and sinusoidal loading cases. Due to the general shortcomings of existing knowledgebase, design and analysis for structures with laminated rubber base isolation devices, design codes and specifications (AASHTO 2010; JRA 1996, 2002, 2012) still generally recommend use of simple bilinear elasto-plastic models, to represent the restoring force-displacement relationship of laminated rubber bearings by omitting rate-dependent behavior of HDRBs.

1.4 Scopes and objectives

On the basis of the background in section 1.3, the current research is performed to meet the following objectives:

1. To investigate the mechanical behavior of HDRBs in terms of elasto-plastic and rate-dependent viscosity behavior at room and low temperatures.

2. To develop an appropriate model that can reproduce nonlinear visco-elastoplastic behavior at room and low temperature behavior of HDRBs.

3. To validate the adequacy of the proposed model by numerical simulation of loading test data.

4. To investigate self heating of HDRBs under cyclic loading at room temperature and low temperatures.

1.5 Contents of dissertation

Chapter 1 gives the background and objectives of the research. The background shows a review on previous work for HDRBs. The main targets of this research are to investigate the fundamental mechanical behavior of high damping rubber bearings under horizontal shear deformation with constant vertical compressive load and to develop a rheology model that can represent the mechanical behavior of the bearings at room and low temperatures.

Chapter 2 presents an experimental investigation of the mechanical behavior of HDRBs at room and low temperatures. An experimental program was conducted by japan rubber bearing association. Preloading was applied to specimens to detach Mullins effect from other inelastic phenomena. Multi-step relaxation tests were carried out to identify the rate-independent equilibrium hysteresis of HDRBs. Simple relaxation tests were conducted to observe the rate-dependent viscosity effect. Finally, cyclic shear tests at high strain rates were carried out to evaluate the instantaneous state of the bearings.

On the basis of the experimental observations in Chapter 2, an improved rheology model is proposed in Chapter 3. In order to improve the rate-dependent behavior in the original rheology model of Bhuiyan et al. (2009), major modifications to the original model are performed. In the new model, a nonlinear elasto-plastic element connected with a dashpot is used to represent the rate-dependent behavior of HDRBs. In addition, a parameter identification procedure is developed in this chapter. The parameters for equilibrium response were identified from multi-step relaxation tests, and the parameters for overstress response were determined from sinusoidal loading tests. Moreover, an optimal technique is introduced in this chapter. The technique is used to determine the overstress parameters, and it is implemented in Matlab software.

Chapter 4 is concerned with the numerical verification of the proposed model. For this purpose, the identified parameters in Chapter 3 are used to simulate experimental results in Chapter 2.

Chapter 5 addresses self heating of rubber bearings, the effect of the inside temperature rise on the mechanical behavior of HDRBs is investigated in this chapter at room and low temperatures.

Chapter 6 presents a summary of the research, major conclusions based on this study, and recommendation for future study.

CHAPTER 2

STRAIN-RATE DEPENDENT BEHAVIOR OF HIGH DAMPING RUBBER BEARINGS UNDER CYCLIC LOADING

2.1 General

The general mechanical behavior of HDRBs mainly concerns with strong nonlinear rate-dependent hysteretic response (Bhuiyan et al., 2009; Dall'Asta and Ragni, 2006) in line with the other inelastic behaviors such as Mullins effect (Amin et al., 2010; Mullins, 1968) and self-heating (Gent and Hindi, 1988; Park et al., 2000; Takaoka et al., 2008). Moreover, the low temperature dependence of the stress-strain relationship of HDRBs is stronger than that of the other laminated rubber bearings (Imai et al., 2010). However, the simplified models in some guide specifications (AASHTO, 2010; EC8, 2004; JRA, 2002) omit the strain-rate dependence behavior of HDRBs, and this omission may cause major errors in predicting the seismic responses of the structures isolated by HDRBs. It is a great concern for engineers designing isolation structures in the areas where are not only very cold but also seismically active such as Hokkaido of Japan (1968 Tokachi Earthquake), Alaska of US (1964 Alaska Earthquake). Therefore, deep knowledge of this behavior of bearings is very necessary for having rational and economic design of seismic isolation structures. For this purpose, HDR bearing tests were conducted by Japan Rubber Bearing Association to observe the mechanical behavior of HDRBs at room and low temperatures in this chapter.

2.2 Specimens and experimental set-up

Cyclic loading tests for HDRBs in room temperature have been presented in the work of Bhuiyan et al. (2009). In this study, loading tests at low temperatures are conducted following similar loading ways and using same HDR material. The experimental data of those loaded at room temperature are also used in this study. Specimens used in room temperature are marked as type A, those served for low temperature test in this study are marked as type B. All specimens had square cross-sectional shape. The dimensions and material properties of the specimens are given in Table 2.1. Type-A specimen follows the ISO standard (ISO, 2005) in Fig. 2.1 and Type-B with smaller dimensions in Fig. 2.2. All

tests were conducted on HDRBs with two different high damping rubber materials, named HDR2 and HDR3.

Table 2.1. Dimension and material properties of HDR bearing specimens

Particulars	Specifications	
	Type A	Type B
Cross-section A (mm^2)	57600 mm^2, 240mm x 240mm	25600 mm^2, 160mm x 160mm
Number of rubber layers	6	5
Thickness of one rubber layer (mm)	5	4
Total rubber thickness h(mm)	30	20
Thickness of one steel plate (mm)	2.3	2.3
Nominal shear modulus (MPa)	1.2	1.2

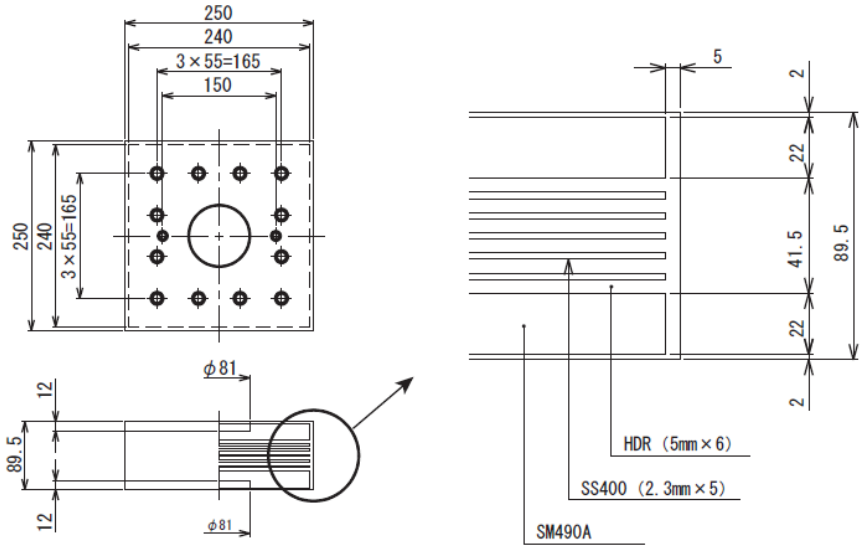

Fig.2.1. Type-A specimen [mm] used at room temperature

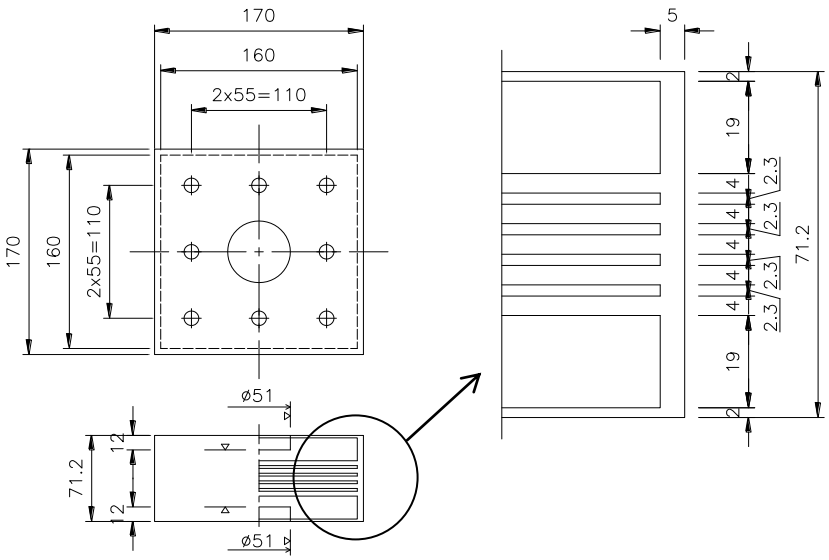

Fig.2.2. Type-B specimen [mm] used at low temperatures

The rubber bearing tests are performed at constant temperature in an environmental test chamber (Fig. 2.3) with a computer-controlled servo-hydraulic testing machine as shown in Fig. 2.4. To ensure homogeneous temperature distribution, the specimen was first let in the temperature chamber at room temperature (23^oC or above) and allowed to cool down under load-free conditions. During this process, the specimen inside the chamber was allowed to change dimensions under stress-free condition. After attaining the test temperature for the particular test, the specimen to be tested was kept inside the test chamber for more 24 hours to equilibrate the temperature inside the specimen. All specimens were tested under shear deformation with a constant vertical compressive average stress of 6 MPa. All tests were carried out with new specimens. Some test data at room temperatures are available in Bhuiyan et al. (2009) and the loading program including new tests in this study and those presented in Bhuiyan et al (2009) is shortly described in Table 2.2.

The average shear stress τ and average shear strain γ are calculated using the as following two equations throughout this dissertation.

$$\tau = \frac{F}{A} \tag{2.1}$$

$$\gamma = \frac{u}{h} \tag{2.2}$$

where F is the horizontal force; A is the area of the cross-section of bearings; u is the horizontal displacement, and h is the total rubber thickness (Table 2.1).

Fig. 2.3. The environmental test chambers

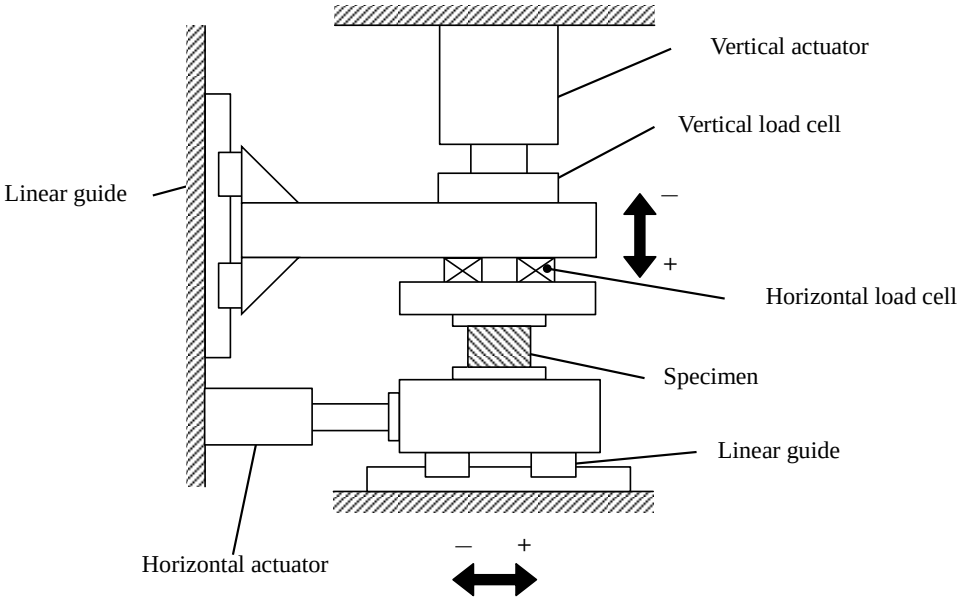

Fig. 2.4. The two axis testing machine. (OILES Industry Co., Ltd.)

Table 2.2. Test Scheme

No.	Test Name	Specimen type	Test temp. (℃)	Test control parameters					
				Max. shear strain (%)	Test protocol	Strain rate (/s)	Freq. (Hz)	Repetitions	Hold time of each strain (s)
1	SR100-30*	B	-30°C	±100	SR	5.50	–	1	1800
2	SR150-30*	B	-30°C	±150	SR	5.50	–	1	1800
3	SR175-30*	B	-30°C	±175	SR	5.50	–	1	1800
4	MSR250-30*	B	-30°C	±250	MSR	5.50	–	1	1200
5	Sin175-30*	B	-30°C	±175	Sin	<5.5	0.50	11	
6	CS175-30-1.5*	B	-30°C	±175	CS	1.50	–	11	–
7	CS175-30-5.5*	B	-30°C	±175	CS	5.50	–	11	–
8	CS175-30-8.7*	B	-30°C	±175	CS	8.75	–	11	–
9	SR100-10*	B	-10°C	±100	SR	5.50	–	1	1800
10	SR150-10*	B	-10°C	±150	SR	5.50	–	1	1800
11	SR175-10*	B	-10°C	±175	SR	5.50	–	1	1800
12	MSR250-10*	B	-10°C	±250	MSR	5.50	–	1	1200
13	Sin175-10*	B	-10°C	±175	Sin	<5.5	0.50	11	
14	CS175-10-1.5*	B	-10°C	±175	CS	1.50	–	11	–
15	CS175-10-5.5*	B	-10°C	±175	CS	5.50	–	11	–
16	CS175-10-8.7*	B	-10°C	±175	CS	8.75	–	11	–
17	SR100-r#	A	23°C	±100	SR	5.50	–	1	1800
18	SR150-r#	A	23°C	±150	SR	5.50	–	1	1800
19	SR175-r#	A	23°C	±175	SR	5.50	–	1	1800
20	MSR250-r*	A	23°C	±250	MSR	5.50	–	1	1200
21	Sin175-r#	A	23°C	±175	Sin	<11	1.00	11	
22	CS175-r-1.5#	A	23°C	±175	CS	1.50	–	11	–
23	CS175-r-5.5#	A	23°C	±175	CS	5.50	–	11	–
24	CS175-r-8.7#	A	23°C	±175	CS	8.75	–	11	–

Source of test data: *: Current study; #: Bhuiyan et al. (2009).

2.3 Loading conditions

There were four kinds of tests included multi-step relaxation (MSR) tests, cyclic shear (CS) tests, sinusoidal loading (Sin) tests, and simple relaxation (SR) tests at -30^{o}C, -10^{o}C and 23^{o}C. Figs. 2.5 and 2.6 illustrate the applied strain histories on the specimens for MSR tests, SR tests, CS tests and Sin tests at different temperatures. As seen in Figs. 2.5(a) and 2.5(b), MSR tests are cyclic loading tests that was conducted at constant strain rate of 5.5/s at each loading step, but after a small part of shear strain application, the specimen was kept on hold at that particular shear strain for 1200s to let the stress in HDRB to relax to its equilibrium state. A number of relaxation periods (hold times) were applied as shown in the figures.

CS tests were loaded under three different loading rates of 1.5 S^{-1}, 5.5 S^{-1}, and 8.75 S^{-1}, to investigate the rate dependent behavior. Loading rate of 8.75 S^{-1} is an unreal value for isolation structure. It was set as "extremely fast" to observe the up-limit of rate dependent state, mentioned as instantaneous state in the following. Sin tests are conducted in this study with loading rate amplitude of 5.5 S^{-1}.

The relaxation behavior induced by viscosity is examined by SR tests. SR tests were carried out in a fashion similar to MSR tests but with only single hold time (1800s) between loading and unloading. The strain histories applied to SR tests were presented in Fig. 2.5(c) with three strain levels of γ=100, 150, and 175%, a strain rate of 5.5/s.

Virgin rubber exhibits a well-known stress-softening phenomenon, referred to as Mullins effect (Mullins 1969), in the first loading cycle. In order to remove Mullins effect, all virgin specimens were first subjected to a preloading sequence before the actual tests (Lion 1997; Amin et al., 2002, 2006a,b; Bhuiyan et al., 2009). The preloading consisted of 6 sinusoidal loading cycles at 1.75 strain level and frequency of 0.05 Hz. The applied maximum strain in preloading was 2.5 for MSR tests.

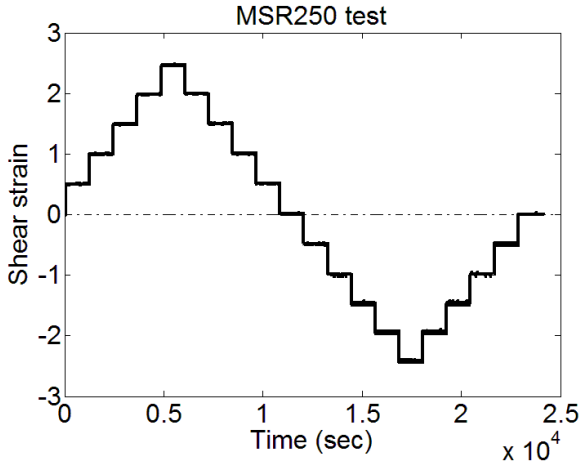

(a)

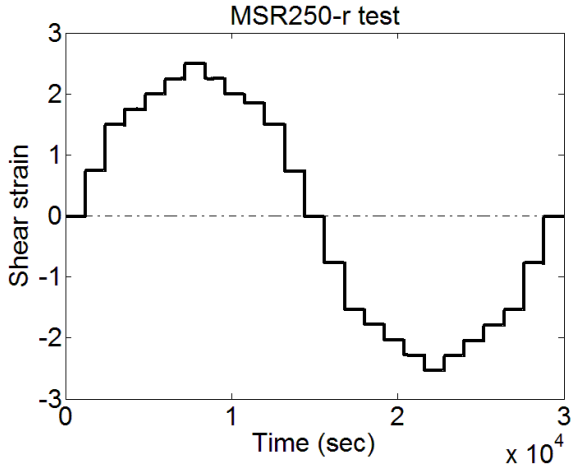

(b)

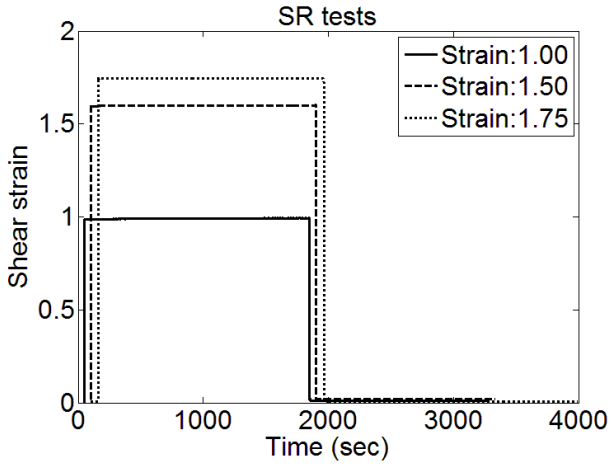

(c)

Fig. 2.5. Applied strain histories of MSR and SR tests: (a) MSR tests at -30°C & -10°C, (b) MSR tests at 23°C, (c) SR tests at -30°C, -10°C & 23°C. The strain histories of SR tests have been separated by 50s to each other in (c) for clear illustration.

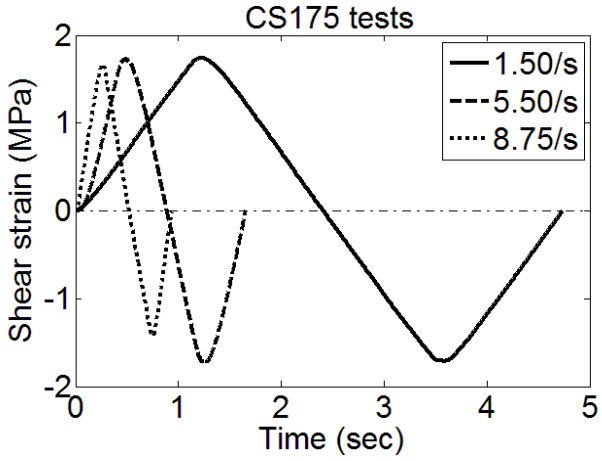

(a)

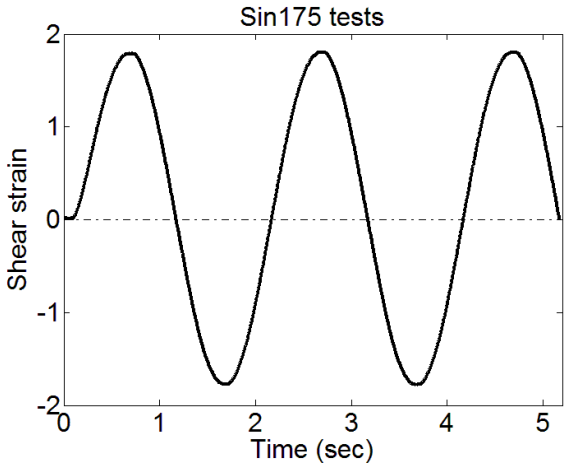

(b)

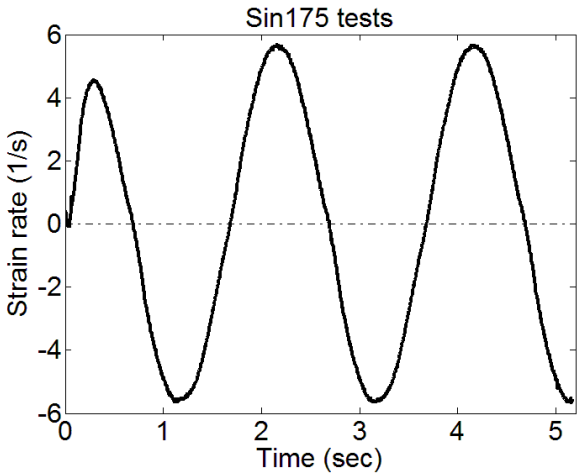

(c)

Fig. 2.6. Applied strain histories: (a) CS tests under constant strain rates of 8.75, 5.5, amd 1.5 1/s, (b) Sin tests at variable strain rate. (c) Resultant strain rate of Sin tests.

2.4 Equilibrium hysteresis behavior from MSR tests

The equilibrium stress-strain responses of HDRBs can only be obtained by applying infinitely slow loading rate, which is difficult in practice (Bergström and Boyce, 1998; Miehe and Keck, 2000). Therefore, MSR tests were suggested to identify the equilibrium state behavior at different temperatures (Figs. 2.5(a) and 2.5(b)). Stress histories recorded in MSR tests at three different temperatures are plotted in Figs. 2.7 and 2.8. It is seen that the stress value drops once the applied strain was on hold. The magnitude of stress relaxation for a particular applied strain level, perceived as the difference between the peak stress (beginning of hold time for a particular strain level) and end stress (end of hold time for particular strain level) is larger during loading than in unloading. Furthermore, from a comparison between the figures, it is clear that the peak stress value recorded at beginning of hold time for a particular strain level is larger than that recorded at the respective strain level but at a lower temperature. Not to mention, all these general observations is indicative of the existence of rate dependence property in HDRBs, but shall be carefully examined further for ruling out the strain history dependence properties via SR tests. This aspect is addressed in Section 2.5 and Section 2.6.

After each relaxation period, the stress was almost stabled, and that value was approximately the stress of equilibrium state. The converged value of stress after a relaxation step is defined as an equilibrium stress. The shear stress-strain relationship in the equilibrium state can be obtained by connecting all the equilibrium state points in Figs. 2.9 and 2.10.

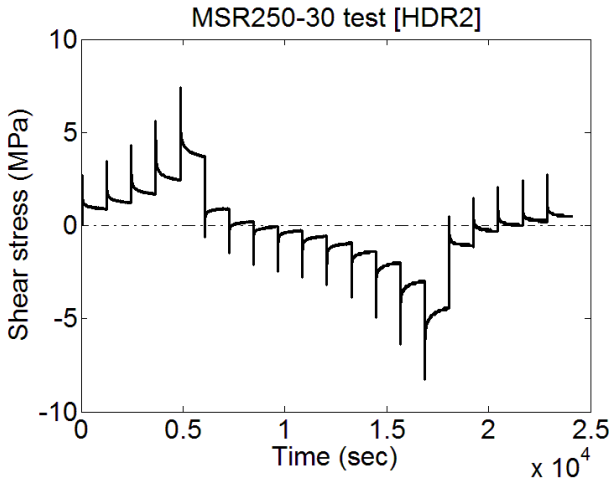

(a)

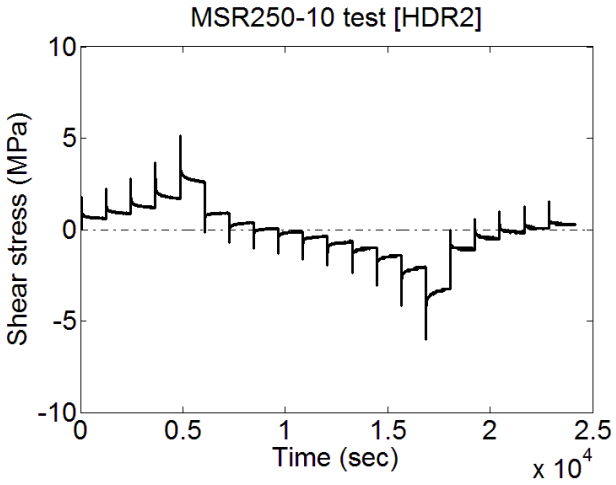

(b)

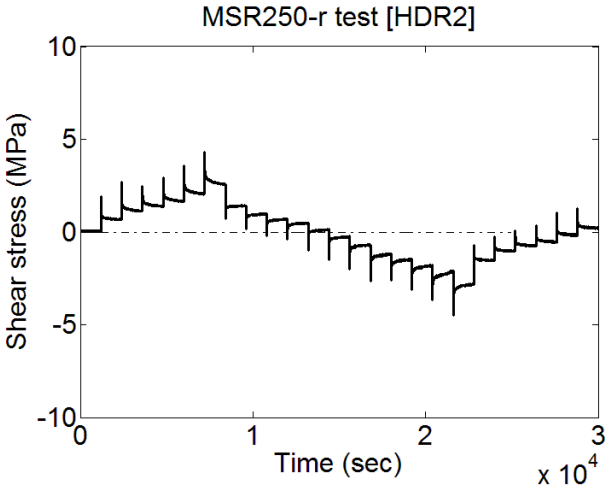

(c)

Fig. 2.7. Stress histories obtained from MSR tests of HDR2 at (a) -30°C (b) -10°C (c) 23°C.

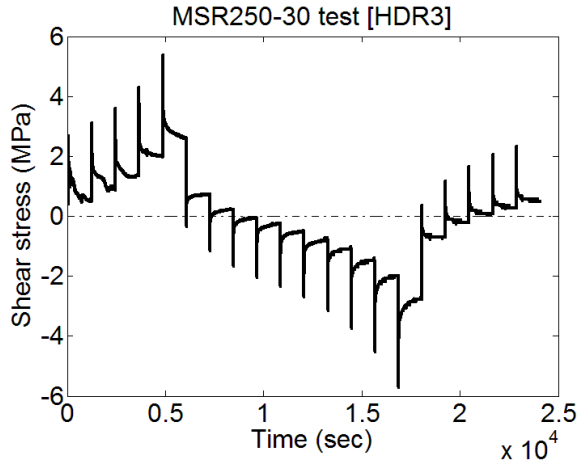

(a)

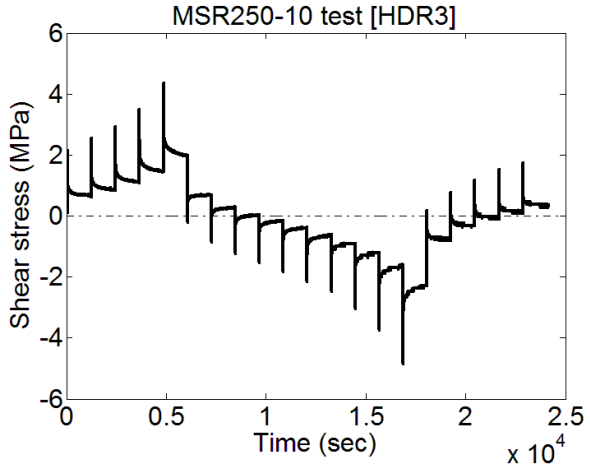

(b)

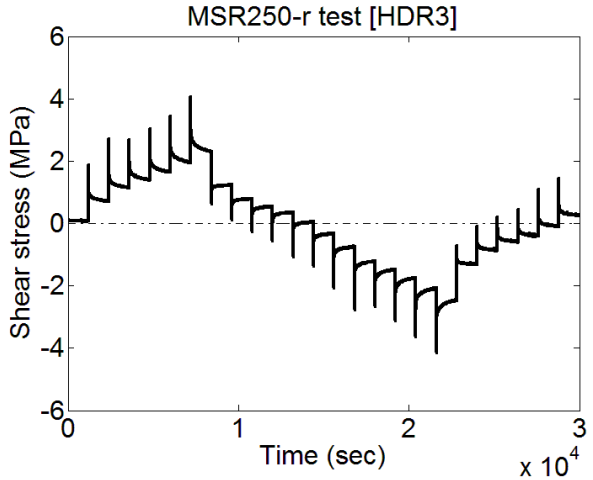

(c)

Fig. 2.8. Stress histories obtained from MSR tests of HDR3 at (a) -30°C (b) -10°C (c) 23°C.

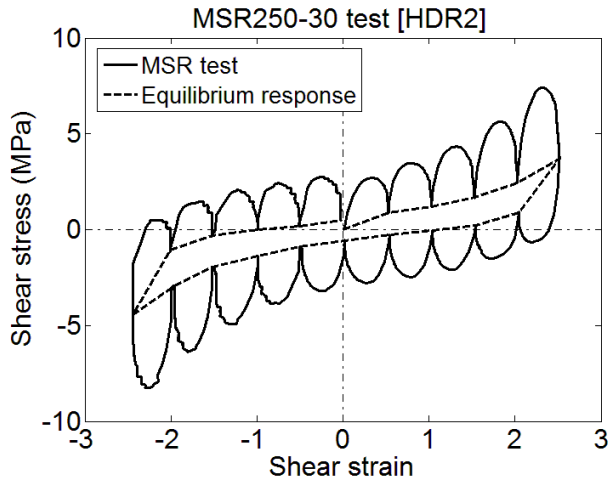

(a)

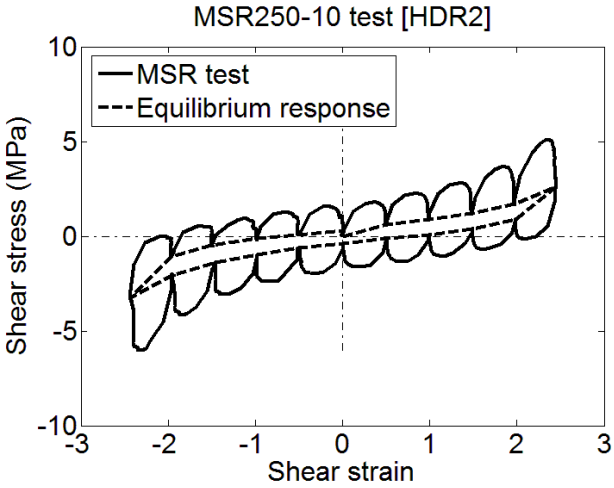

(b)

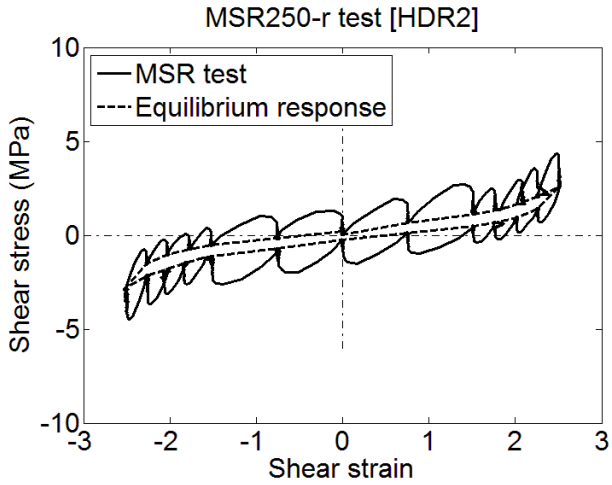

(c)

Fig. 2.9. Stress-strain responses obtained from MSR tests of HDR2 at (a) -30^{o}C (b) -10^{o}C (c) 23^{o}C

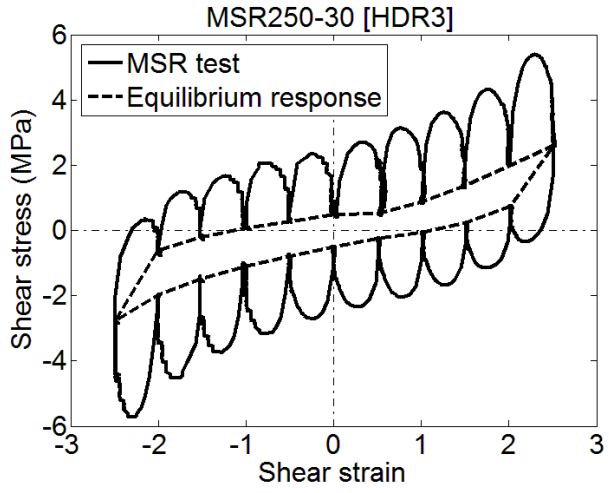

(a)

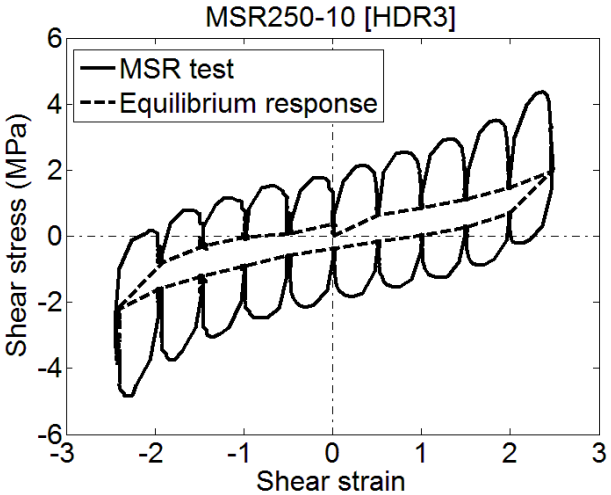

(b)

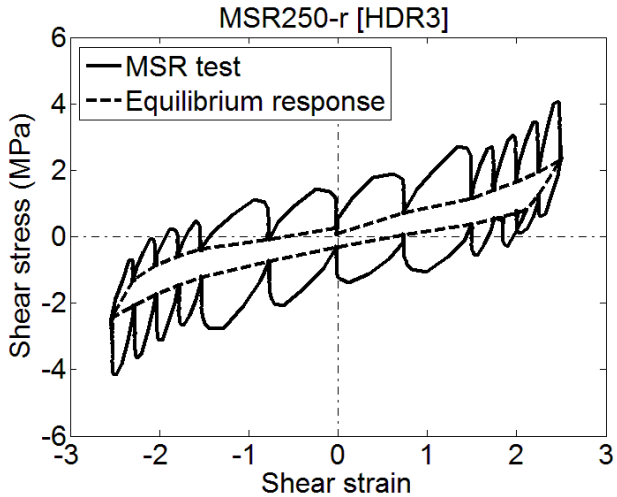

(c)

Fig. 2.10. Stress-strain responses obtained from MSR tests of HDR3 at (a) -30^{o}C (b) -10^{o}C (c) 23^{o}C

2.5 Instantaneous state from CS tests

Instantaneous response from a solid is the state when the specimen is loaded at an extremely high rate so that the rate-dependent part of stress is near to their uppermost limit (Huber and Tsakmakis 2000; Amin et al., 2002). In practice, high speed cyclic shear tests or high frequency sinusoidal loading tests are usually used to estimate the instantaneous response of rubber bearings. A series of CS tests were carried out to identify the instantaneous of HDRBs in this study. As shown in Fig. 2.6, the strain rate of these tests changes from 1.5/s to 8.75/s with an absolute maximum shear strain of 1.75. In addition, the Sin tests were conducted using an amplitude of 1.75 with a strain rate amplitude of 5.5/s (Fig. 2.6(c)) to compare with the instantaneous stress-strain responses obtained from CS tests.

To avoid self-heating appearing in the bearing when subjected to cyclic loading, only the 1st cycle of the stress-strain relationship obtained from CS tests is presented and discussed in this section. Figs. 2.11 and 2.12 show the 1st cycle of corresponding shear stress-strain relationships of CS tests at different temperatures. The absolute values of maximum stresses are larger than those of minimum stresses in CS tests, especially at low temperatures. These stress-softening behaviors seem to result from the healing of Mullins effect (Amin et al., 2010; Mullins., 1969) occurring with the time lapse between finish of the preloading and start of the actual test. However, the temperature rise inside HDRBs is remarkable at low temperatures(Cardone et al., 2011; Nguyen et al. 2013). This rise also may cause some effect on stress responses in the 1st cycle of CS tests.

It can be observed from these figures that the stress occurred larger in the specimen which was loaded faster. However, this increase in stress converged near 8.75/s as the difference in stresses between tests with strain rates of 5.5/s and 8.75/s are very small. This is in conformity to the experimental observations reported first in Amin et al. (2002) on NR and HDR. It implies that the instantaneous stress-strain response of HDRBs can be approximately obtained by loading tests in a strain rate of 8.75/s. Furthermore, hysteresis exhibited by HDRB upon cyclic loading, indicated by the areas enclosed by the stress-strain loops, are larger for lower ambient temperatures. Together with the experimental results gathered in Sections 2.4 and 2.5 on equilibrium hysteresis and stress relaxation behaviors and their experimentally observed temperature dependence properties, it is

apparent that increase in hysteresis as seen in SS and Sin tests at lower ambient temperatures are due to the main increase in the rate-dependent overstress.

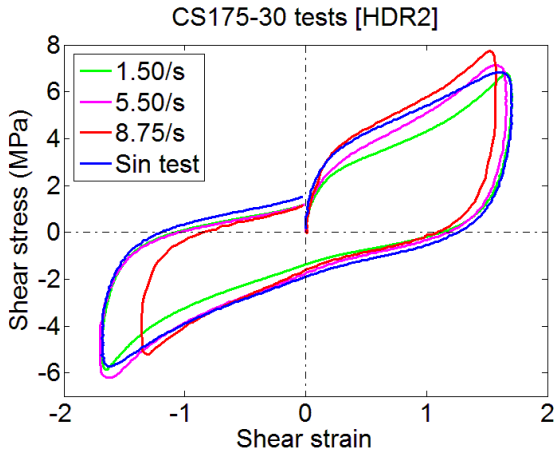

(a)

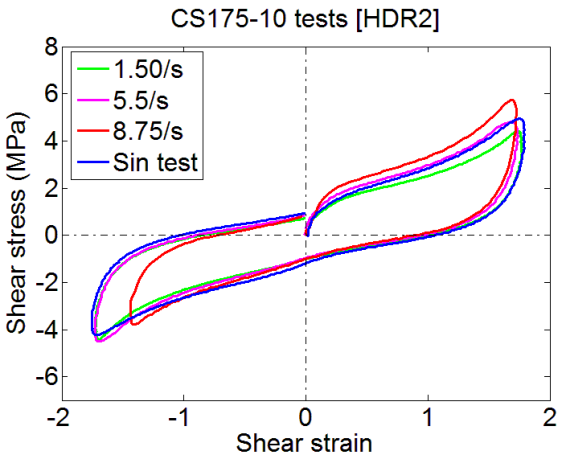

(b)

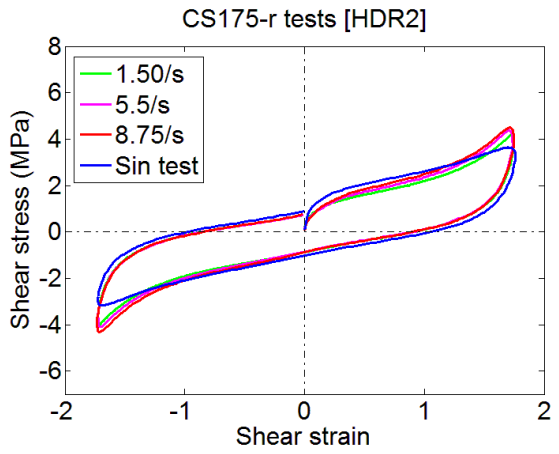

(c)

Fig. 2.11. Stress-strain responses obtained from CS tests of HDR3 at (a) -30^{o}C (b) -10^{o}C (c) 23^{o}C.

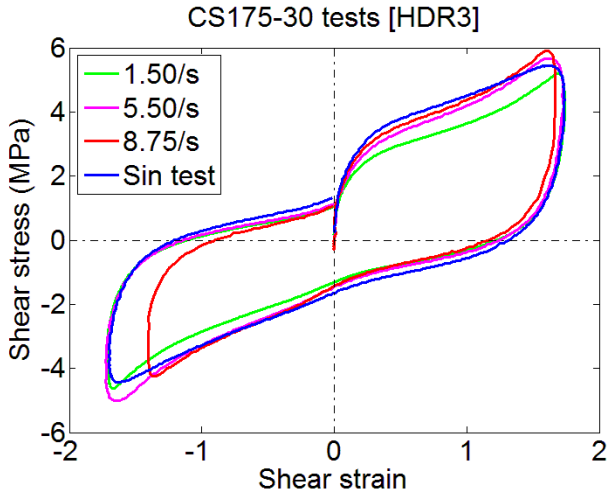

(a)

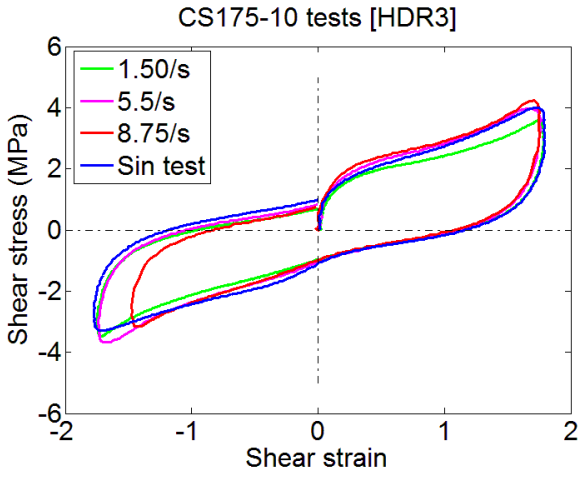

(b)

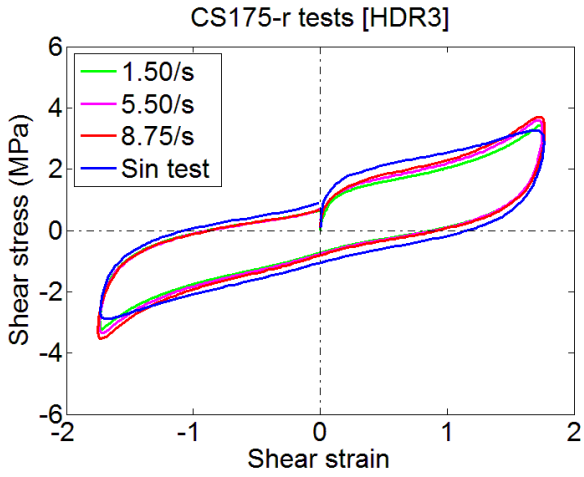

(c)

Fig. 2.12. Stress-strain responses obtained from CS tests of HDR3 at (a) -30^{o}C (b) -10^{o}C (c) 23^{o}C.

2.6 Stress relaxation behavior from SR tests

The relaxation behavior induced by viscosity property is examined by a series of SR tests at different temperatures. The stress histories obtained from SR tests are shown in Figs.2.13 and 2.14. The relaxation of the stress is very quickly in the beginning few minutes then it reaches in an asymptotically converged state. The value of the stress at the end of the relaxation period can be considered as the rate-independent equilibrium stress, the difference between the equilibrium stress and the total stress is the rate-dependent overstress.

Figs.2.13 and 2.14 compare the stress histories having same strain level at different temperatures. It is clear that the equilibrium stresses at the end of the relaxation period are similar to each other, especially in the unloading part of the SR tests. It seems that the equilibrium state is temperature-independent. However, the initial stresses at the beginning of the relaxation period are strong temperature-dependent. This behavior can be attributed to the temperature dependence of the viscosity property of HDRBs. This dependence can explain the CS test results in which the stress-strain curves increase when temperature decreases.

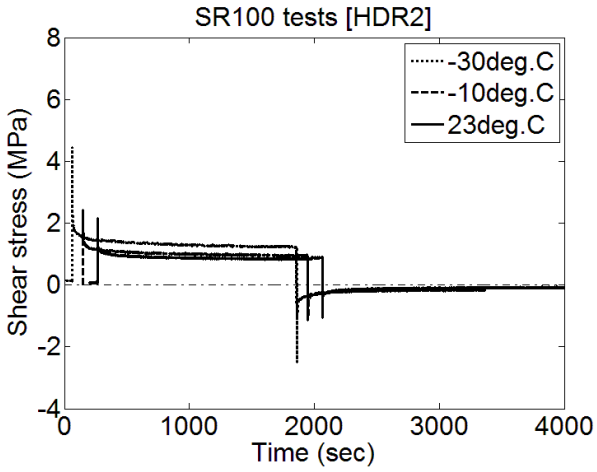

(a)

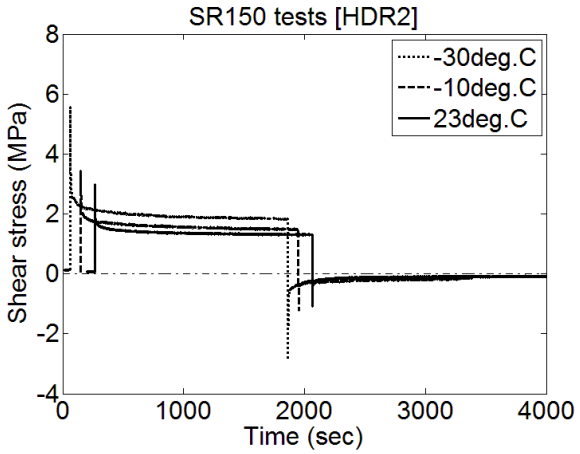

(b)

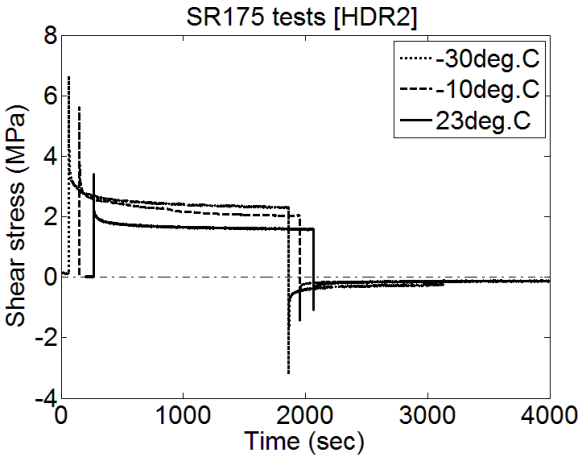

(c)

Fig. 2.13. Stress histories obtained from SR tests of HDR2 at (a) SR100 (b) SR150 (c) SR175. The stress histories have been separated by 50s to each other for clear illustration.

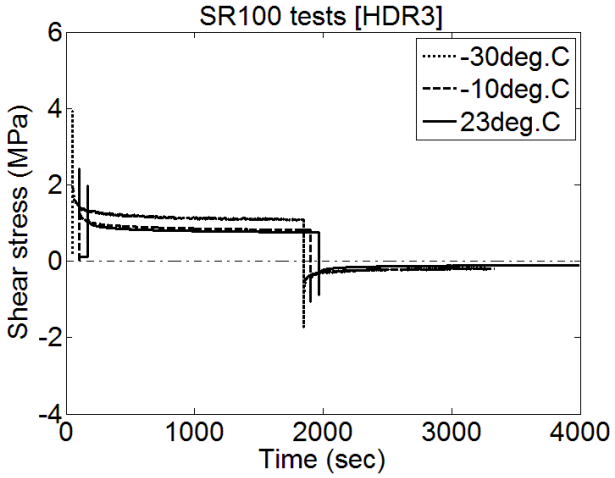

(a)

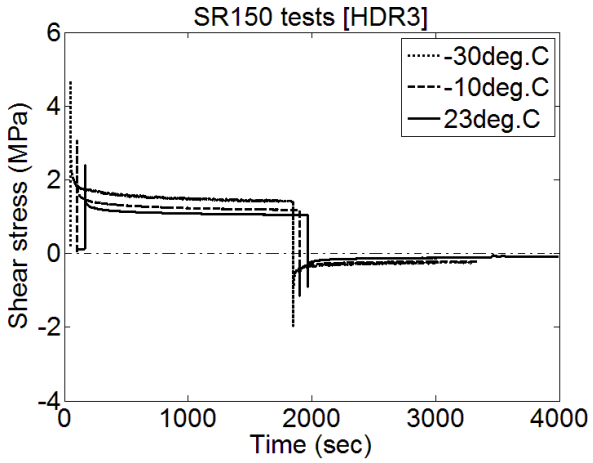

(b)

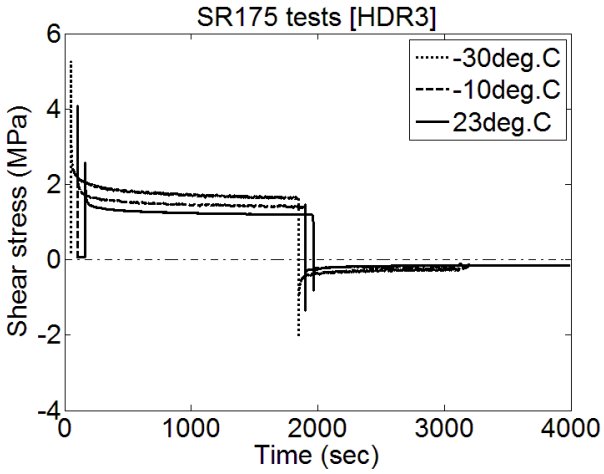

(c)

Fig. 2.14. Stress histories obtained from SR tests of HDR3 at (a) SR100 (b) SR150 (c) SR175. The stress histories have been separated by 50s to each other for clear illustration.

2.7 Summary

The mechanical behavior of HDRBs was investigated with a test program performed at constant ambient temperatures in an environmental test chamber. The test program was conducted under shear deformation with a constant vertical compressive average stress of 6 MPa.

Multi-step relaxation tests were employed to identify the equilibrium state behavior of HDRBs. The experimental observations showed an increase in the equilibrium stress with decreasing ambient temperatures. However, this increase is smaller than the increase in the overstress when ambient temperature is reduced.

A series of cyclic shear tests were carried out to identify the instantaneous response of HDRBs. The stress response at a strain rate of 5.5/s accords almost with the response at the rate of 8.75/s. It means that the instantaneous response of HDRBs can be obtained at 8.75/s.

The relaxation behavior induced by viscosity was examined by a series of simple relaxation tests. The overstress responses are larger at lower temperatures in all strain levels. This behavior can be attributed to the temperature dependence of the viscosity of HDRBs. Moreover, the temperature dependence of overstress is much larger than the dependence of the equilibrium stress at the end of relaxation period.

CHAPTER 3
AN IMPROVED RHEOLOGY MODEL

3.1 General

The experimental observations in Chapter 2 showed the strain rate-dependent behavior of HDRBs and this behavior was more obvious at low temperatures. The equilibrium response obtained from multi-step relaxation tests presented the hysteresis property and the strain hardening effect at high strain level. In addition, simple relaxation tests and cyclic shear tests also described the viscosity induced the strain rate-dependent overstress. These properties of HDRBs are reproduced in a new proposed rheology model in this section.

3.2 Layout of the improved rheology model

Based on the experimental observations at room temperature, the rheology model (Bhuiyan et la, 2009) is proposed to represent the mechanical behaviors of HDRBs. This model can adequately represent the equilibrium response of the bearings. However, it could not closely predict the instantaneous response due to the assumption of the linear spring in Maxwell element. Then, the rate-dependent parameters obtained from simple relaxation tests could not simulate the sinusoidal loading test data. The use of two parameter sets representing the experiments makes the stability and convenience of the model under question. In order to overcome the limitation of the rheology model in the prediction of the instantaneous response, a nonlinear stress-strain relation is proposed in the third branch. The new proposed model can improve the stability and convenience of the rheology model. On the basis of the original experimental observations reported in Chapter 2, a layout of a rheology model is proposed as in Fig. 3.1. Here, the total stress of HDRBs τ is presented as the resultant of rate-independent equilibrium stress τ_e and rate-dependent overstress τ_{oe}.

$$\tau = \tau_e + \tau_{oe} \tag{3.1}$$

As shown in Fig. 3.1, the equilibrium stress τ_e is expressed as three elements: spring A_1, slider S_1, and spring B_1. Spring A_1 is in series with slider S_1, so that these stresses are equal to each other.

$$\tau_{a1} = \tau_{s1} \tag{3.2}$$

Meanwhile, spring A_1 and slider S_1 share the total strain as shown in Fig. 3.1.

$$\gamma = \gamma_{a1} + \gamma_{s1} \tag{3.3}$$

The first branch consisting of spring A_1 and slider S_1 represents elasto-plastic stress τ_{ep}. The second branh including (spring B_1) describes the nonlinear elastic stress τ_{ee}. These three elements can be used to simulate bi-linear-model behavior with kinematic hardening. The equilibrium stress calculated by this model can present rate-independent bilinear stress-strain relation, such as those curves observed in MSR tests, as shown in Figs. 2.9 and 2.10. Accordingly, the equilibrium stress τ_e can be calculated from the following equation.

$$\tau_e = \tau_{ep} + \tau_{ee} \tag{3.4}$$

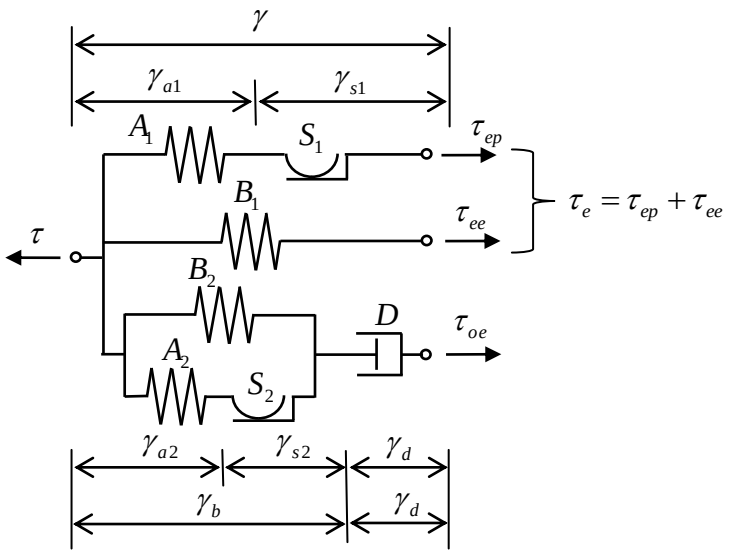

Fig. 3.1. Layout of the proposed model. Three branches define elasto-plastic stress τ_{ep}, nonlinear elastic stress τ_{ee}, and rate-dependent overstress τ_{oe}.

Fig. 3.2 shows the instantaneous state obtained from CS tests that are presented in section 2.6. It is clear from the figures that the initial stiffness is very high, due to well-known Fletcher-Gent effect (Amin et al., 2006a). The second stiffness is however lower. These aspects can be simulated by a bilinear model. Therefore, a similar structure to the equilibrium part is used in the rate-dependent overstress part, where the three elements A_2, S_2, and B_2 present elasto-plastic behavior. This elasto-plastic part is connected with a dashpot, as shown in Fig. 3.1, to construct an expanded Maxwell model. This layout for overstress can also be seen as a Maxwell model installed in a nonlinear elasto-plastic

spring instead of the original linear elastic spring. Thus, when the bearing is loaded at low strain rate, the overstress is low, Maxwell model performs its relaxation property by letting the dashpot to absorb most of the deformation. On the other hand, when the bearing is loaded at a high strain rate, the deformation of dashpot is locked-up, and the overstress shows bilinear behavior.

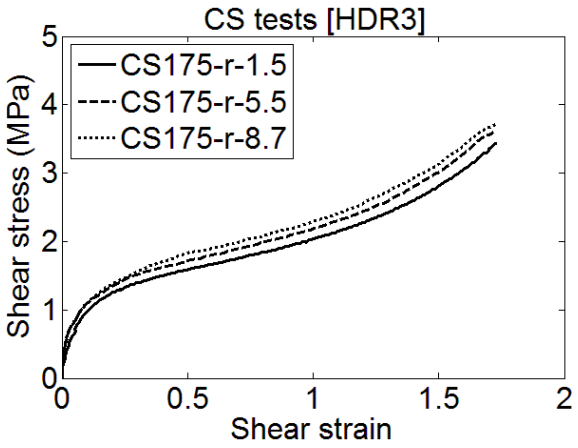

Fig. 3.2. Instantaneous state obtained from CS tests of HDR3 at 23°C

3.3 Rate-independent equilibrium part

Stress-strain relationship of spring A_1 is modeled as

$$\tau_{ep} = C_1^{(EQ)} \gamma_{a1} \tag{3.5}$$

where $C_1^{(EQ)}$ is a constant for spring A_1.

Slider S_1 will be activated and start to slide, if τ_{ep} reaches a critical stress $\tau_{cr}^{(EQ)}$

$$\begin{cases} \dot{\gamma}_{s1} \neq 0 & for \quad \left|\tau_{ep}\right| = \tau_{cr}^{(EQ)} \\ \dot{\gamma}_{s1} = 0 & for \quad \left|\tau_{ep}\right| < \tau_{cr}^{(EQ)} \end{cases} \tag{3.6}$$

where $\tau_{cr}^{(EQ)}$ is represented as the half of the stress difference of equilibrium hysteresis loop at the same strain level. This value also affects the energy dissipation capacity.

Spring B_1 is defined as the following nonlinear equation to simulate the experimental observation of hardening behavior of rubber bearings in large strain domain.

$$\tau_{ee} = C_2^{(EQ)} \gamma + C_3^{(EQ)} \left|\gamma\right|^m \operatorname{sgn}(\gamma) \tag{3.7}$$

where $C_2^{(EQ)}$, $C_3^{(EQ)}$, and m are parameters and

$$\mathrm{sgn}(x)=\begin{cases}+1 & : \quad x>0\\ 0 & : \quad x=0\\ -1 & : \quad x<0\end{cases} \tag{3.8}$$

The $C_1^{(EQ)}$, $C_2^{(EQ)}$, $C_3^{(EQ)}$, m parameters are determined by a standard nonlinear least square method to fit the equilibrium curves obtained by MSR tests (Figs. 2.9 and 2.10) as illustrated in Figs. 3.3 and 3.4. The parameters for equilibrium behavior identified at room and low temperatures are listed in Table 3.1.

Table 3.1: Equilibrium parameters obtained from MSR tests

Specimen ID	Temperature	$C_1^{(EQ)}$ (MPa)	$C_2^{(EQ)}$ (MPa)	$C_3^{(EQ)}$ (MPa)	$\tau_{cr}^{(EQ)}$ (MPa)	m
HDR2	-30°C	14.7	0.619	0.0199	0.715	4.92
	-10°C	10.6	0.524	0.0130	0.399	5.10
	23°C	8.28	0.505	0.0071	0.328	5.48
HDR3	-30°C	13.4	0.511	0.0055	0.561	5.62
	-10°C	8.84	0.442	0.0181	0.405	3.94
	23°C	7.12	0.486	0.0079	0.355	5.03

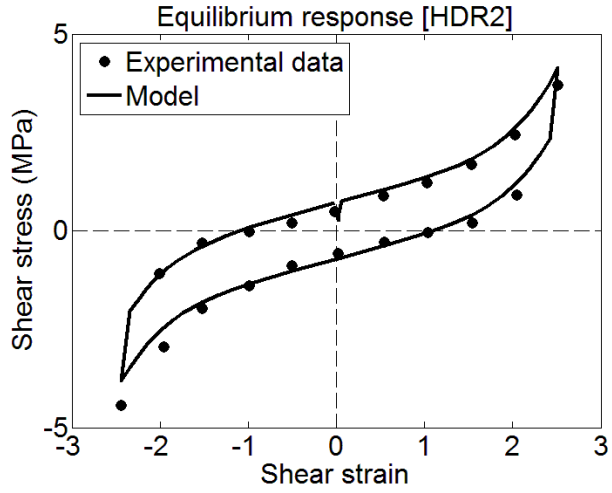

(a)

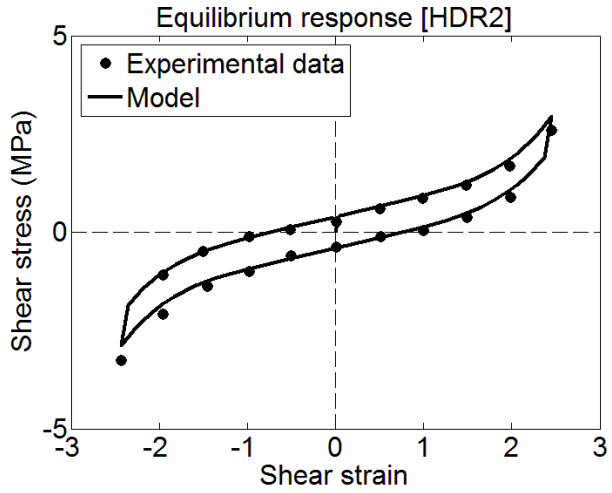

(b)

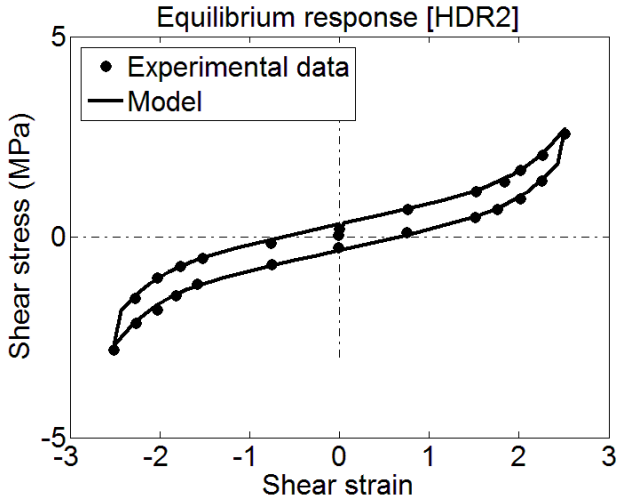

(c)

Fig. 3.3. Identification of equilibrium parameters of HDR2 at (a) -30°C (b) -10°C (c) 23°C

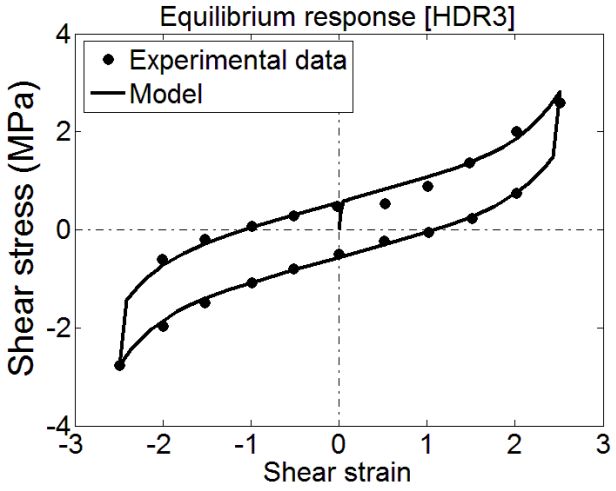

(a)

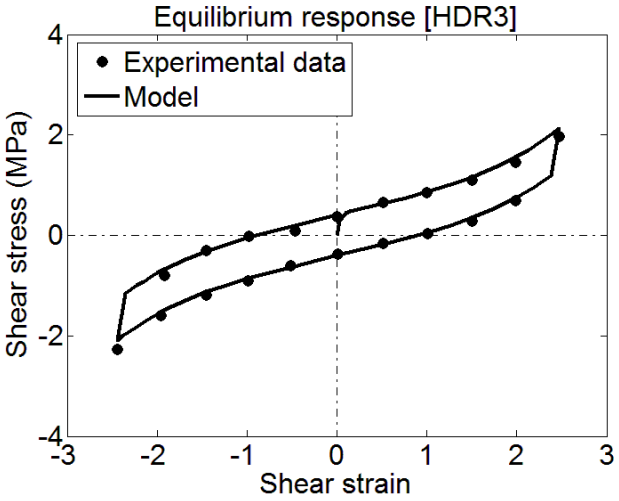

(b)

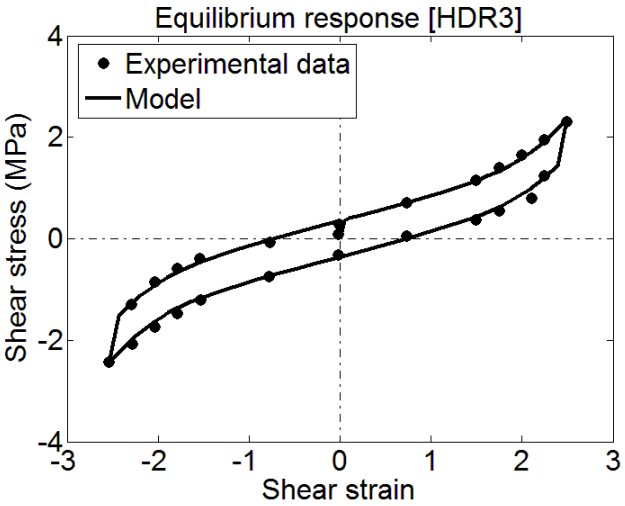

(c)

Fig. 3.4. Identification of equilibrium parameters of HDR3 at (a) -30°C (b) -10°C (c) 23°C

3.4 Rate-dependent overstress part

The overstress in the dashpot D is equal to the nonlinear elasto-plastic part stress, which is logically the sum of the stress τ_a in spring A_2 and the stress τ_b in spring B_2 as:

$$\tau_{oe} = \tau_a + \tau_b \tag{3.9}$$

The assumed stress-strain relationships of elements A_2 and S_2 are similar to the relationships of the equilibrium stress.

The stress-strain relationship of spring A_2 is then defined as:

$$\tau_a = C_1^{(OE)} \gamma_{a2} \tag{3.10}$$

Element S_2 is a friction slider defined as:

$$\begin{cases} \dot{\gamma}_{s2} \neq 0 & for \quad |\tau_a| = \tau_{cr}^{(OE)} \\ \dot{\gamma}_{s2} = 0 & for \quad |\tau_a| < \tau_{cr}^{(OE)} \end{cases} \tag{3.11}$$

The linear stress-strain relationship of spring B_2 can be obtained by

$$\tau_b = C_2^{(OE)} \gamma_b \tag{3.12}$$

where $C_1^{(OE)}$, $\tau_{cr}^{(OE)}$,and $C_2^{(OE)}$ are rate-dependent overstress parameters.

3.4.1 Viscosity behavior obtained from simple relaxation tests

The overstress and dashpot strain rate relationship of element D in the proposed model is established from SR tests in this section. For this work, the overstress τ_{oe} in Eq. (3.9) is determined from SR tests. The converged stress at the end of each relaxation period is recognized as the equilibrium stress, and accordingly the overstress is obtained by subtracting the equilibrium stress from the total stress of SR test. The parameters in Eq. (3.10) to (3.12) are determined from the instantaneous state obtained from CS tests then strain γ_b can be obtained by solving Eq. (3.9). The dashpot strain γ_d can be calculated as $\gamma_d = \gamma - \gamma_b$ in Fig. 3.1. The dashpot strain rate is obtained by taking the time derivative of the dashpot strain history. Following this method, the overstress and dashpot strain rate obtained from SR tests are presented in Figs. 3.5 and 3.6.

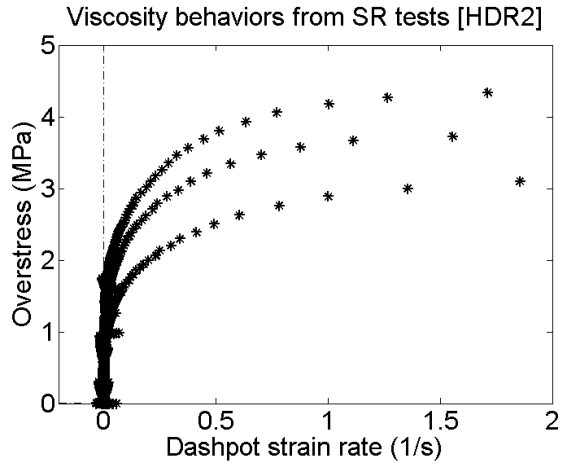

(a)

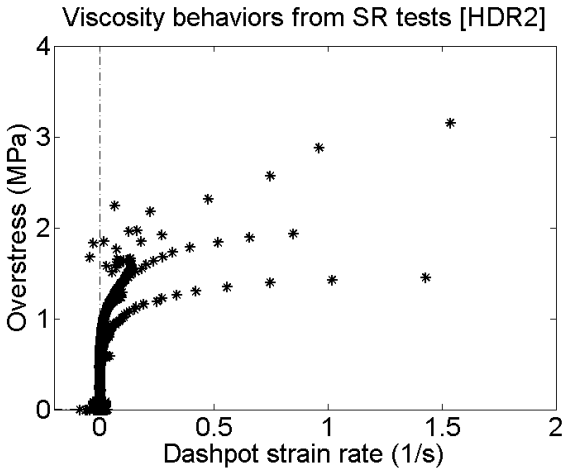

(b)

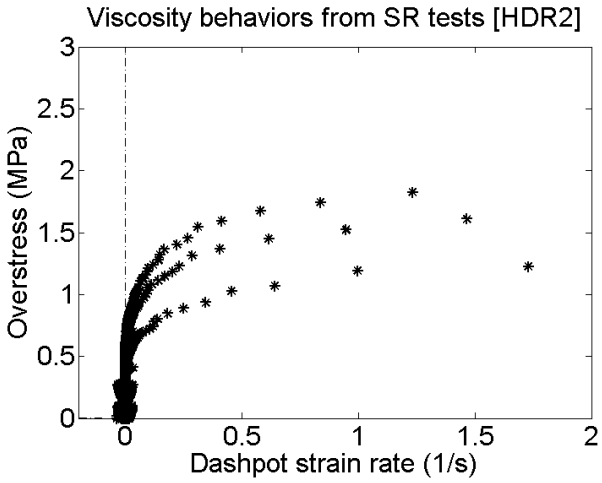

(c)

Fig. 3.5. Overstress-dashpot strain rate relationships obtained from SR tests of HDR2 at (a) -30^{o}C (b) -10^{o}C (c) 23^{o}C.

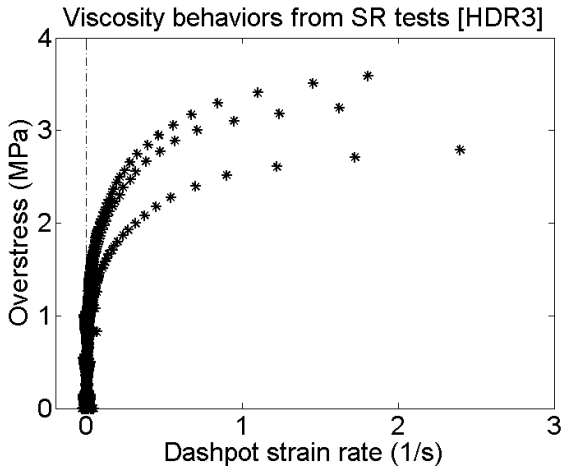

(a)

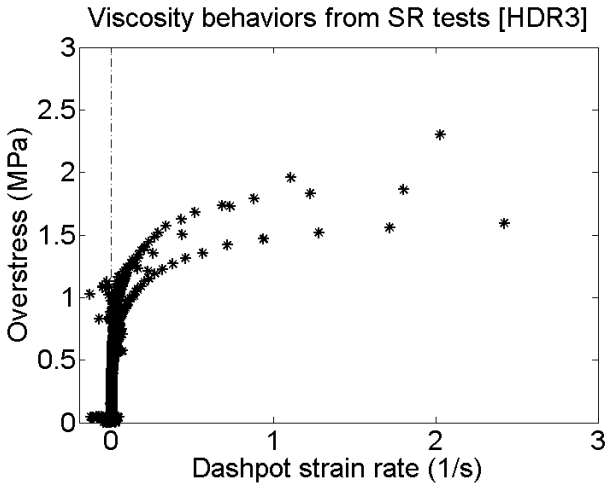

(b)

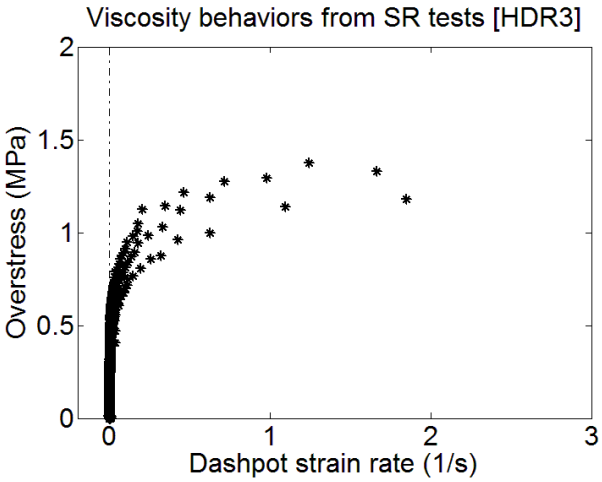

(c)

Fig. 3.6. Overstress-dashpot strain rate relationships obtained from SR tests of HDR3 at (a) -30^{o}C (b) -10^{o}C (c) 23^{o}C.

Based on the experimental observations presented in Figs. 3.5 and 3.6, the stress of D can be presented by following equation:

$$\tau_{oe} = a\left|\frac{\dot{\gamma}_d}{\dot{\gamma}_0}\right|^n \operatorname{sgn}\left(\dot{\gamma}_d\right) \tag{3.13}$$

where $\dot{\gamma}_0 = 1/(s)$ is a reference strain rate of the dashpot, a is the damping coefficient due to viscosity and n $(n<1)$ is damping exponent. The overstress parameters are determined from SIN tests in the following section.

3.4.2 Scheme to identify optimal overstress parameters

In order to determine the overstress parameters, $C_1^{(OE)}$, $\tau_{cr}^{(OE)}$, $C_2^{(OE)}$, a, and n; an optimizing technique is employed. The similarity of numerical result comparing to experimental result is defined here by the following equation:

$$R^2 = 1 - \frac{\sum_{i=1}^{N}\left(\tau_{oe}^{\exp,i} - \tau_{oe}^{M,i}\right)^2}{\sum_{i=1}^{N}\left(\tau_{oe}^{\exp,i} - \bar{\tau}_{\exp}\right)^2} \tag{3.14}$$

$$\text{with} \quad \begin{cases} \tau_{oe}^{\exp,i} = \tau_{\exp,i} - \tau_{eq,i} \\ \bar{\tau}_{\exp} = \dfrac{\sum_{i=1}^{N}\tau_{oe}^{\exp,i}}{N} \end{cases} \tag{3.15}$$

where N is the total number of data points, while $\tau_{oe}^{\exp,i}$ and $\tau_{oe}^{M,i}$ are the overstress obtained from the experiment and the model, respectively, in i step. $\bar{\tau}_{\exp}$ is the average value of experimental result. $\tau_{\exp,i}$ and $\tau_{eq,i}$ are the total shear stress and the equilibrium stress due to experiment, respectively.

Fig. 3.7 presents the flow chart of the optimizing algorithm. At step 1, the input data include the experimental data, initial values of overstress parameters and values of $S_l, S_r, \varepsilon_{Di}$. The step length D_i is selected to equal 10% of the parameter value at this step. Based on the input data, the stress of the model τ_M and function R are calculated at step 2.

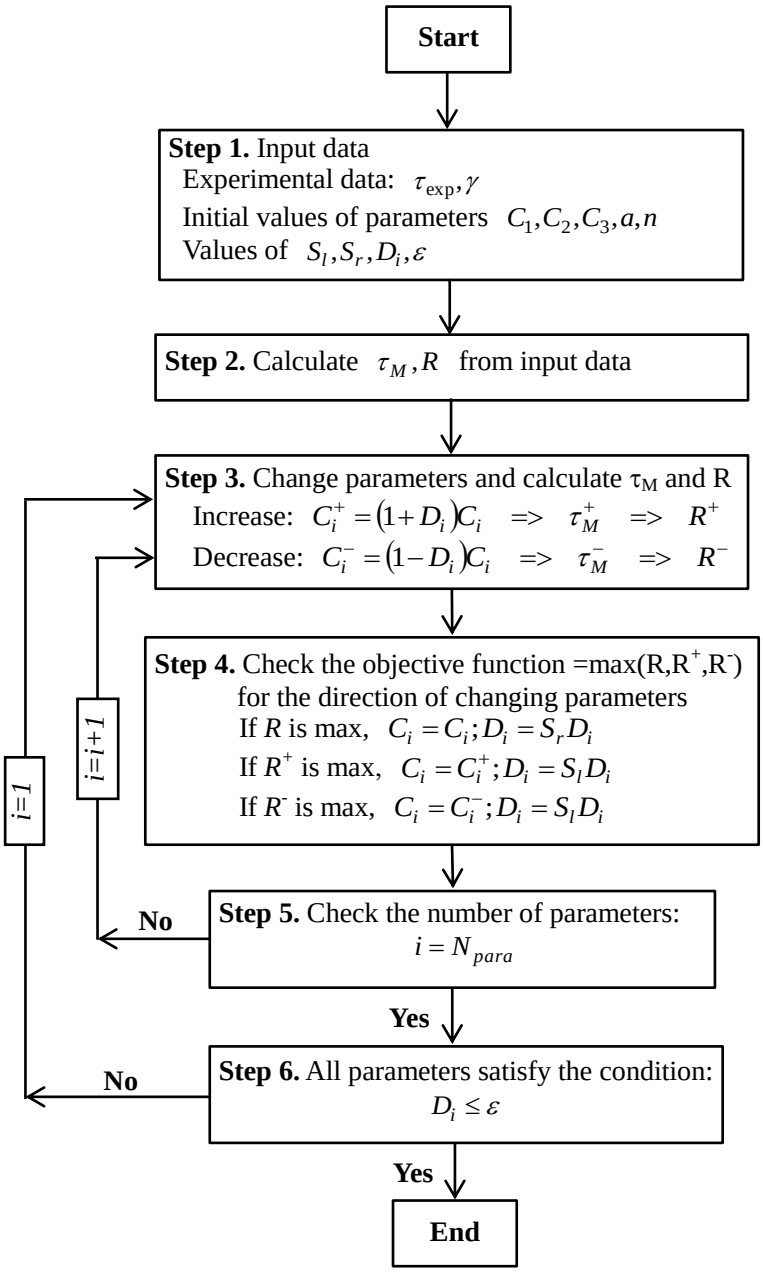

Fig. 3.7. Flow chart to determine the optimal overstress parameters. Notations: τ_{exp}, γ = the experimental stress and strain, respectively; τ_M = the stress obtained from the model; C_i = the i^{th} parameter; S_l = the increasing rate; S_r = the decreasing rate; D_i = the step length for parameter C_i; ε_{Di} = the minimum value of the step rate D_i; N_{para} = the number of overstress parameters.

At step 3, parameter C_i is varied by Eq. (3.16) in which C_i increases by $D_i C_i$ into C_i^+ and C_i decreases by $D_i C_i$ into C_i^-. Values of R^+ and R^- can be obtained from C_i^+ and C_i^- by Eq. (3.14), respectively.

$$\begin{cases} C_i^+ = (1+D_i)C_i \\ C_i^- = (1-D_i)C_i \end{cases} \tag{3.16}$$

At step 4, the maximum value of $\left(R, R^{+}, R^{-}\right)$ is identified to find the optimal direction variation of the parameter. After finding the optimal direction variation of the parameter, the corresponding parameter $\left(C, C_i^{+}, C_i^{-}\right)$ is selected and the step length D_i is changed by Eq. (3.17) for the next step $i+1$.

$$\begin{cases} C_i = C_i; & D_i = S_r D_i \quad if \quad R = \max\left(R, R^{+}, R^{-}\right) \\ C_i = C_i^{+}; & D_i = S_l D_i \quad if \quad R^{+} = \max\left(R, R^{+}, R^{-}\right) \\ C_i = C_i^{-}; & D_i = S_l D_i \quad if \quad R^{-} = \max\left(R, R^{+}, R^{-}\right) \end{cases} \tag{3.17}$$

This direct step-by-step iteration of C_i parameter identification is finished when the optimal condition is satisfied: $D_i \le \varepsilon_{Di}$ at step 5 and the optimum program is completed when all parameters are identified at step 6.

Figs. 3.8 and 3.9 show the identification of overstress parameters by using the optimum program. The 1st cycle of shear stress-strain responses of Sin tests are used in the parameter identification procedure. There are some differences between the experimental and numerical results due to the stress-softening phenomenon occuring in the 1st cycle of sinusoidal loading tests, especially in the hysteresis loops at low temperatures. The model could still present the set of experimental result effectively. The optimized parameters are listed in Table 3.2.

Table 3.2: Overstress parameters obtained from Sin tests.

Specimen ID	Temperature	$C_1^{(OE)}$ (MPa)	$C_2^{(OE)}$ (MPa)	$\tau_{cr}^{(OE)}$ (MPa)	a (MPa)	n
HDR2	-30°C	23.1	1.583	1.465	4.32	0.283
	-10°C	11.8	0.998	0.944	2.88	0.235
	23°C	9.16	0.687	0.798	2.13	0.233
HDR3	-30°C	19.2	1.253	1.365	3.93	0.248
	-10°C	10.4	0.681	0.932	2.53	0.251
	23°C	10.2	0.652	0.711	1.45	0.238

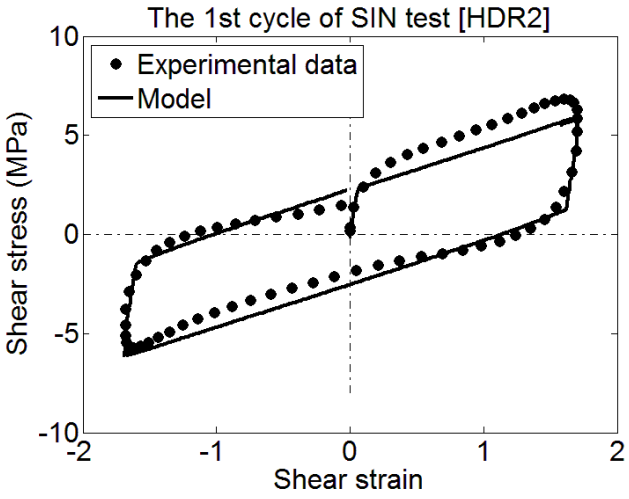

(a)

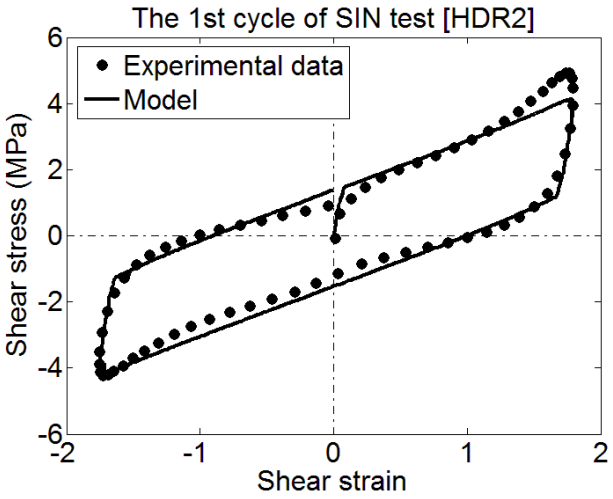

(b)

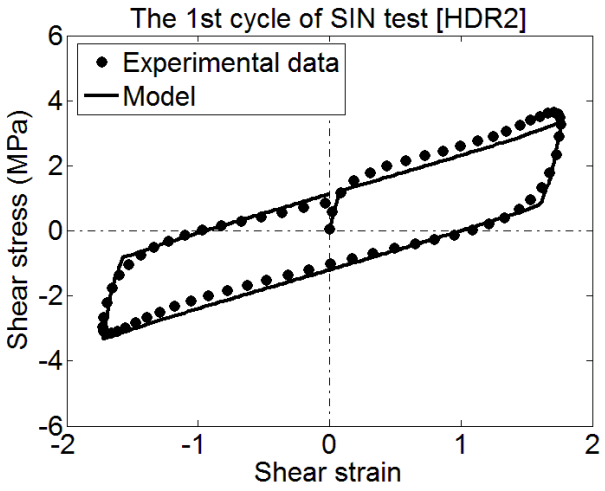

(c)

Figure 3.8. Identification of overstress parameters of HDR2 at (a) -30°C (b) -10°C (c) 23°C.

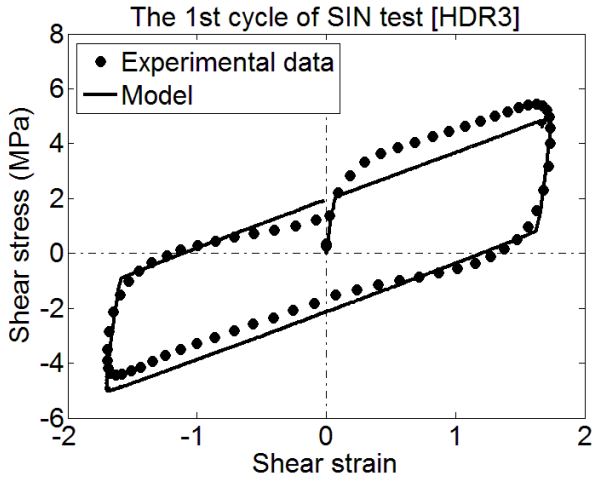

(a)

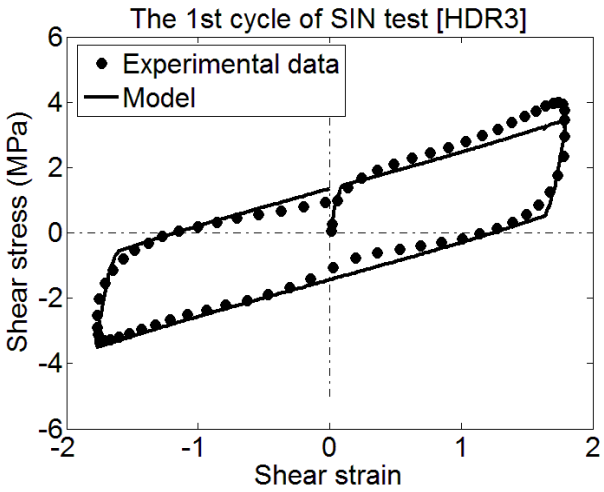

(b)

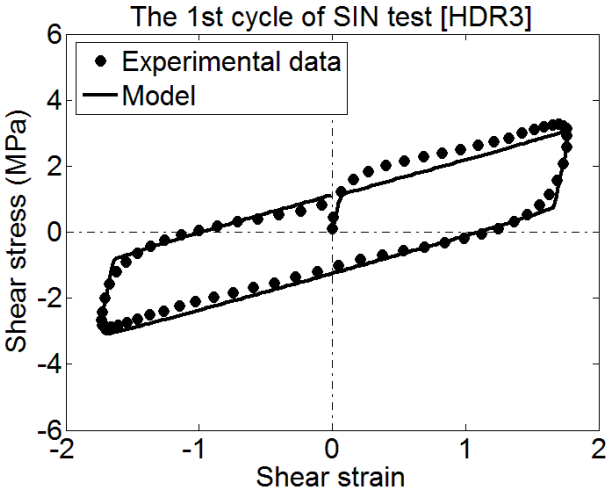

(c)

Figure 3.9. Identification of overstress parameters of HDR3 at (a) -30°C (b) -10°C (c) 23°C.

3.5 Summary

The experimental results presented high strain hardening at high strain level in the equilibrium hysteresis. These behaviors are represented by a rate-independent model that is constructed by combining a nonlinear spring and an ideal elasto-plastic model (spring-slider) in parallel.

On the basis of the experimental observations of instantaneous state obtained from CS tests, a structure similar to the rate-independent part is used in the rate-dependent overstress part. This part is connected with a dashpot that represents the rate-dependent behavior of HDRBs. The proposed relationship between the overstress and the strain rate of the dashpot is based on the nonlinear viscosity law deduced from the experimental results of SR tests.

The equilibrium parameters are identified from MSR tests by a standard nonlinear least square method. An optimizing technique is also employed to determine the overstress parameters in this chapter.

CHAPTER 4
NUMERICAL SIMULATION OF EXPERIMENTAL DATA AND VERIFICATION OF THE PROPOSED RHEOLOGY MODEL

4.1 General

On the basis of the experimental observations in Chapter 2, a rheology model is proposed to describe the mechanical behavior of HDRBs in Chapter 3. The basic layout of the proposed model is to divide the total stress into two contributions including rate-independent equilibrium stress and rate-dependent overstress. The parameters of equilibrium part are identified from MSR tests, and the parameters of overstress part are determined from Sin tests. In this chapter, in order to evaluate the capability of the proposed model in Chapter 3, the identified parameters in Table 3.1 and 3.2 are used in the model to simulate MSR tests, CS tests and SR tests. Though part of these test data have been used in parameter identification, reversibility and the global simulation performance are needed to be checked.

4.2 Simulation results

4.2.1 Relaxation tests

Figs. 4.1 to 4.4 present the comparison between the numerical simulation results and MSR test results of HDR2 and HDR3 specimens at different temperatures. The stress-strain points obtained from tests and the proposed model at equilibrium state agree well with each other. As can be seen in these figures, there are some difference in the instantaneous responses in unloading path. The instantaneous responses appearing at the beginning of each relaxation step are underestimated by the proposed model. However, the capability of the model in capturing the long-term and short-term relaxation behavior of the bearings is clearly illustrated in loading path.

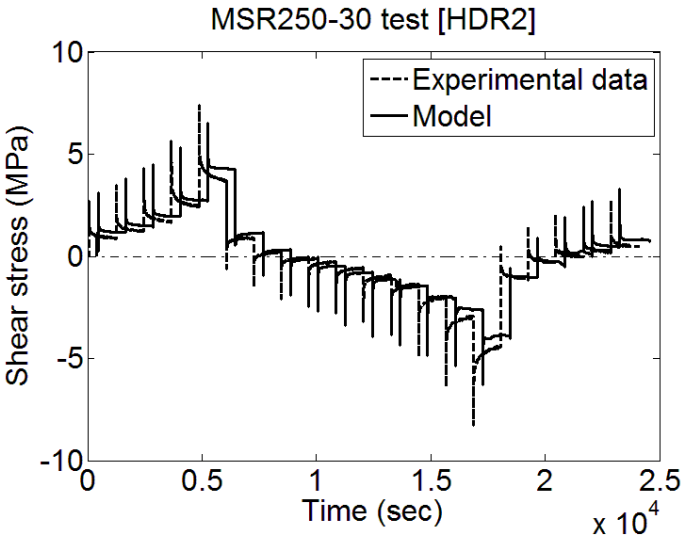

(a)

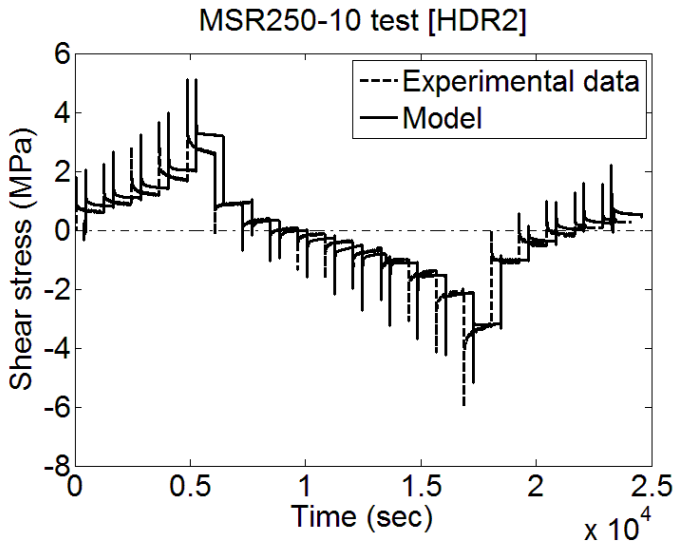

(b)

Fig. 4.1. Numerical simulation of MSR tests of HDR2. Stress histories at (a) -30^{o}C (b) -10^{o}C. The stress histories have been separated by 400s to each other for clear illustration.

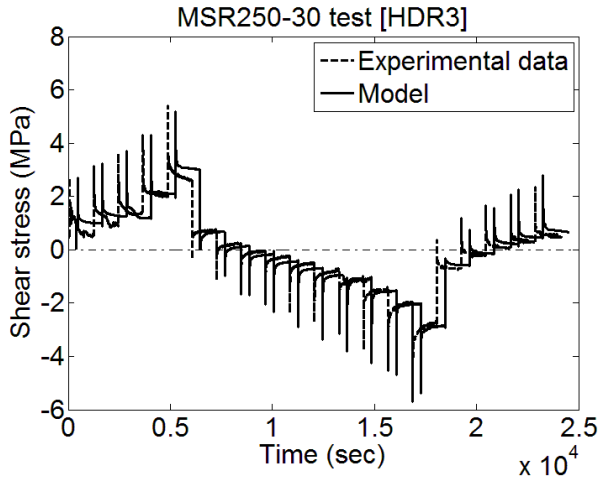

(a)

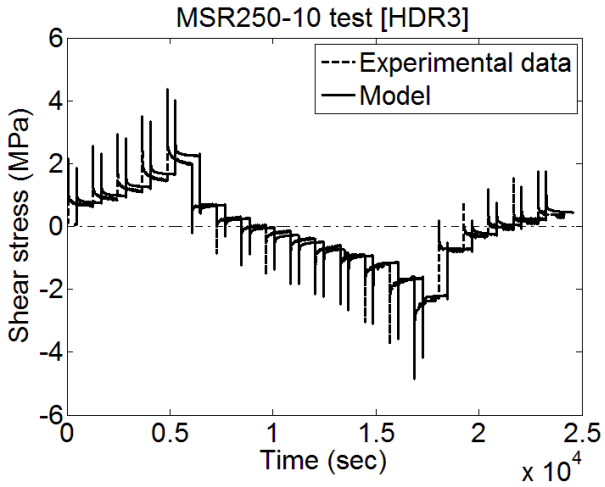

(b)

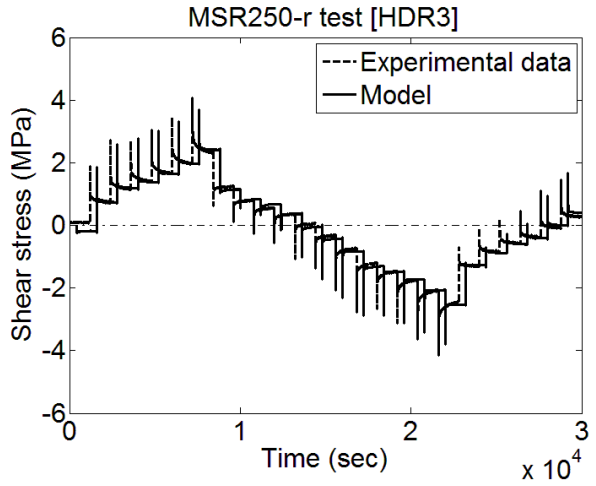

(c)

Fig. 4.2. Numerical simulation of MSR tests of HDR3. Stress histories at (a) -30°C (b) -10°C. The stress histories have been separated by 400s to each other for clear illustration..

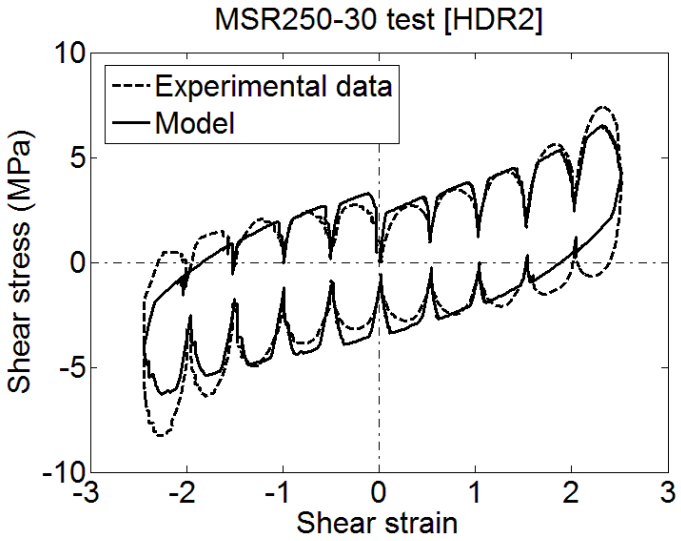

(a)

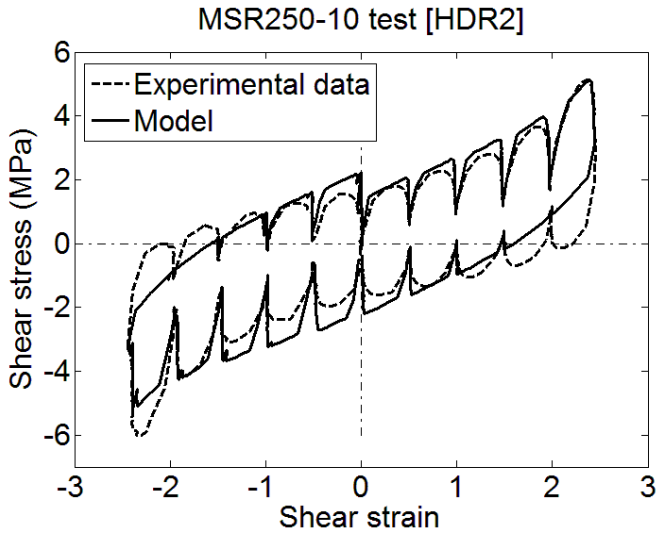

(b)

Figure 4.3. Numerical simulation of MSR tests of HDR2. Stress-strain responses at (a) -30^{o}C (b) -10^{o}C.

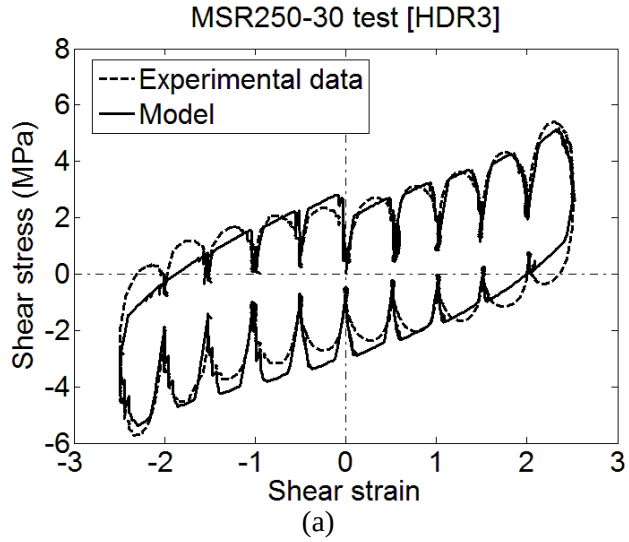

(a)

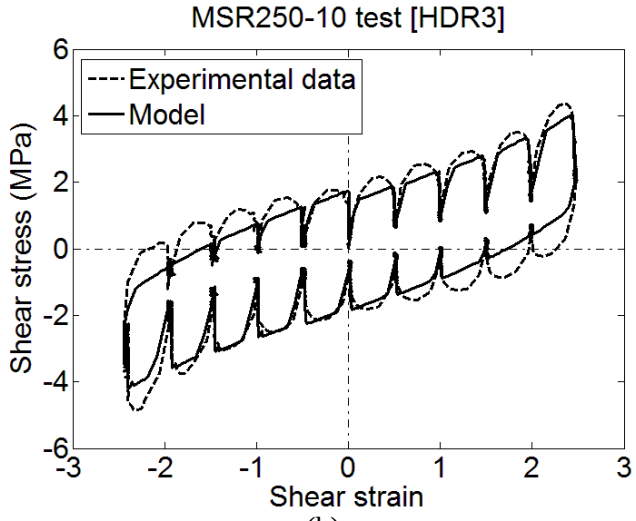

(b)

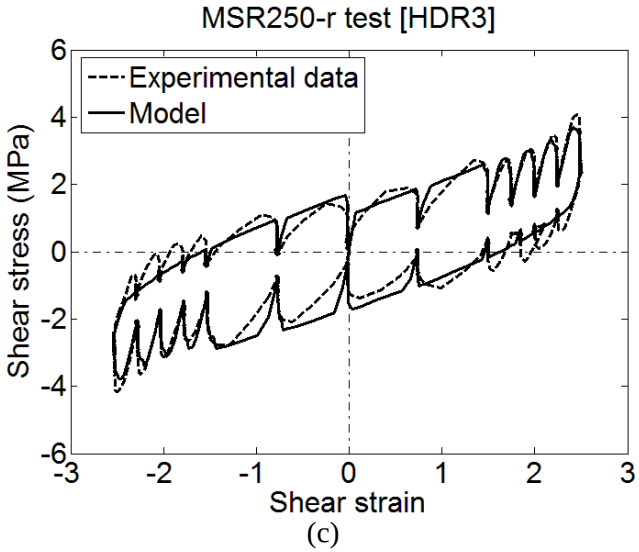

(c)

Figure 4.4. Numerical simulation of MSR tests of HDR3. Stress-strain responses at (a) -30°C (b) -10°C.

The simulation results for SR tests are plotted in Figs. 4.5 to 4.23 in comparison to experimental results. Confident simulation can be observed in all the cases. The simulation results are closely comparable with the experiment results in representing the instantaneous response and the equilibrium state that appear at the beginning and the end of relaxation processes, respectively. The simulation of the relaxation behaviors at the first three seconds of the relaxation processes also matches very closely with the experiments as compared in Figs. 4.5(b) to 4.23(b). These results show the capability of the proposed model for reproducing the relaxation behavior induced by viscosity of HDRBs.

Furthermore, in some seismic design specifications (AASHTO 2010; JRA 2002) for bridges with HDRBs, a bilinear model is recommended to reproduce the nonlinear characteristics of the bearings. The parameters of the bilinear model are determined based on a stress-strain relationship obtained from sinusoidal loading tests with a constant frequency of 0.5 Hz. However, natural frequencies of recent base-isolated bridges vary widely. In particular, base-isolated bridges with sliding bearings, in which HDRBs are often installed as a stiffness and damping device, have a natural frequency of around 0.2Hz. In fact, the first and second natural frequencies of Imakirigawa bridge (Matsuda et al., 2013), which employs both sliding bearings and HDRBs, are 0.06 and 0.19 Hz respectively. In those bridges, dominant strain rate of HDRBs under earthquake excitation may become about 20% of that in the sinusoidal loading test with 0.5 Hz frequency. Obviously, the bilinear model base on 0.5 Hz frequency tests is not applicable to these wide range strain-rate problems. The proposed model is intended to simulate wide range of strain-rate behavior of HDRBs, inducing bridges with very small natural frequencies.

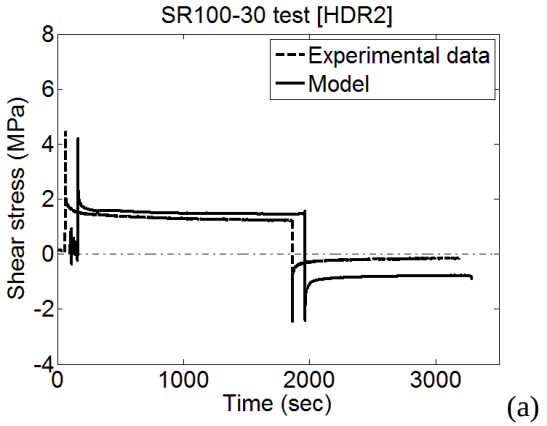

(a)

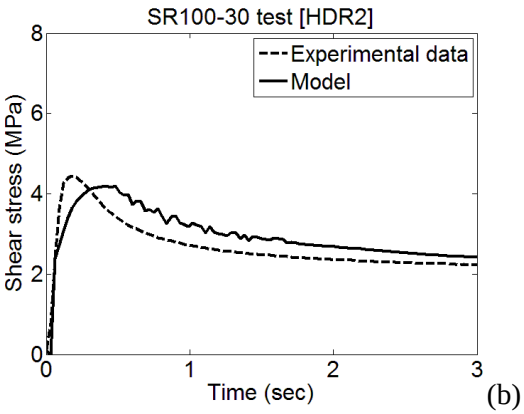

(b)

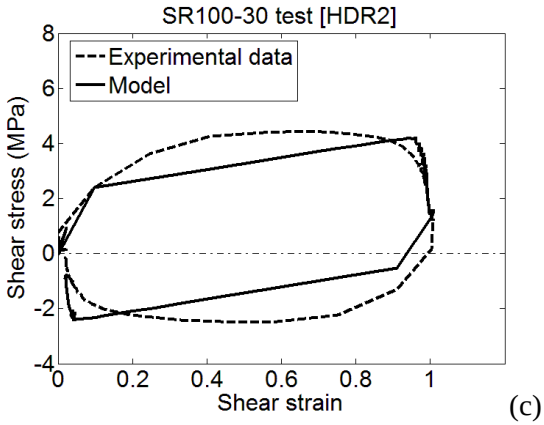

(c)

Fig. 4.5. Numerical simulation of SR100-30 test of HDR2 at -30°C (a) stress history of the test (b) close up view of first 3 sec (c) stress-strain response.

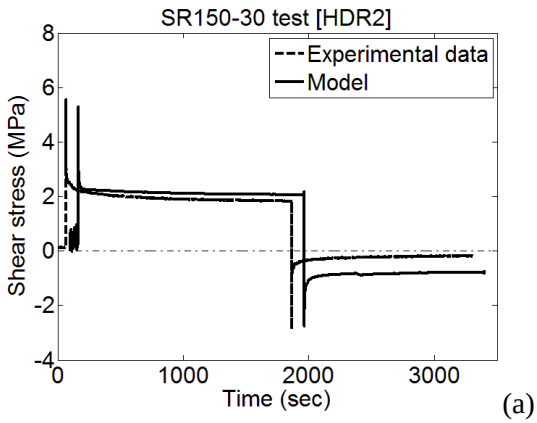

(a)

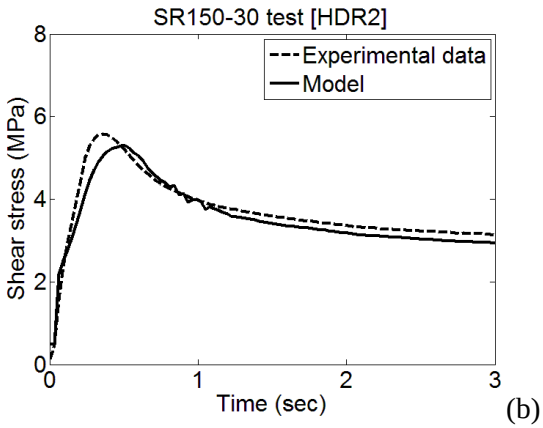

(b)

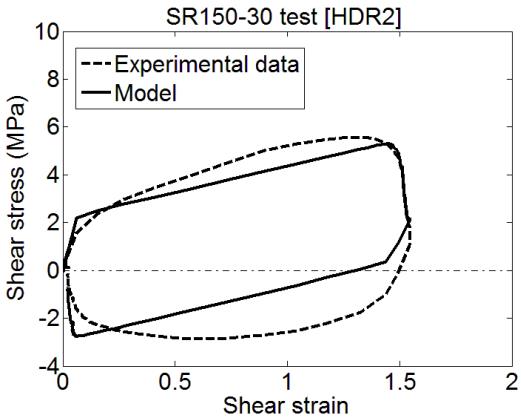

(c)

Fig. 4.6. Numerical simulation of SR150-30 test of HDR2 at -30°C (a) stress history of the test (b) close up view of first 3 sec (c) stress-strain response.

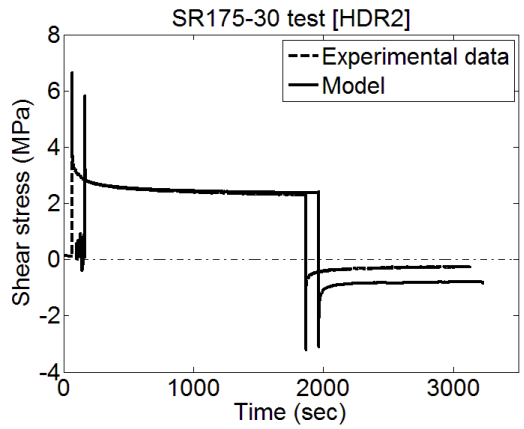

(a)

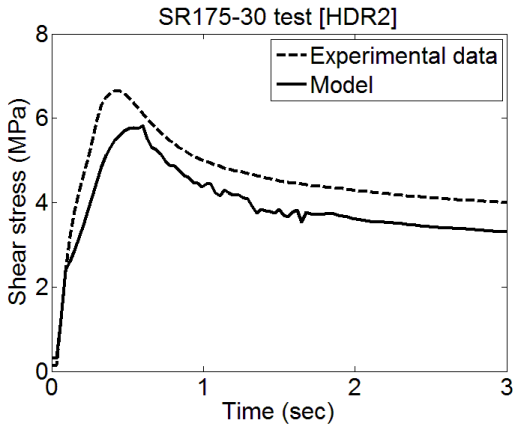

(b)

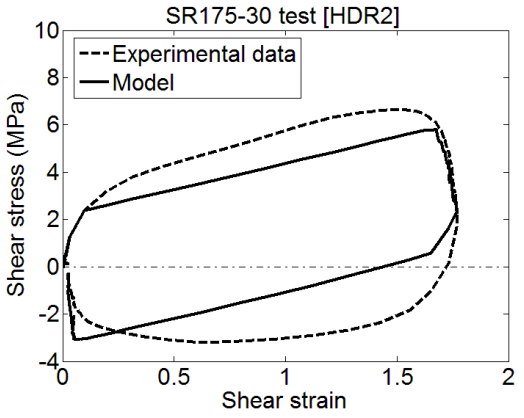

(c)

Fig. 4.7. Numerical simulation of SR175-30 test of HDR2 at -30°C (a) stress history of the test (b) close up view of first 3 sec (c) stress-strain response.

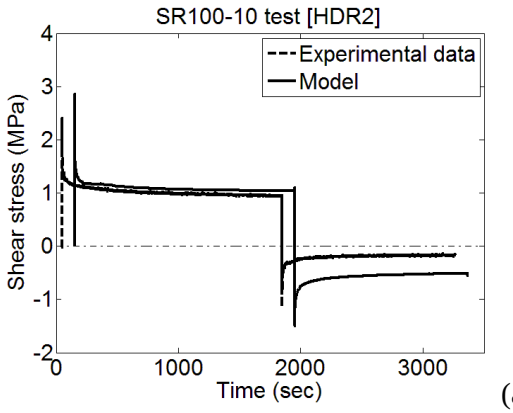

(a)

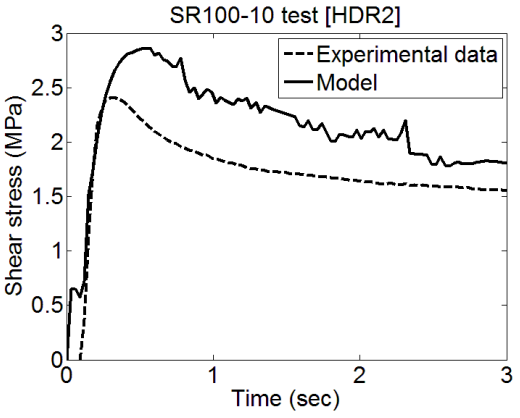

(b)

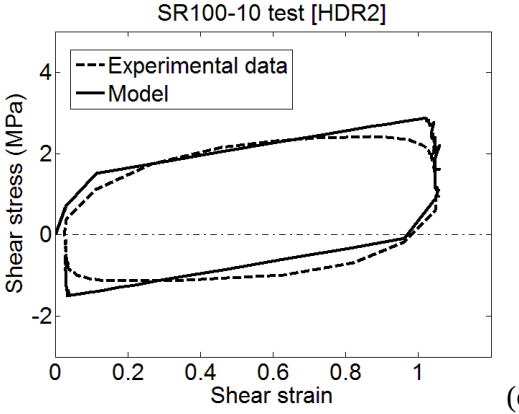

(c)

Fig. 4.8. Numerical simulation of SR100-10 test of HDR2 at -10°C (a) stress history of the test (b) close up view of first 3 sec (c) stress-strain response.

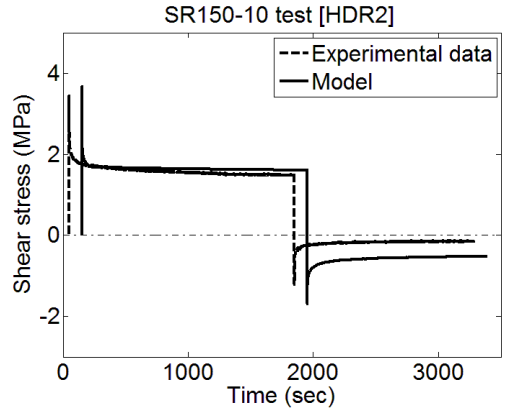

(a)

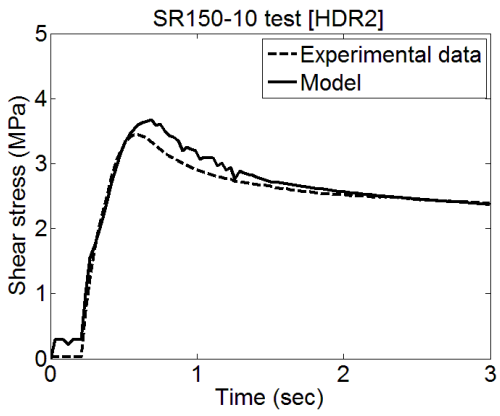

(b)

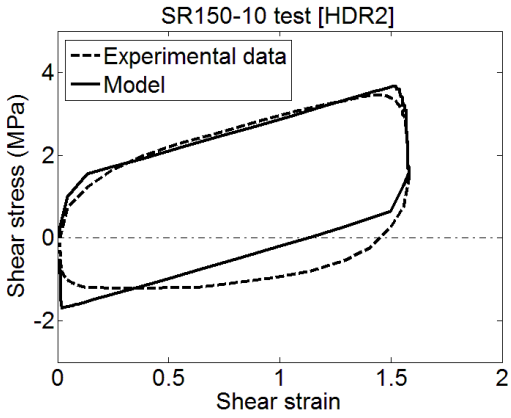

(c)

Fig. 4.9. Numerical simulation of SR150-10 test of HDR2 at -10^{o}C (a) stress history of the test (b) close up view of first 3 sec (c) stress-strain response.

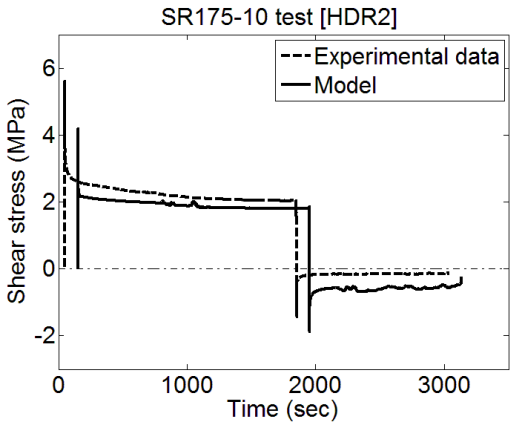

(a)

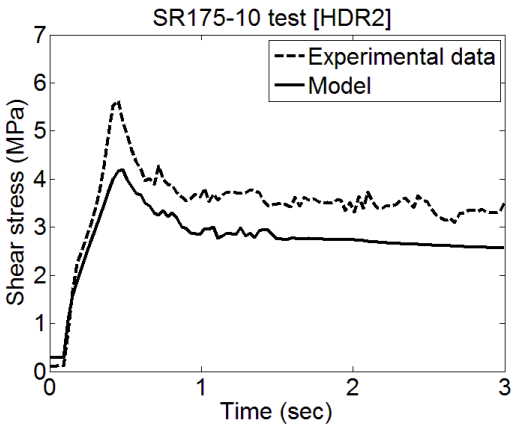

(b)

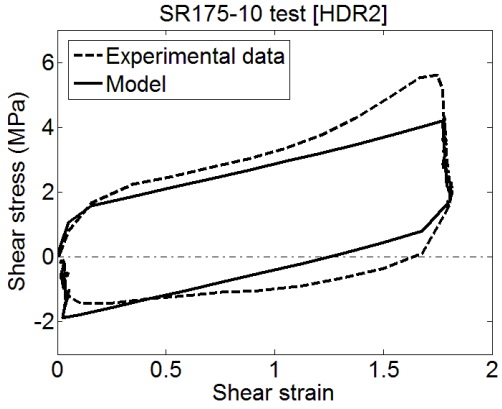

(c)

Fig. 4.10. Numerical simulation of SR175-10 test of HDR2 at -10^{o}C (a) stress history of the test (b) close up view of first 3 sec (c) stress-strain response.

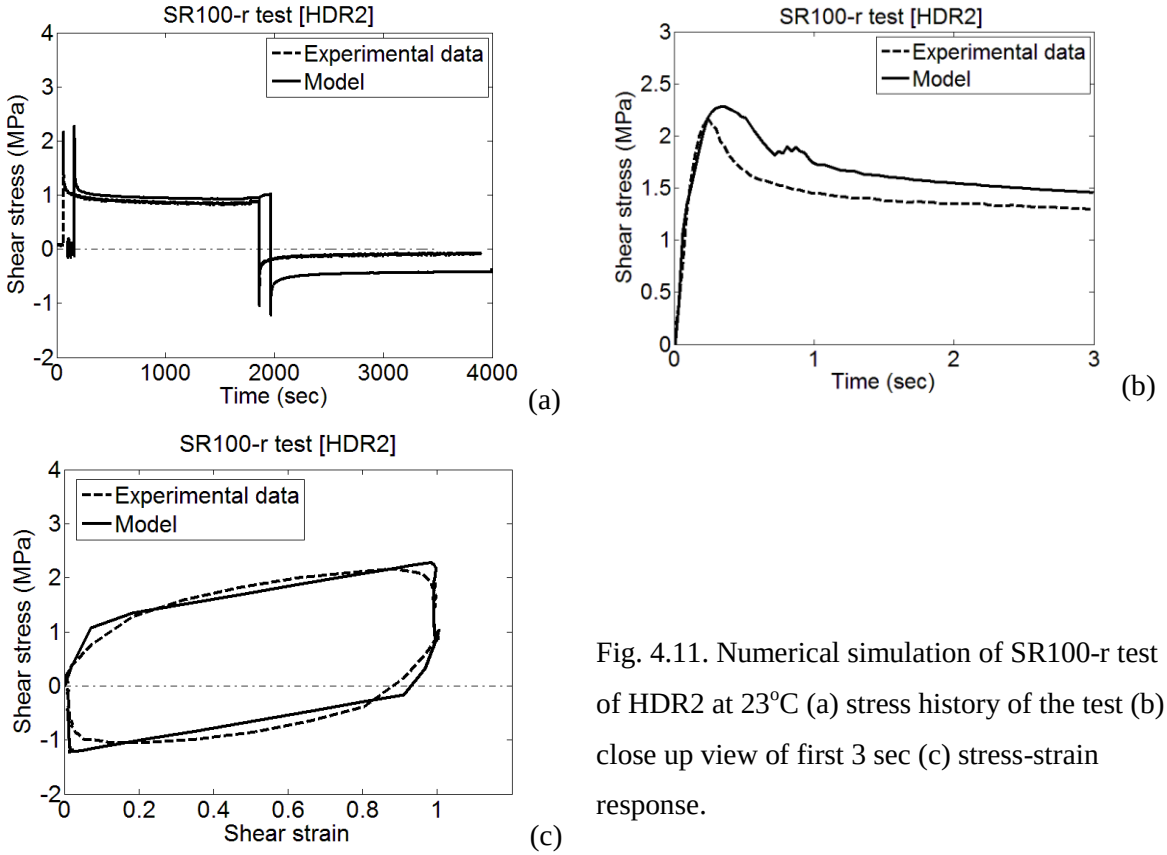

Fig. 4.11. Numerical simulation of SR100-r test of HDR2 at 23°C (a) stress history of the test (b) close up view of first 3 sec (c) stress-strain response.

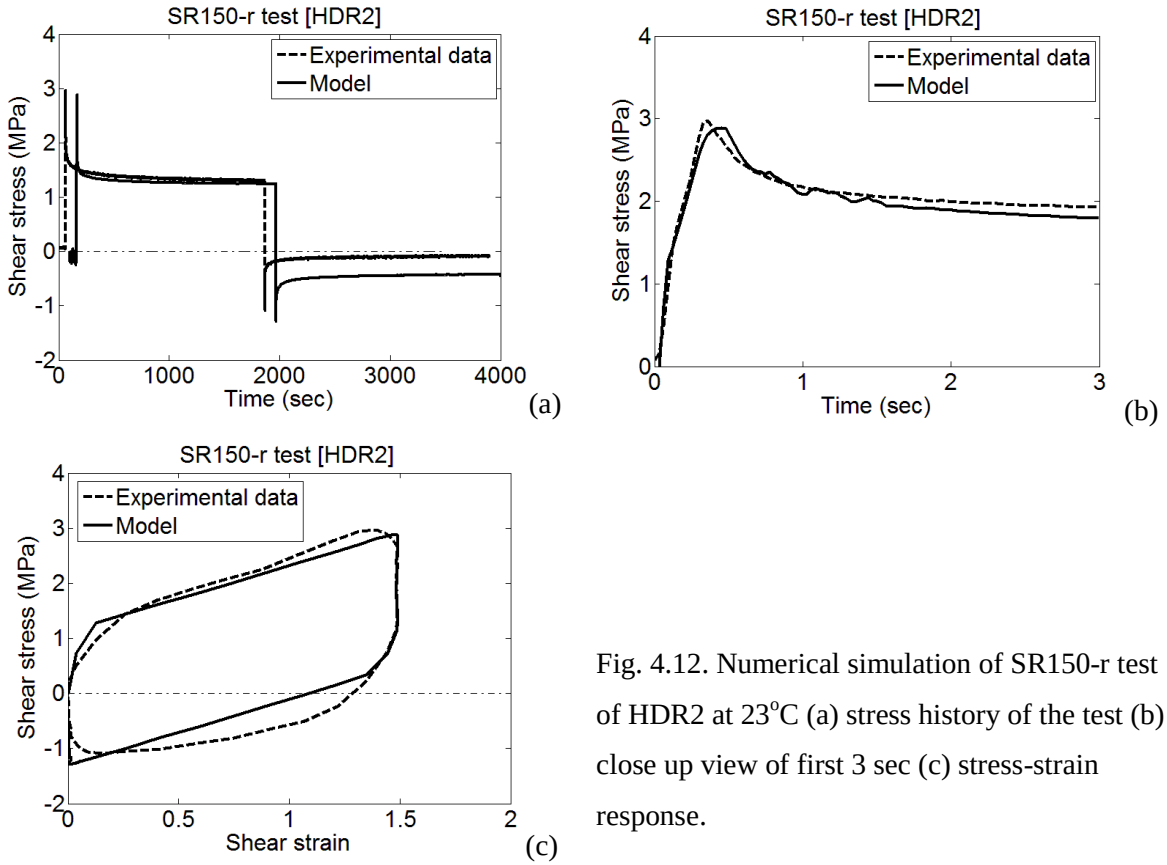

Fig. 4.12. Numerical simulation of SR150-r test of HDR2 at 23°C (a) stress history of the test (b) close up view of first 3 sec (c) stress-strain response.

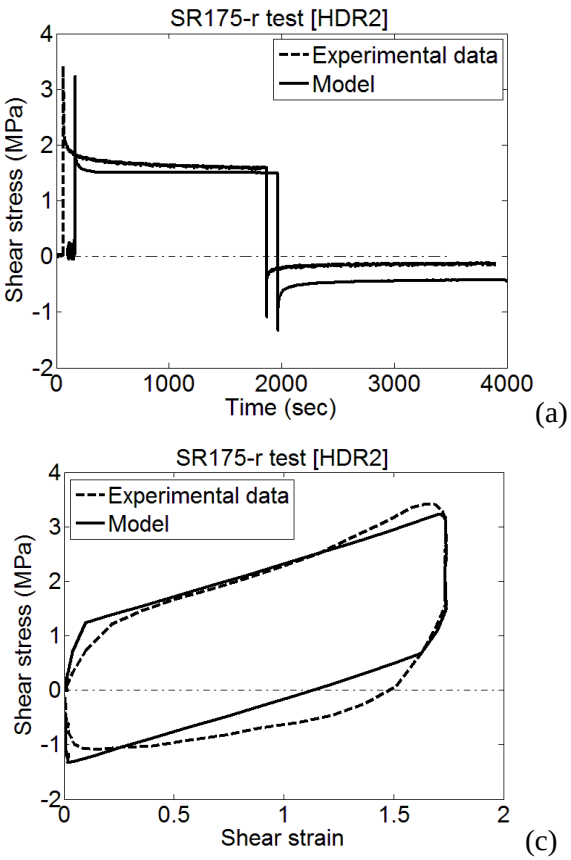

Fig. 4.13. Numerical simulation of SR175-r test of HDR2 at 23^{o}C (a) stress history of the test (b) close up view of first 3 sec (c) stress-strain response.

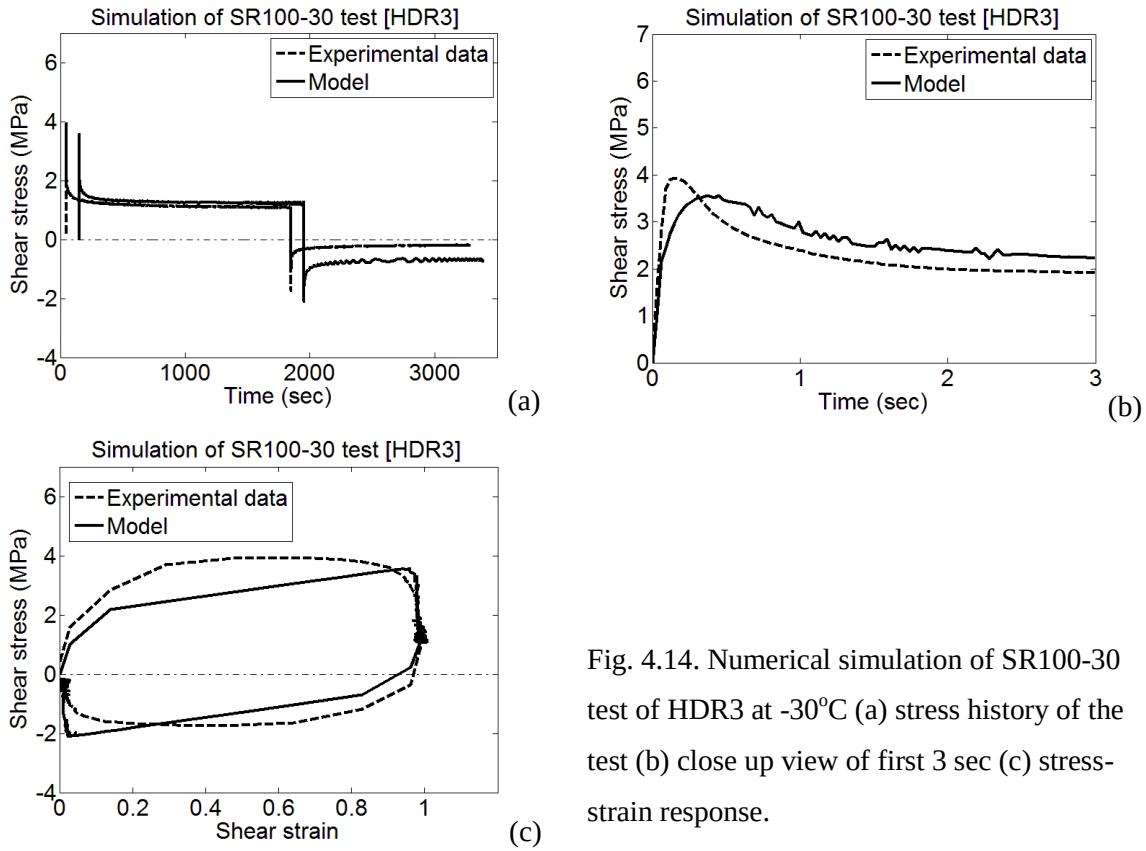

Fig. 4.14. Numerical simulation of SR100-30 test of HDR3 at -30^{o}C (a) stress history of the test (b) close up view of first 3 sec (c) stress-strain response.

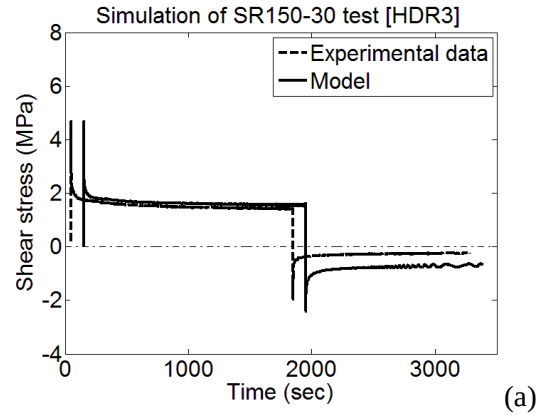

(a)

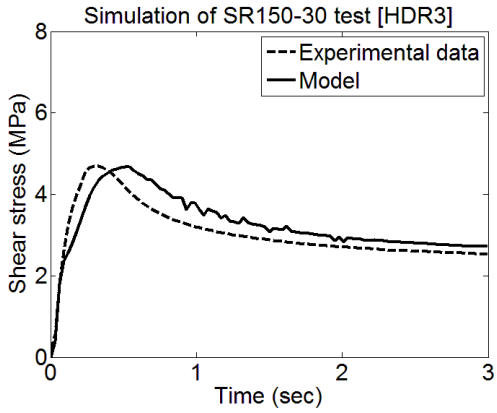

(b)

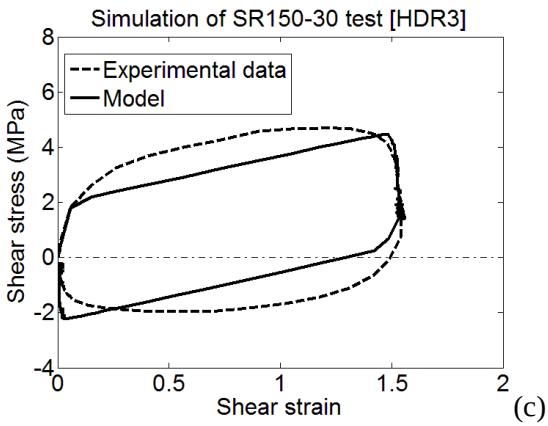

(c)

Fig. 4.15. Numerical simulation of SR150-30 test of HDR3 at -30°C (a) stress history of the test (b) close up view of first 3 sec (c) stress-strain response.

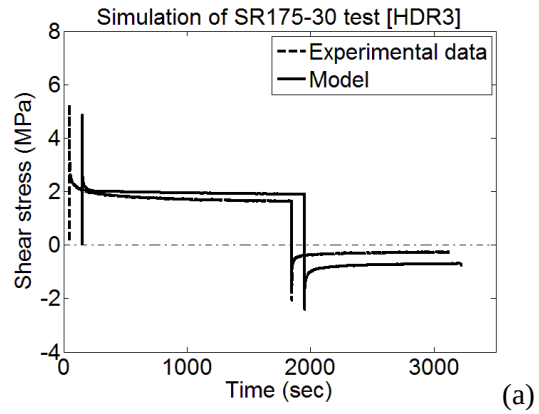

(a)

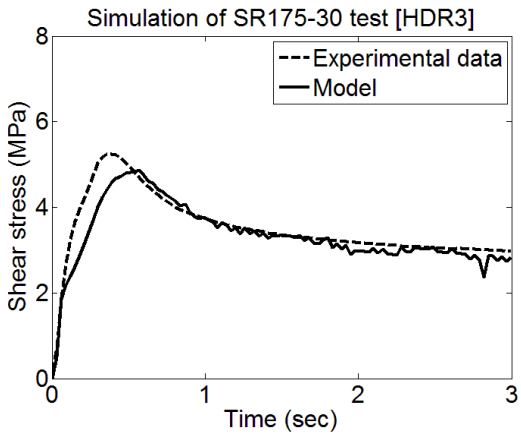

(b)

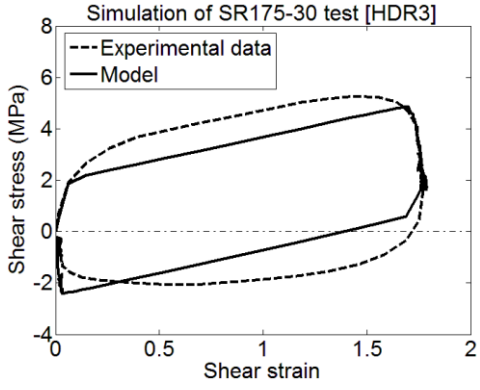

(c)

Fig. 4.16. Numerical simulation of SR175-30 test of HDR3 at -30°C (a) stress history of the test (b) close up view of first 3 sec (c) stress-strain response.

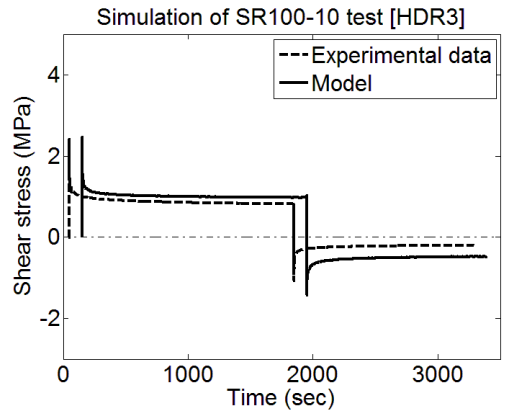

(a)

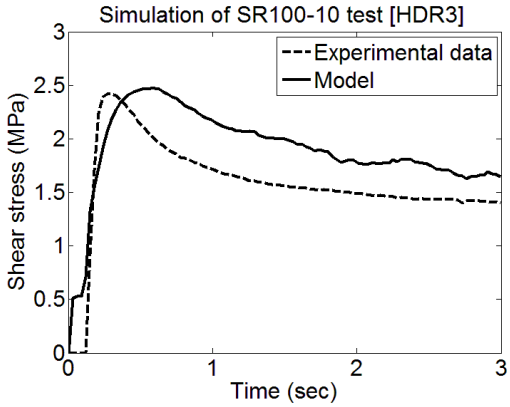

(b)

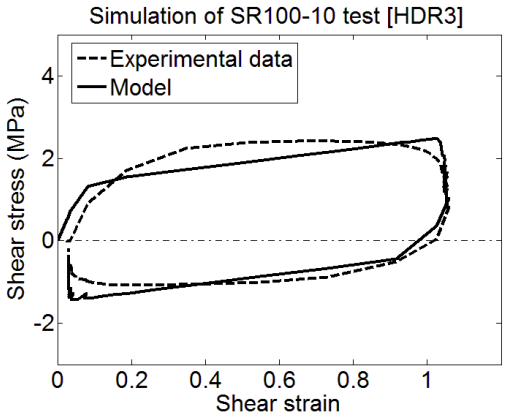

(c)

Fig. 4.17. Numerical simulation of SR100-10 test of HDR3 at -10°C (a) stress history of the test (b) close up view of first 3 sec (c) stress-strain response.

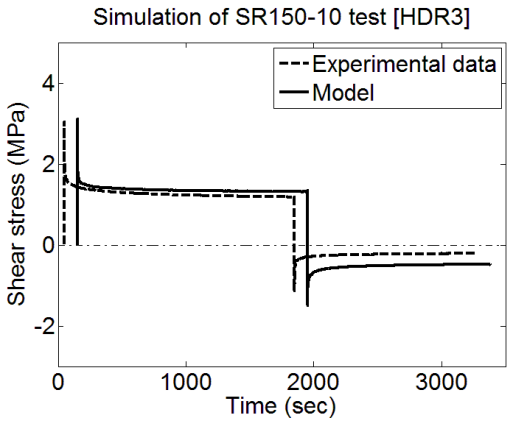

(a)

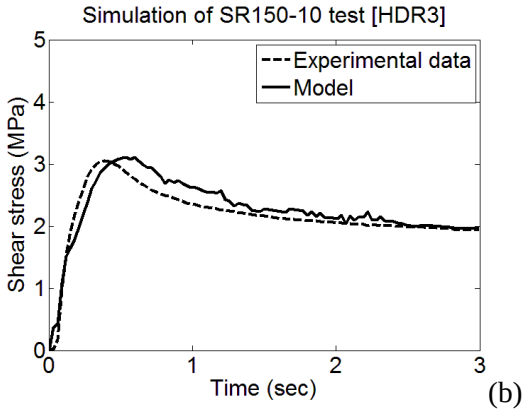

(b)

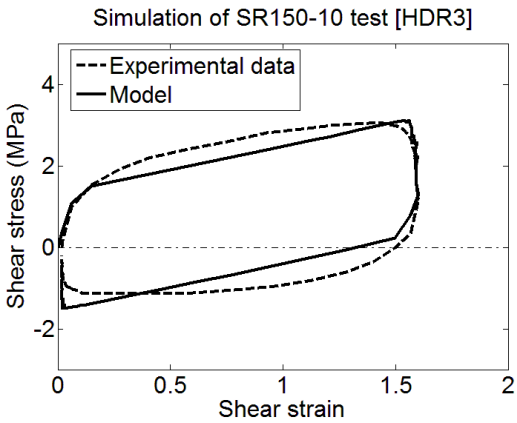

(c)

Fig. 4.18. Numerical simulation of SR150-10 test of HDR3 at -10°C (a) stress history of the test (b) close up view of first 3 sec (c) stress-strain response.

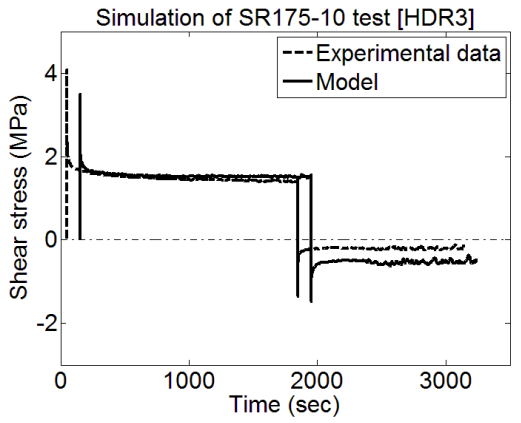

(a)

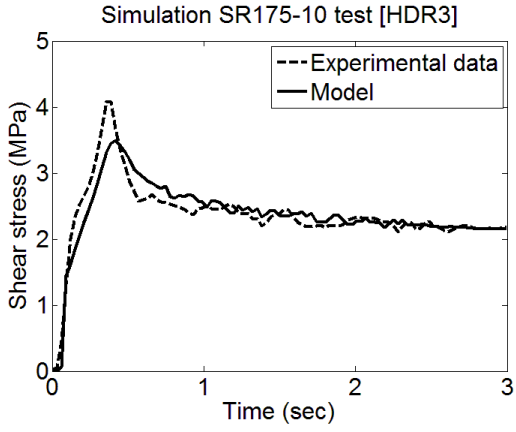

(b)

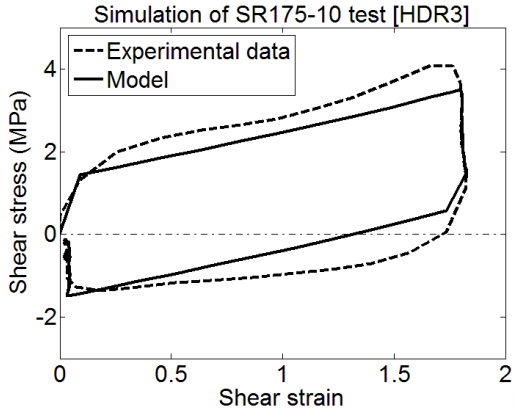

(c)

Fig. 4.19. Numerical simulation of SR175-10 test of HDR3 at -10°C (a) stress history of the test (b) close up view of first 3 sec (c) stress-strain response.

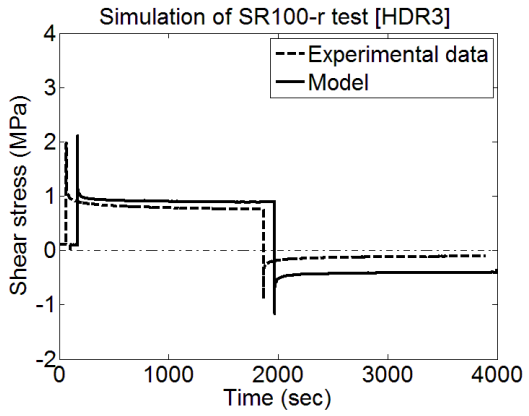

(a)

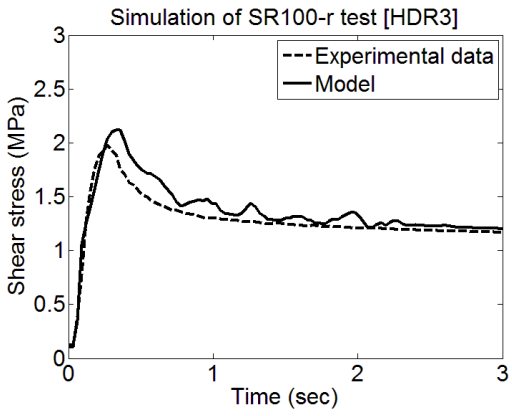

(b)

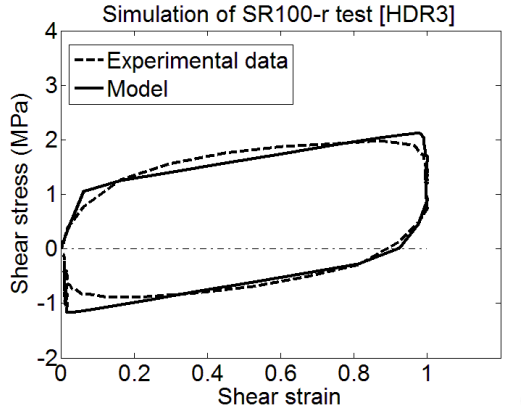

(c)

Fig. 4.20. Numerical simulation of SR100-r test of HDR3 at 23°C (a) stress history of the test (b) close up view of first 3 sec (c) stress-strain response.

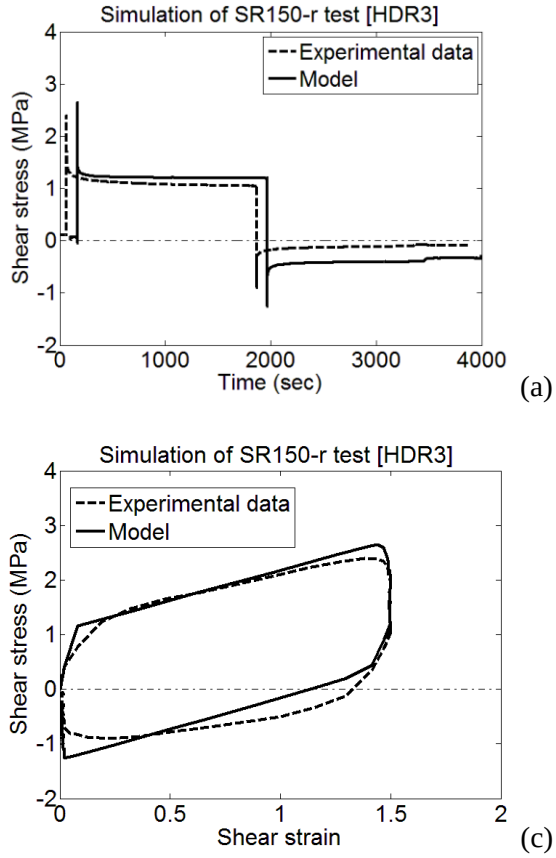

Fig. 4.21. Numerical simulation of SR150-r test of HDR3 at 23^{o}C (a) stress history of the test (b) close up view of first 3 sec (c) stress-strain response.

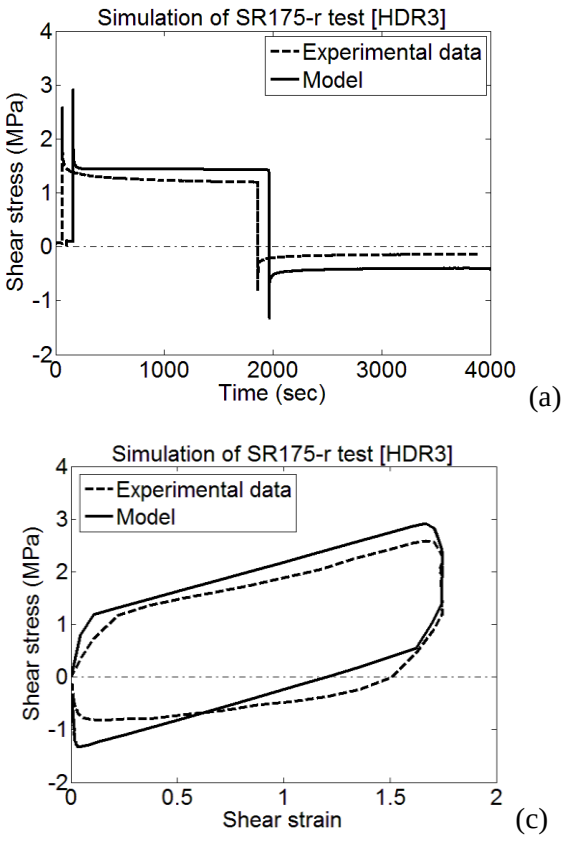

Fig. 4.22. Numerical simulation of SR175-r test of HDR3 at 23^{o}C (a) stress history of the test (b) close up view of first 3 sec (c) stress-strain response.

4.2.2 Cyclic shear tests

Figs. 4.23 to 4.28 present the 1st cycle of stress-strain relationship of CS tests obtained by experimental data and numerical model. Because of the stress-softening phenomena appearing in the 1st cycle of stress-strain responses, there are some difference between the numerical results and the experimental results. However, it is clear that simulation results are close to the experimental data in almost cases.

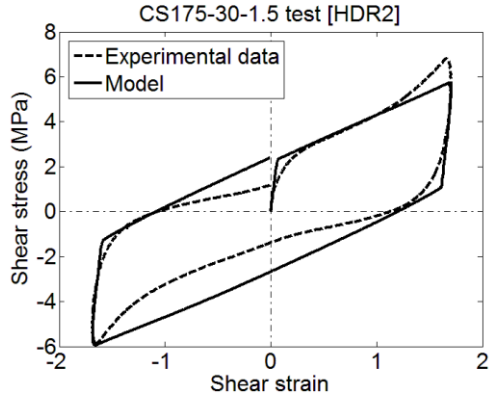

(a)

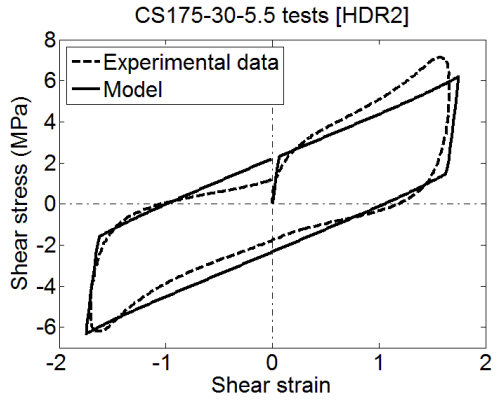

(b)

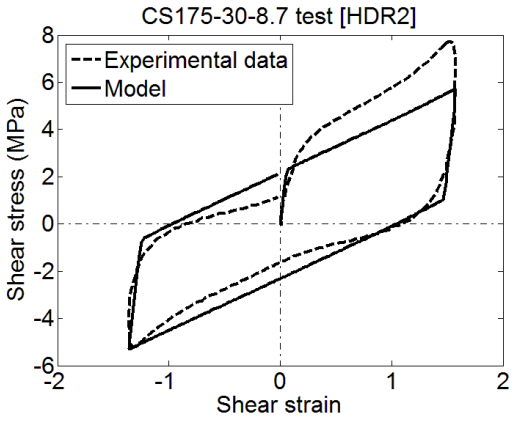

(c)

Fig. 4.23. Numerical simulation of CS-30 tests of HDR2 at (a) 1.5/s (b) 5.5/s (c) 8.75/s.

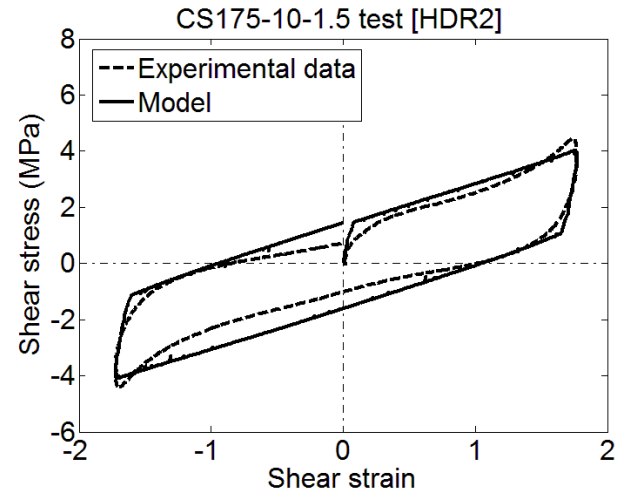

(a)

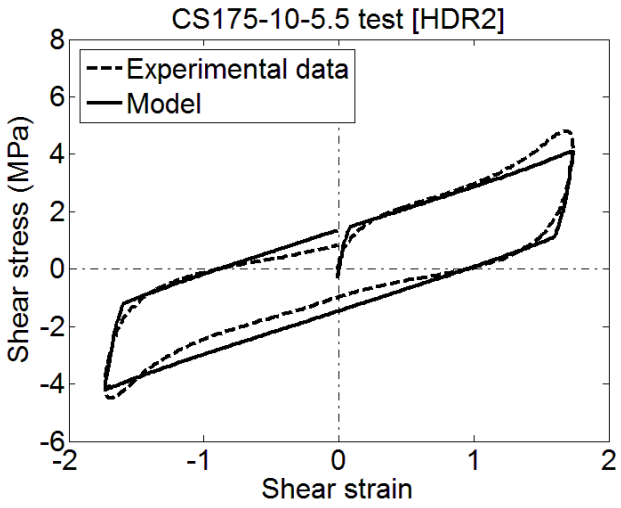

(b)

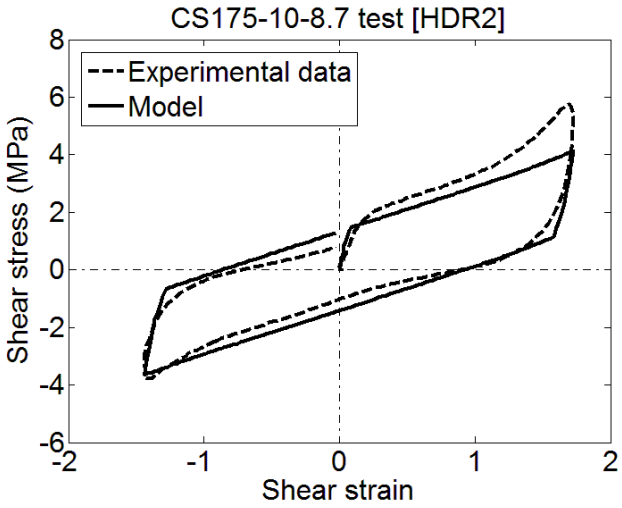

(c)

Fig. 4.24. Numerical simulation of CS-10 tests of HDR2 at (a) 1.5/s (b) 5.5/s (c) 8.75/s.

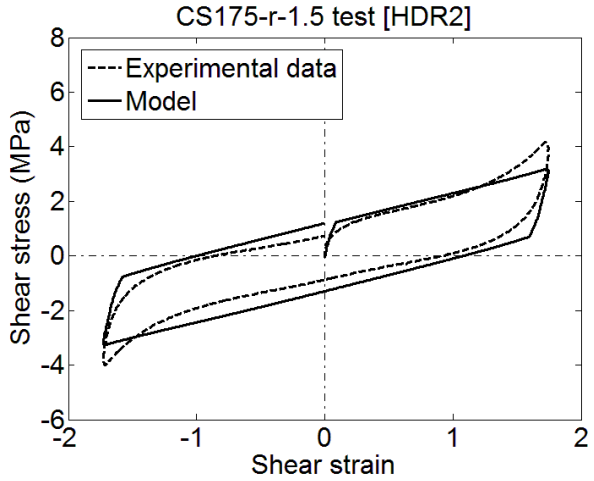

(a)

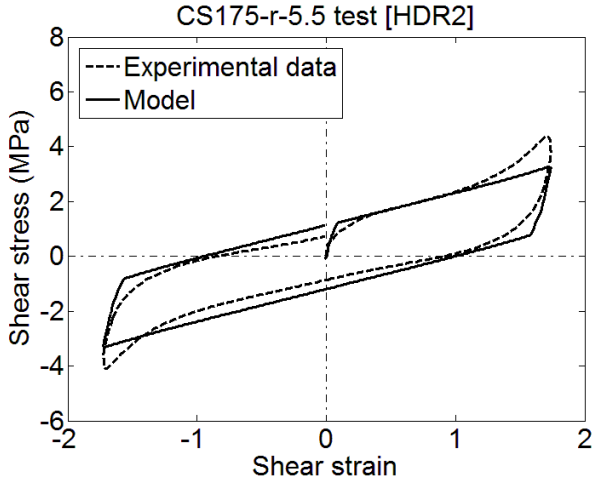

(b)

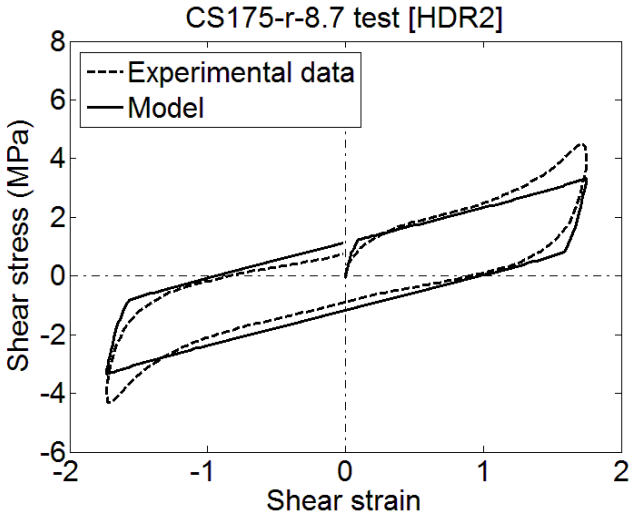

(c)

Fig. 4.25. Numerical simulation of CS-r tests of HDR2 at (a) 1.5/s (b) 5.5/s (c) 8.75/s.

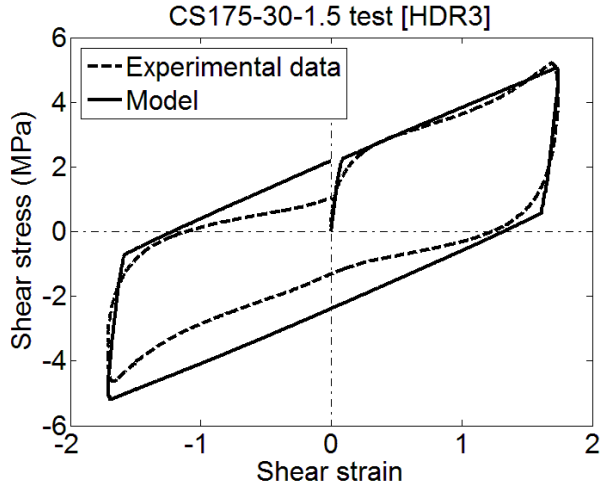

(a)

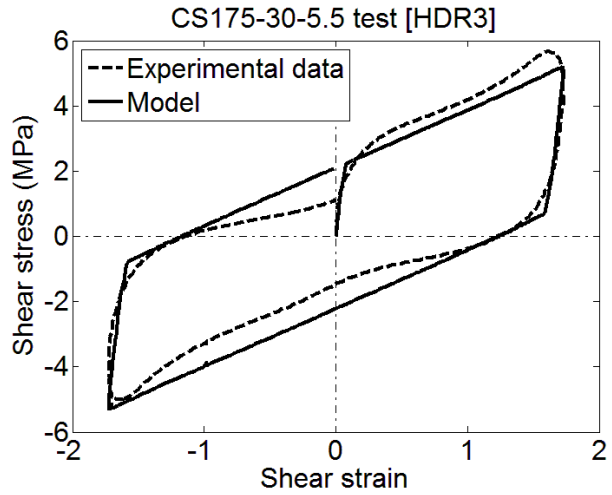

(b)

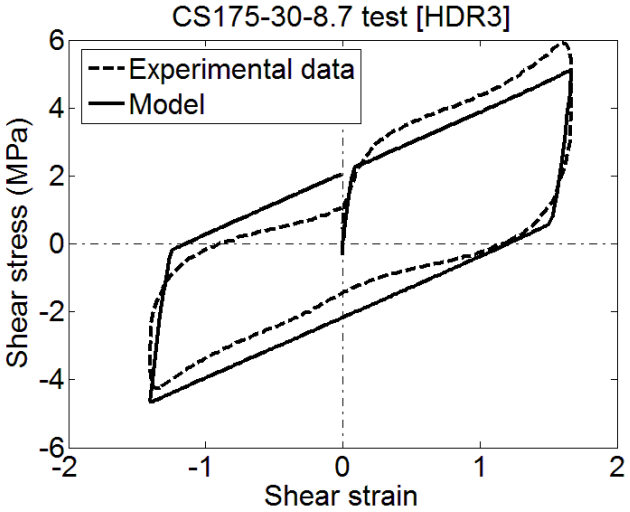

(c)

Fig. 4.26. Numerical simulation of CS-30 tests of HDR3 at (a) 1.5/s (b) 5.5/s (c) 8.75/s.

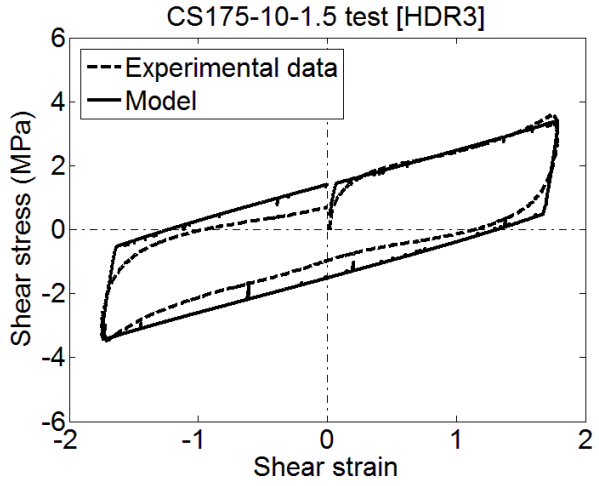

(a)

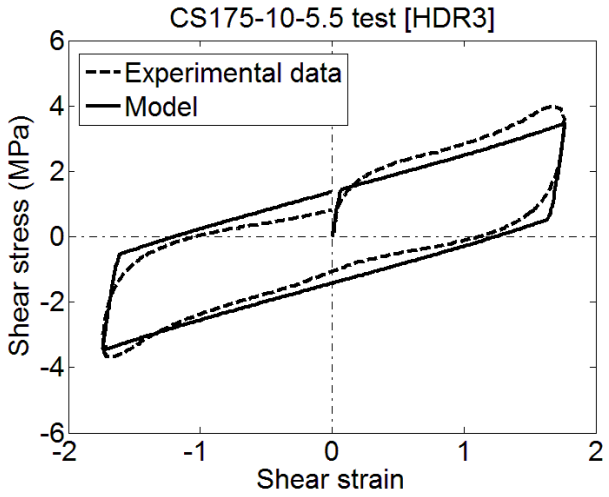

(b)

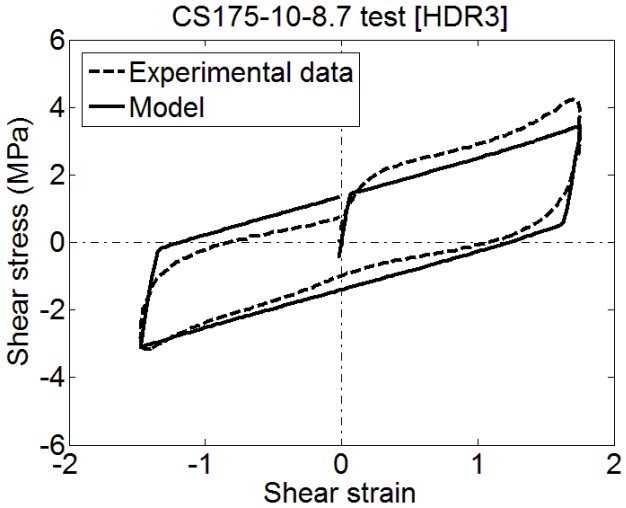

(c)

Fig. 4.27. Numerical simulation of CS-10 tests of HDR3 at (a) 1.5/s (b) 5.5/s (c) 8.75/s.

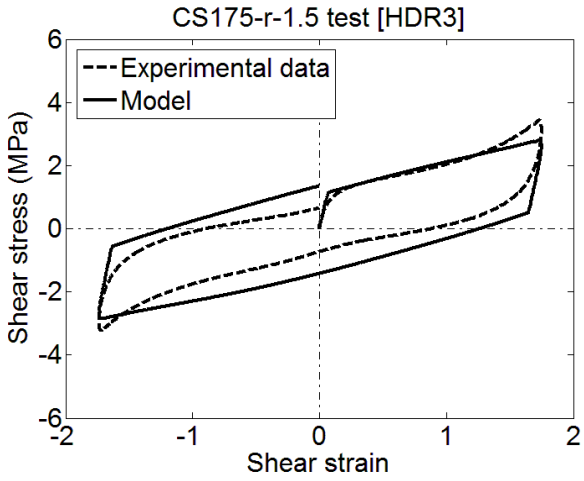

(a)

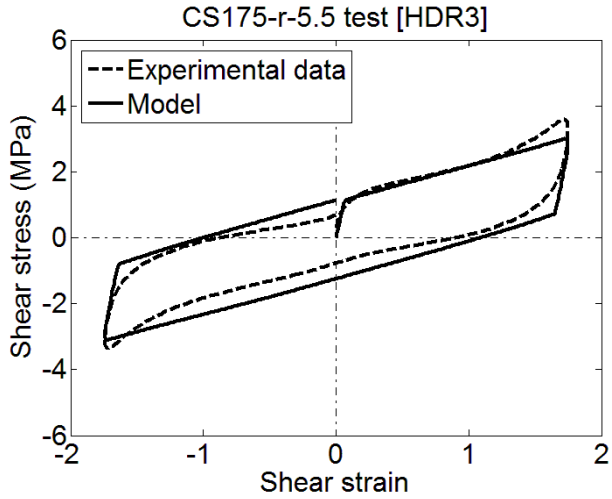

(b)

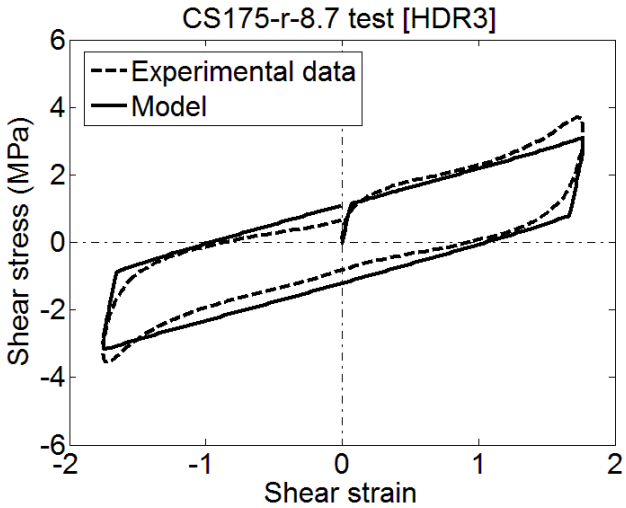

(c)

Fig. 4.28. Numerical simulation of CS-r tests of HDR3 at (a) 1.5/s (b) 5.5/s (c) 8.75/s.

However, Figs. 4.23 to 4.28 show minor discrepancies between experimental and numerical results in terms of energy dissipation and lateral effective stiffness. These discrepancies are presented more clearly by comparing three seismic parameters i.e. energy loss per cycle D, equivalent damping ratio h_{eq} and, equivalent shear modulus G_{eq} defined by

$$h_{eq} = \frac{D}{2\pi W} \tag{4.1}$$

$$G_{eq} = \frac{\tau_{\max} - \tau_{\min}}{\gamma_{\max} - \gamma_{\min}} \tag{4.2}$$

where W is the elastic strain energy, which equals the area of the shaded triangle in Fig. 4.29; $\tau_{\max}$ and $\tau_{\min}$ are the maximum and minimum shear stresses; $\gamma_{\max}$ and $\gamma_{\min}$ are the corresponding shear strains at $\tau_{\max}$ and $\tau_{\min}$, respectively. The differences between experimental and numerical results of HDR3 specimens are compared in Fig. 4.30 and Table 5. The differences of the energy loss per cycle and the equivalent damping ratio are quite clear (Figs. 4.30(a) and 4.30(b)), whereas the equivalent shear modulus obtained from numerical results are closely comparable with the modulus obtained from the experimental results (Fig. 4.30(c)). Such difference also appears in the overstress parameter identification. The difference between experimental and numerical results seems to be caused by the healing of Mullins effect (Amin et al., 2010; Mullins., 1969) occurring in the time interval between the preloading and the actual test. This situation will not exist when the overstress parameters are determined based on a stress-strain relationship obtained from sinusoidal loading tests after several cycles of loading. In that case, self-heating effect (Cardone et al., 2010; Takaoka et al., 1969) should be taken into account. It is the current study of the authors to address self-heating effect. The preliminary result of this topic is presented in Nguyen et al (2013). Moreover, the difference between experimental data and simulation results has been discussed in the chapter 6. However, the ability of the proposed model for representing the rate-dependent behavior induced by viscosity property of HDRBs is verified by the simulations of relaxation tests. This ability remarkably affects the accuracy of the model in predicting the structures' seismic performance with HDRBs, especially in designing isolation structures in seismically active cold areas.

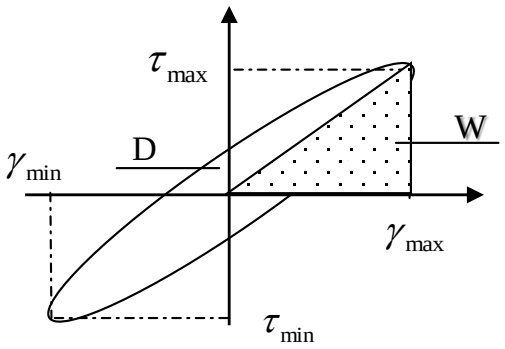

Fig. 4.29. Hysteresis loop in the stress-strain curve of rubber bearings under cyclic loading.

Table 4.1. Comparison between experimental and numerical results in terms of the energy loss per cycle D, equivalent damping ratio h_B, and equivalent shear modulus G for HDR3 specimen.

Temperature	Strain rate (1/s)	D (MJ/m^3)		h_{eq}		G_{eq} (MPa)		ΔD (%)	Δh_{eq} (%)	ΔG_{eq} (%)
		Test	Model	Test	Model	Test	Model			
-30°C	1.5	11.1	14.8	0.20	0.27	2.94	2.99	24.9	25.2	1.88
	5.5	12.7	14.3	0.22	0.25	3.28	3.05	10.7	12.2	7.20
	8.75	11.2	12.4	0.19	0.23	3.43	3.19	9.83	19.5	7.04
-10°C	1.5	7.61	9.80	0.19	0.26	2.08	1.95	22.4	27.2	6.20
	5.5	8.67	9.41	0.21	0.26	2.28	2.04	7.82	20.4	10.2
	8.75	7.79	8.53	0.17	0.22	2.36	2.04	8.64	23.6	13.6
23°C	1.5	5.87	8.42	0.16	0.28	1.93	1.64	30.3	43.1	15.1
	5.5	6.28	7.80	0.16	0.24	2.02	1.77	19.6	32.7	12.1
	8.75	6.72	7.73	0.17	0.23	2.08	1.79	13.1	26.8	14.1

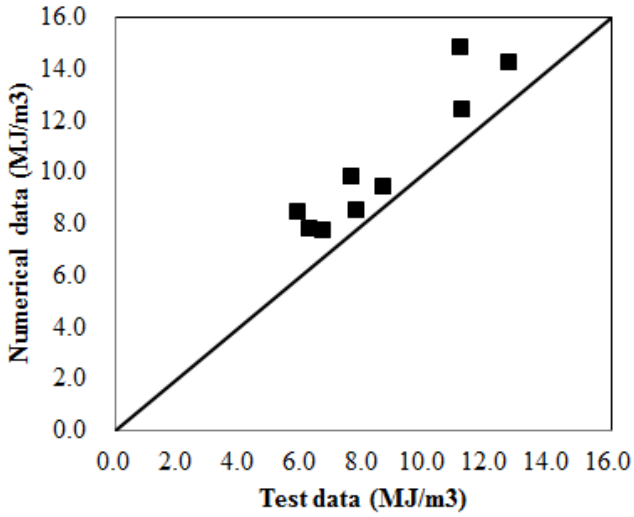

(a)

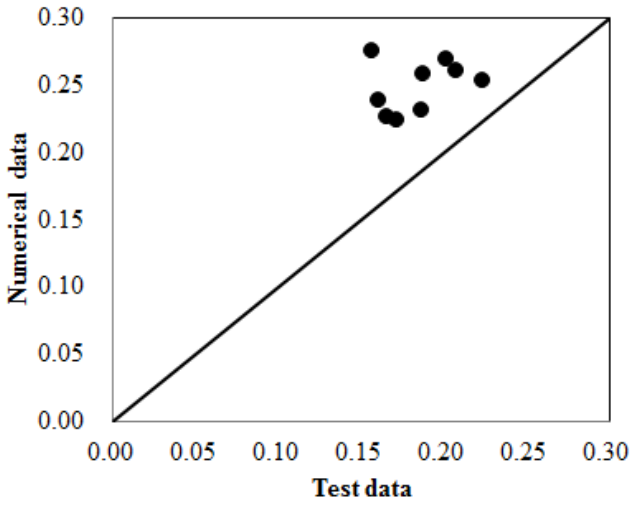

(b)

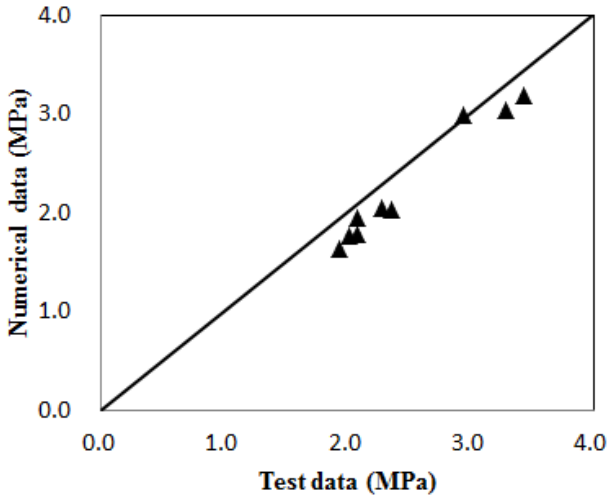

(c)

Fig. 4.30. Comparison between experimental and numerical results (a) dissipated energy per cycle (b) equivalent damping ratio (c) equivalent shear modulus.

Figs. 4.31 and 4.32 are finally devoted to give further evidences to describe the capability of the proposed model in representing the rate-dependent behavior of HDRBs by simulating CS responses at slow for fast strain rates at different temperatures using the identified parameters. The model has produced logical results in each of the cases, indicating its inherent promises at the design desk.

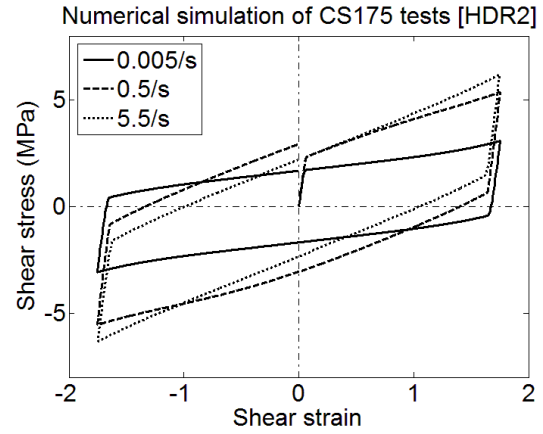

(a)

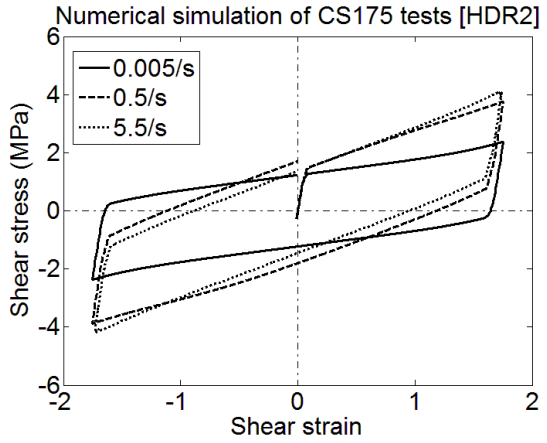

(b)

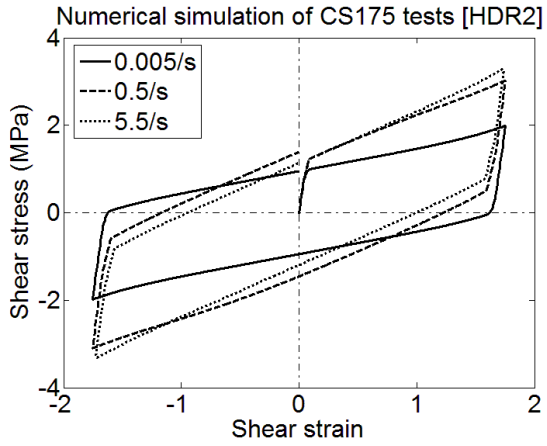

(c)

Fig. 4.31. Shear stress-strain relationships obtained from numerical simulation of CS175 tests of HDR2 at (a) -30^{o}C (b) -10^{o}C (c) 23^{o}C.

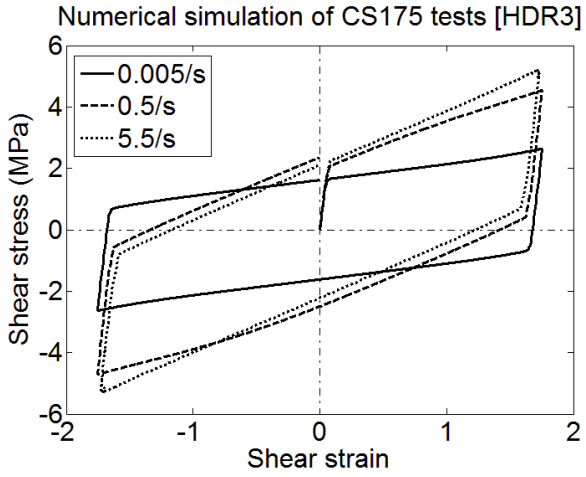

(a)

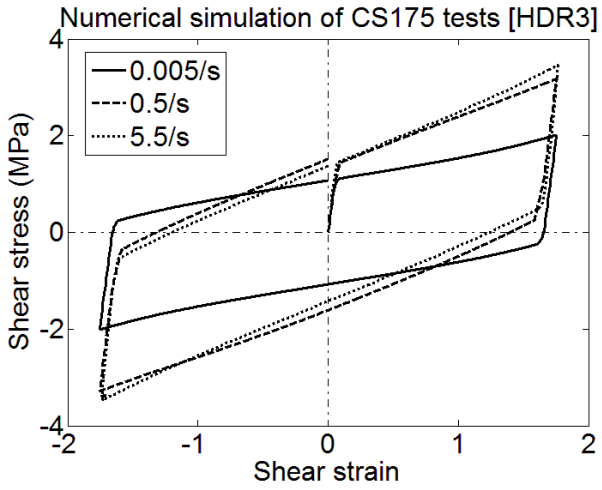

(b)

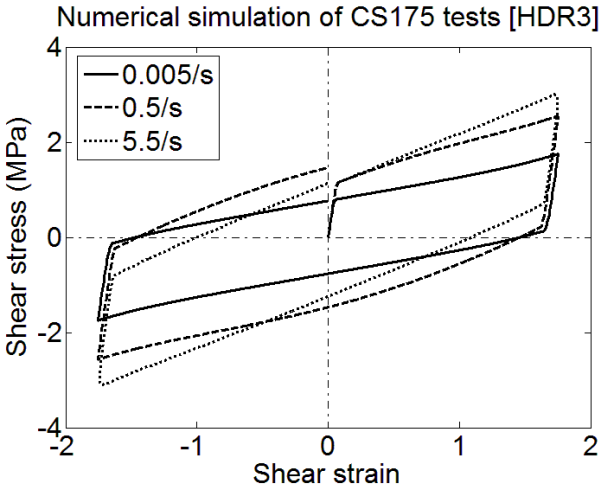

(c)

Fig. 4.32. Shear stress-strain relationships obtained from numerical simulation of CS175 tests of HDR3 at (a) -30°C (b) -10°C (c) 23°C.

4.3 Summary

A series of numerical simulations of the experimental data were conducted to verify the adequacy of the proposed rheology model. The numerical simulation results of relaxation tests (SR tests and MSR tests), and cyclic shear tests describe the capability of the proposed model in reproducing the mechanical behavior of HDRBs. The model effectively simulates the experimental data in all cases at both room and low temperatures.

The numerical simulation results of CS responses at slow and fast strain rates present the ability of the model to logically reproduce the rate-dependent behavior of HDRBs, and its inherent promises at the design desk. However, a detail comparison between experimental data and simulation results of the first cycle of Sin tests points out the existence of some differences, especially at low temperatures. These differences may be caused by self-heating effect.

CHAPTER 5
SELF-HEATING OF HIGH DAMPING RUBBER BEARINGs

5.1 General

On the basis of the experimental observations in Chapter 2, a rheology model is proposed to describe the mechanical behavior of HDRBs in Chapter 3. The model is verified by simulating relaxation and cyclic loading tests in Chapter 4. In order to minimize the self-heating effect on the overstress parameter identification, the first cycle of the sinusoidal loading test is employed. However, the stress-strain relationship in the first cycle is different from that in the other cycles of the sinusoidal loading tests due to the stress-softening phenomenon. When the parameters are determined based on a stress-strain relationship obtained from sinusoidal loading tests after several cycles of loading to avoid the phenomenon, self-heating effect should be taken into account. This chapter is devoted to investigate the self-heating effect on the mechanical characteristics of HDRBs under sinusoidal loading at room and low temperatures.

5.2 Specimens and test conditions

The test set-up of the experiments in this chapter is same as the test set-up in Chapter 2. All specimens used in this investigation are type-A in Fig. 2.1. The rubber bearing tests were carried out by Japan Rubber Bearing Association in an environmental test chamber at -30°C, -20°C, and 23°C ambient temperatures. In order to remove stress-softening due to Mullins effect, all specimens were preloaded before the actual tests. The temperatures in the specimens were measured with thermocouples. The positions of temperature measurement in the central section are shown in Fig. 5.1. The tests consisted of eleven sinusoidal loading cycles at 1.75 strain level and frequency of 0.5 Hz shown in Fig. 5.2. Although the target strain level is 1.75, the actual strain level of few first cycles is smaller than this value such as the strain level of first cycles of the tests carried out at -30°C and -20°C shown in Fig. 5.2(a) and (b).

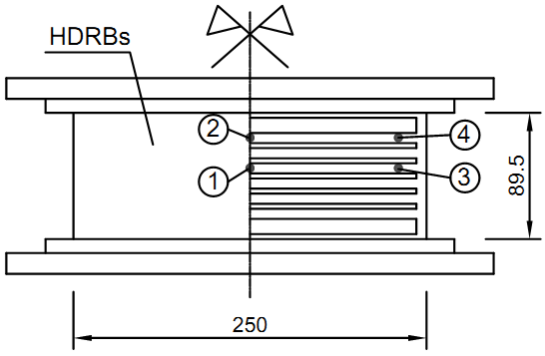

Fig. 5.1. Measure points of temperatures

5.3 Effect of inside temperature of HDRBs on their mechanical characteristics under sinusoidal loading

Fig. 5.3 (a) to (c) show the shear stress-strain relationships obtained from the sinusoidal loading tests at different ambient temperatures. It is obvious that the 1st cycle is different from the other cycles of the sinusoidal loading tests, and this difference is larger at the lower ambient temperatures.

The measured temperatures inside the specimens and the cumulative dissipated energy density are presented in Fig. 5.4. The cumulative dissipated energy density up to j^{th} cycle is calculated from

$$D = \sum_{i=1}^{j} D_i \tag{5.1}$$

where D_i is the dissipated energy density of the i^{th} cycle, and D_i can be calculated from the enclosed area of a stress-strain hysteresis loop for the ith cycle.

Fig. 5.4 shows that the temperatures in the bearings are increased by cyclic loading. The rise in the inside temperature and the cumulative dissipated energy are larger at lower ambient temperatures.

Assuming that all dissipated energy is converted into the heat energy, the temperature increase ΔT in a sinusoidal test is estimated from the dissipated energy density under the adiabatic condition for only rubber part:

$$DV_r = C_{pr} m_r \Delta T \tag{5.2}$$

where C_{pr} is the specific heat of rubber; m_r and V_r are the mass and volume of rubber, respectively.

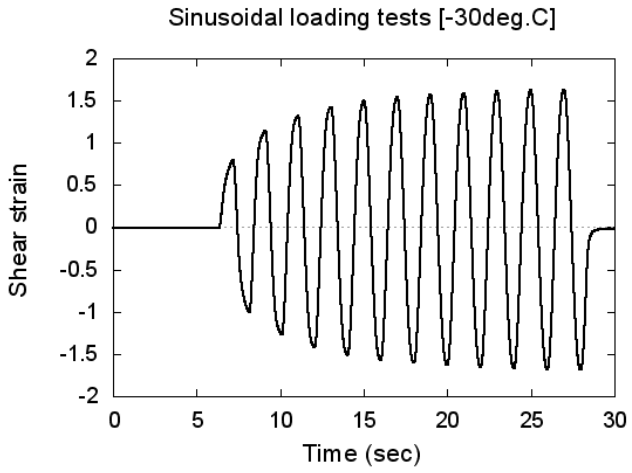

(a)

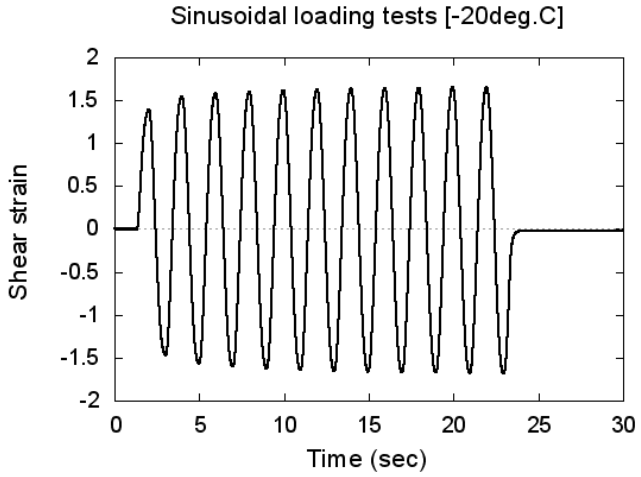

(b)

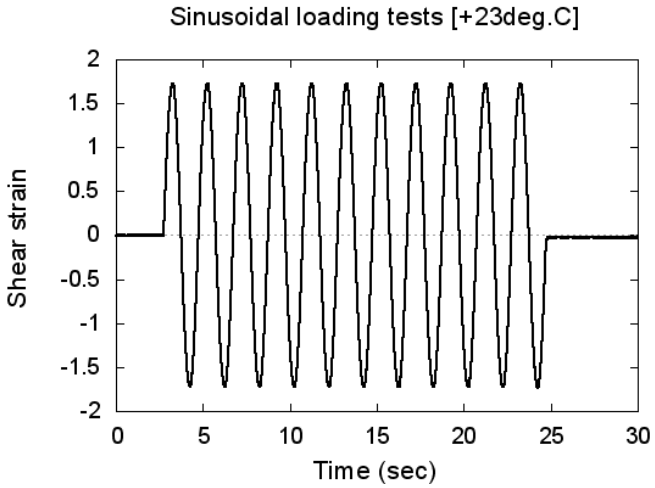

(c)

Fig. 5.2. Strain history applied in sinusoidal loading tests at (a) -30^{o}C (b) -20^{o}C (c) 23^{o}C

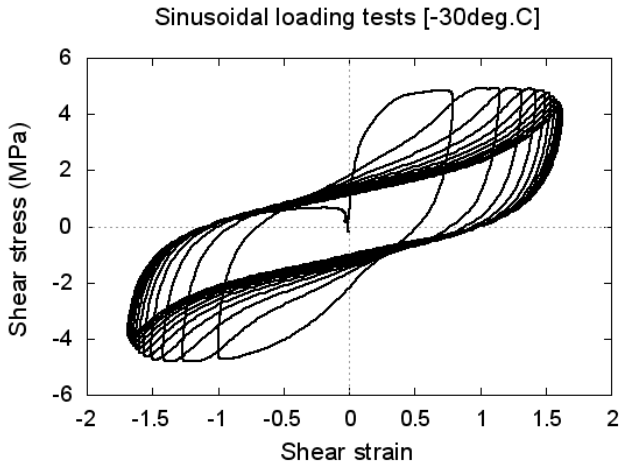

(a)

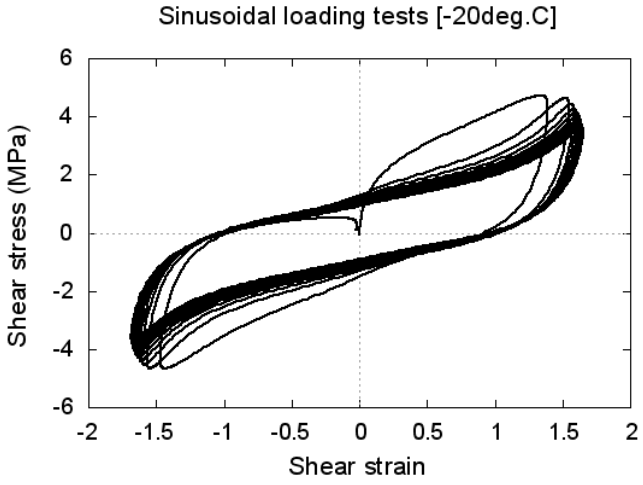

(b)

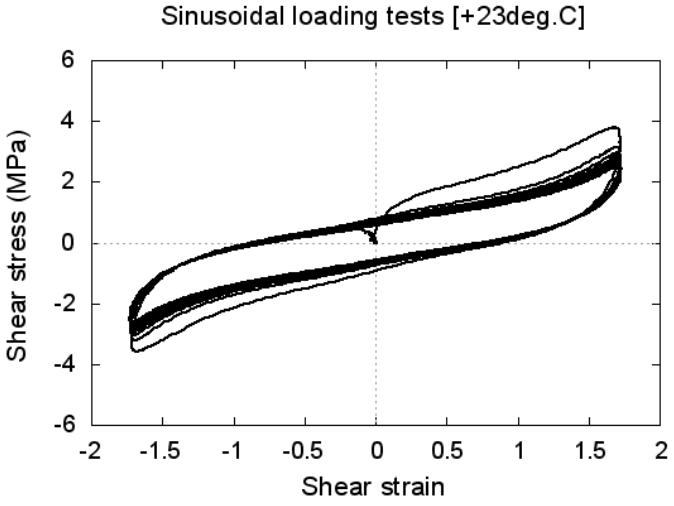

(c)

Fig. 5.3. Stress-strain relationships obtained from sinusoidal tests at (a) -30^{o}C (b) -20^{o}C (c) 23^{o}C

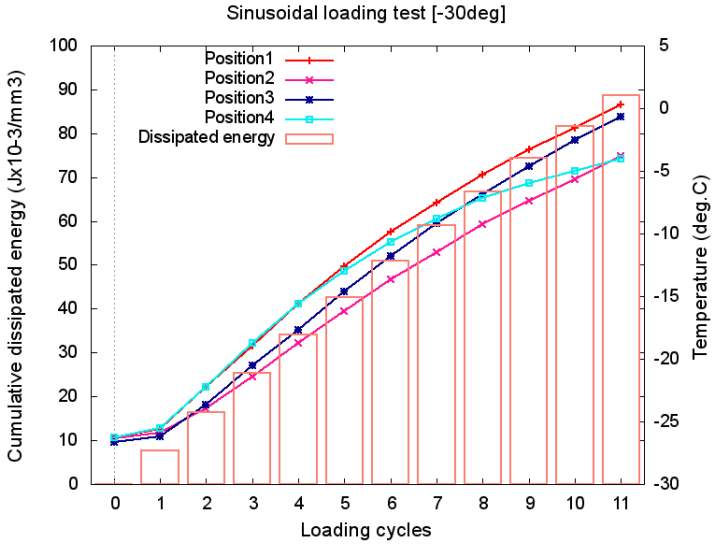

(a)

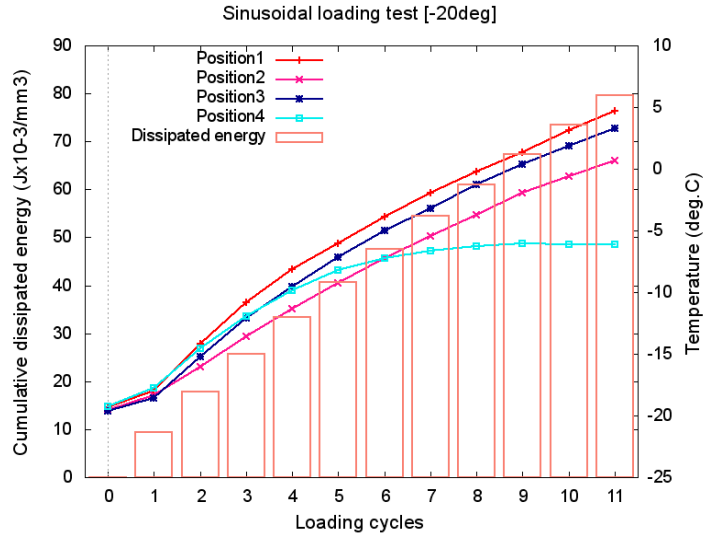

(b)

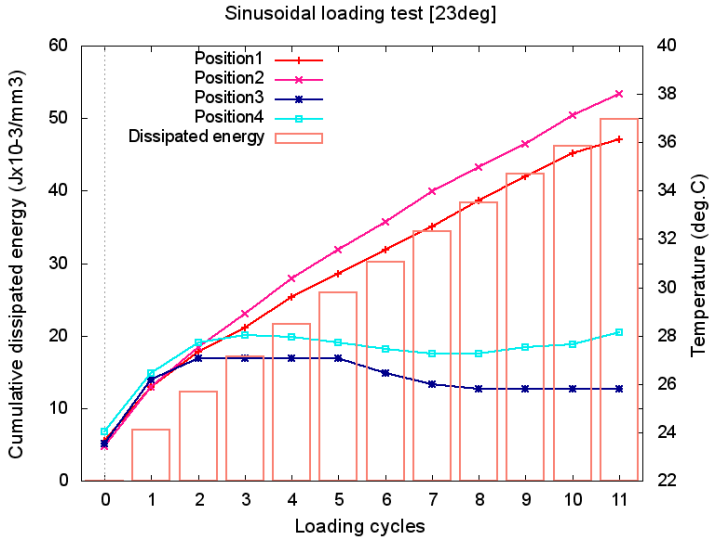

(c)

Fig.5.4. Cumulative dissipated energy and temperatures inside the bearings at ambient temperatures (a) -30°C (b) -20°C (c) 23°C.

On the other hand, considering a rubber bearing as composite of steel and rubber, and assuming that the temperature increases in the rubber and steel are the same, the temperature increase can be estimated from

$$DV_r = \left[C_{pr} f + C_{ps}(1-f)\right] m_r \Delta T \qquad (5.3)$$

where C_{ps} is the specific heat of steel; $m=m_r+m_s$ stands for the total mass; m_s is the mass of steel; $f = m_r / m$ is the mass fraction of rubber.

In this calculation, the specific heats for rubber and steel are assigned to C_{pr} = 1.732 J/g.K, and C_{ps} = 0.432 J/g.K, respectively (Uruta et al., 2004). The estimated temperatures are higher than the measured temperatures as shown in Fig. 5.5, because the some amount of heat transfers from the specimen to the ambient environment in the actual tests.

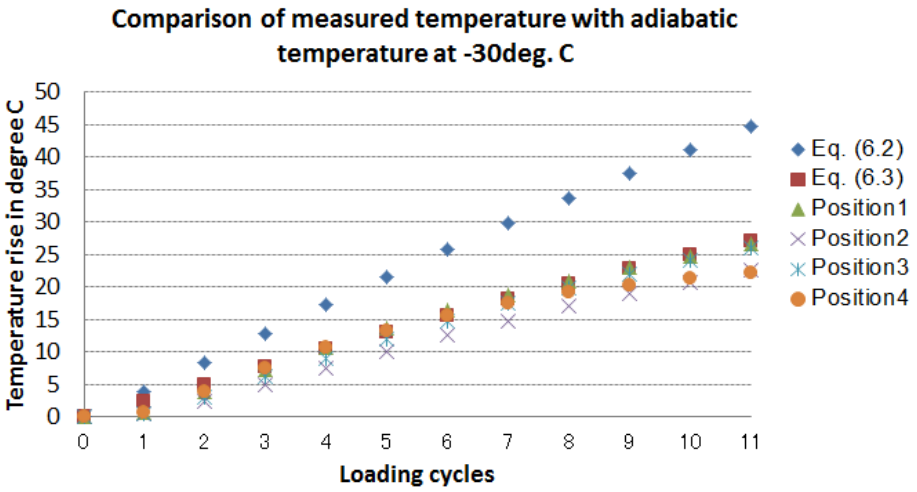

Fig.5.5. Comparison of measured temperature with theoretical temperature at -30°C ambient temperature.

Fig. 5.6 presents the stress-strain relationships obtained from a loading cycle with the same inside temperatures in position 1 but different ambient temperatures. HDRBs with the same inside temperatures exhibit the identical stress-strain curves in these figures. It means that the stress-strain relationships of HDRBs are governed by the inside temperatures, but not by the ambient temperature. Therefore, a seismic model for HDRBs at low temperatures should be based on the inside temperatures.

A detail comparison between experimental data and simulation results by the proposed model in Chapter 3 points out the existence of some obvious difference in the 1st cycle of

sinusoidal loading tests in Fig. 3.8 and 3.9. This difference is caused by self-heating effect. Therefore, the overstress parameters of the proposed model should be determined based on a stress-strain cycle obtained from sinusoidal loading tests after several cycles of loading. Meanwhile, the design temperature of the model is chosen to be the inside temperature of the bearings in the selected cycle of the sinusoidal loading tests.

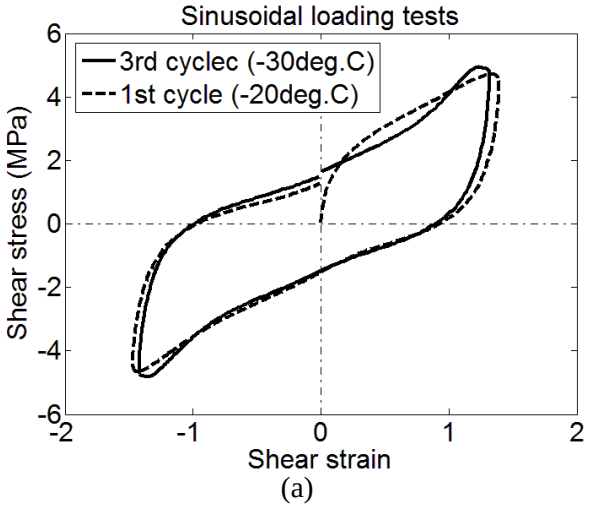

(a)

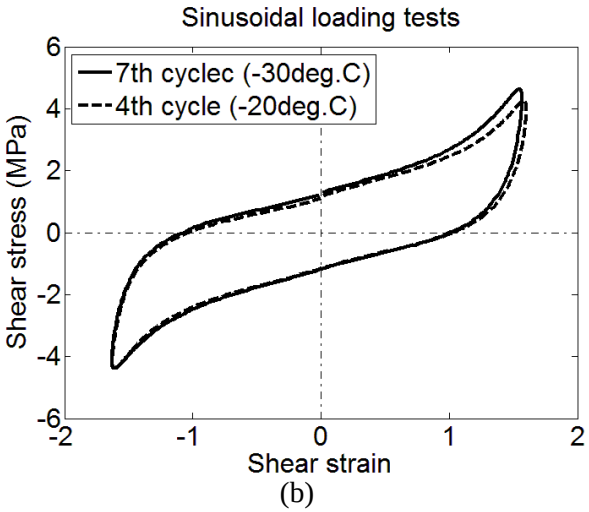

(b)

Fig. 5.6. Stress-strain relationships obtained at the same inside temperatures (a) -20°C (b) -10°C

Fig. 5.7 presents the inside temperature dependence of stress-strain relationship of HDRBs. It is clear that the area of hysteresis loop and the strain hardening of HDRBs increase with decreasing inside temperatures.

The shear modulus G_{eq} and the damping constant h_{eq} are calculated from the experimental results, G_{eq} and h_{eq} are defined in Eqs. 4.1 & 4.2.

The values of G and h_B at different inside temperatures are shown in Fig. 5.8. While the inside temperature increases from -22°C to 35°C, G and h_B decrease 180% and 79%, respectively. It is clear that these parameters are significantly affected by the inside temperature variations.

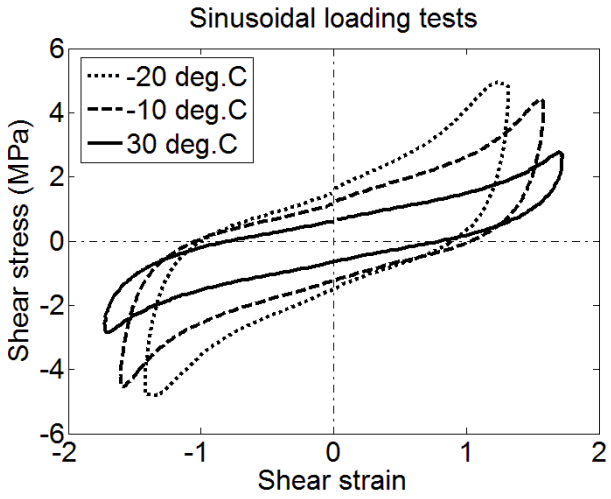

Fig.5.7. Stress-strain relationships of sinusoidal loading tests at different inside temperatures.

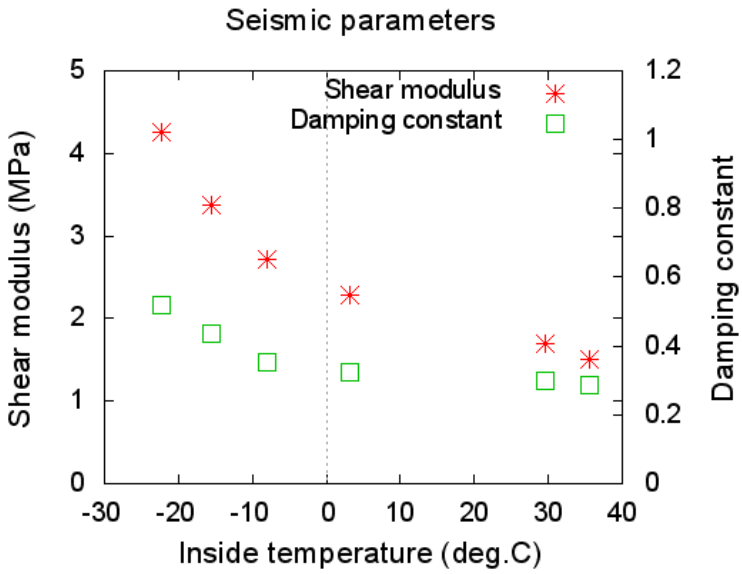

Fig.5.8. Temperature dependence of shear modulus and damping constant

5.4 Effect of self-heating on the design practice

5.4.1 Seismic analysis of single degree of freedom (SDOF) system

In order to investigate the effect of self-heating in the design practice, a seismic analysis of SDOF system is conducted to predict the seismic responses at the top of HDRBs then the dissipated energy under earthquakes can be calculated. On the basis of the dissipated energy, the temperature rise inside HDRBs under earthquakes can be obtained by Eq. (5.3). The SDOF system describes a bridge superstructure supported by an isolation bearing on a rigid foundation. The analytical model of a SDOF system is presented in Fig. 5.9.

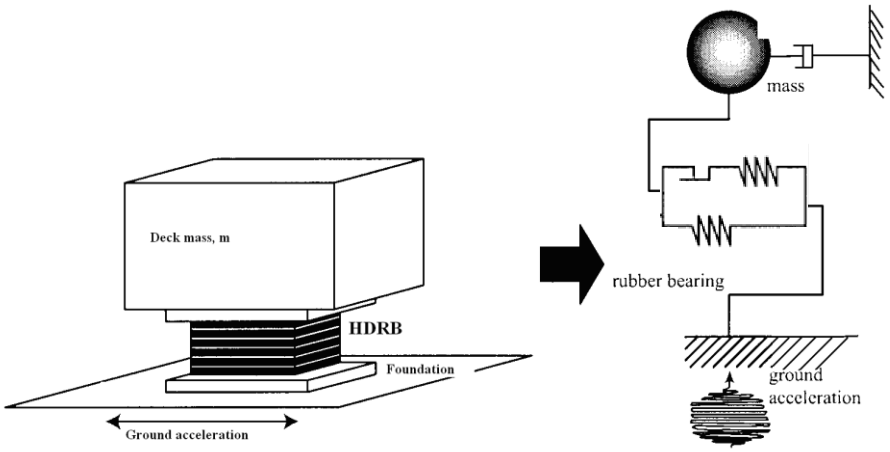

Fig. 5.9. Analytical model of a SDOF system

5.4.1.1 Motion equation and time-stepping procedure

The equation of motion at the mass point as

$$m\ddot{u} + c\dot{u} + f_b = p \tag{5.4}$$

where m and c are the mass and damping coefficient of the superstructure, respectively. f_b is the force of the bearing, p is an external force. u is displacement at the top of bearing. The equation of motion at the time i+1 step

$$\left(\hat{f}_S\right)_{i+1} = p_{i+1} \tag{5.5}$$

where $$\left(\hat{f}_S\right)_{i+1} = m\ddot{u}_{i+1} + c\dot{u}_{i+1} + \left(f_b\right)_{i+1} \tag{5.6}$$

The objective is to determine u_{i+1}, $\dot{u}_{i+1}$, $\ddot{u}_{i+1}$ at time i+1 step.

The bearing force is a function of displacement. Thus, we can adapt the Taylor series expansion for Eq. (5.6), interpret $\left(\hat{f}_S\right)_{i+1}$ as a function of u_{i+1} as

$$\left(\hat{f}_S\right)_{i+1}^{(j+1)} \approx \left(\hat{f}_S\right)_{i+1}^{(j)} + \frac{\partial \hat{f}_S}{\partial u_{i+1}} \Delta u^{(j)} = p_{i+1} \tag{5.7}$$

where $\Delta u^{(j)} = u_{i+1}^{(j+1)} - u_{i+1}^{(j)}$

Differentiating Eq. (5.7) at the known displacement $u_{i+1}^{(j)}$ to define the tangent stiffness

$$\left(\hat{k}_T\right)_{i+1}^{(j)} = \frac{\partial \hat{f}_S}{\partial u_{i+1}} = m\frac{\partial \ddot{u}}{\partial u_{i+1}} + c\frac{\partial \dot{u}}{\partial u_{i+1}} + \frac{\partial f_b}{\partial u_{i+1}} \tag{5.8}$$

The difference between the external force p_{i+1} and $\left(\hat{f}_S\right)_{i+1}^{(j)}$ is defined as the residual force $R_{i+1}^{(j)}$

$$R_{i+1}^{(j)} = p_{i+1} - \left(\hat{f}_S\right)_{i+1}^{(j)} = \left(\hat{k}_T\right)_{i+1}^{(j)} \Delta u^{(j)} \tag{5.19}$$

Newmark developed a family of time-stepping methods based on the following equations

$$u_{i+1} = u_i + (\Delta t)\dot{u}_i + (0.5-\beta)\Delta t^2 \ddot{u}_i + \beta \Delta t^2 \ddot{u}_{i+1} \tag{5.10}$$

$$\dot{u}_{i+1} = \dot{u}_i + (1-\gamma)\Delta t \ddot{u}_i + (\gamma \Delta t)\ddot{u}_{i+1} \tag{5.11}$$

From Eq. (5.10), $\ddot{u}_{i+1}$ can be expressed in terms of u_{i+1}

$$\ddot{u}_{i+1} = \frac{1}{\beta \Delta t^2}\left(u_{i+1} - u_i\right) - \frac{1}{\beta \Delta t}\dot{u}_i - \left(\frac{1}{2\beta} - 1\right)\ddot{u}_i \tag{5.12}$$

Substitute Eq. (5.12) into Eq. (5.11), $\dot{u}_{i+1}$ can be expressed in terms of u_{i+1}

$$\dot{u}_{i+1} = \frac{\gamma}{\beta \Delta t}\left(u_{i+1} - u_i\right) + \left(1 - \frac{\gamma}{\beta}\right)\dot{u}_i + \Delta t\left(1 - \frac{\gamma}{2\beta}\right)\ddot{u}_i \tag{5.13}$$

To differentiate Eq. (5.12) and (5.13)

$$\begin{cases} \dfrac{\partial \ddot{u}}{\partial u_{i+1}} = \dfrac{1}{\beta \Delta t^2} \\ \dfrac{\partial \dot{u}}{\partial u_{i+1}} = \dfrac{\gamma}{\beta \Delta t} \end{cases} \tag{5.14}$$

Substitute Eq. (5.14) into Eq. (5.8) to obtain the tangent stiffness $\left(\hat{k}_T\right)_{i+1}^{(j)}$

$$\left(\hat{k}_T\right)_{i+1}^{(j)} = \frac{1}{\beta \Delta t^2} m + \frac{\gamma}{\beta \Delta t} c + \left(k_T\right)_{i+1}^{(j)} \tag{5.15}$$

where $\left(k_T\right)_{i+1}^{(j)}$ is the stiffness of the bearing

Substitute Eq. (5.12) and (5.13) into Eq. (5.6) then substitute $\left(\hat{f}_S\right)_{i+1}^{(j)}$ into Eq. (5.9) to obtain the residual force $R_{i+1}^{(j)}$.

$$R_{i+1}^{(j)} = p_{i+1} - \left(f_b\right)_{i+1}^{(j)} - \left(\frac{1}{\beta\Delta t^2}m + \frac{\gamma}{\beta\Delta t}c\right)\left(u_{i+1}^{(j)} - u_i\right) + \left[\frac{1}{\beta\Delta t}m + \left(\frac{\gamma}{\beta} - 1\right)c\right]\dot{u}_i + \left[\left(\frac{1}{2\beta} - 1\right)m + \Delta t\left(\frac{\gamma}{2\beta} - 1\right)c\right]\ddot{u}_i \tag{5.16}$$

The bearing force $\left(f_b\right)_{i+1}^{(j)}$ and bearing stiffness $\left(k_T\right)_{i+1}^{(j)}$ can be obtained by the current design bilinear model.

The time-stepping procedure of the seismic analysis is represented in the flow-chart in Fig. 5.10.

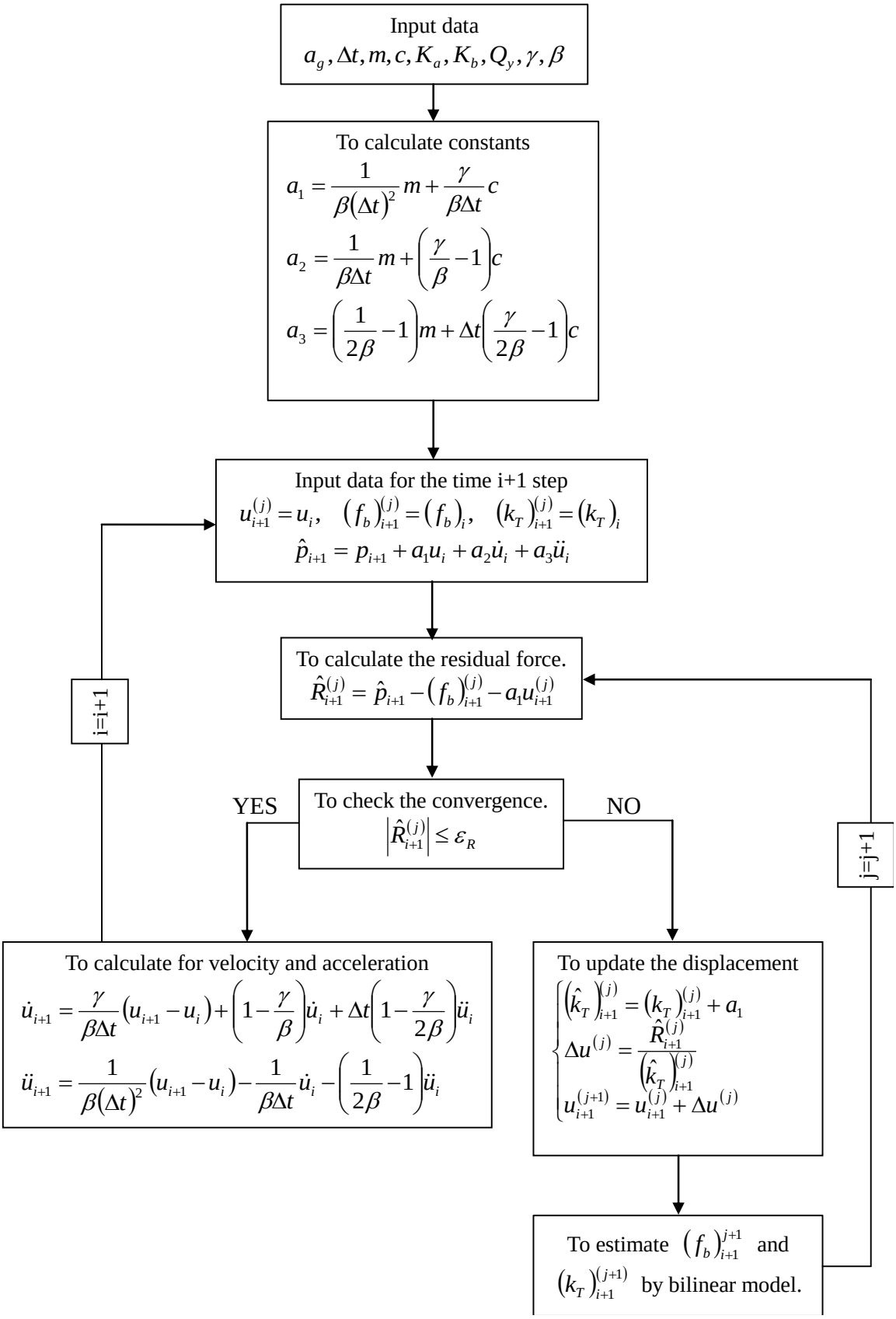

Fig. 5.10. Flow-chart to estimate the seismic response of a SDOF system.

5.4.1.2 Bilinear model

The bilinear model of the bearings can be represented using a structure of rheology model in Fig. 5.11.

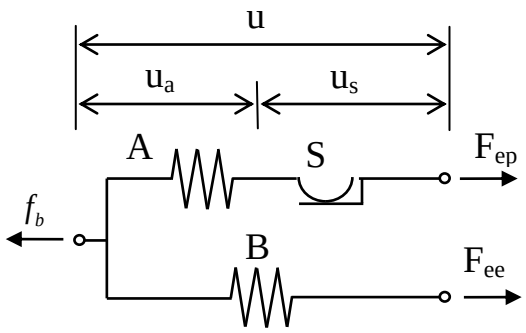

Fig. 5.11. Bilinear model represented using a structure of rheology model

The bearing force can be determine as

$$f_b = F_{ep} + F_{ee} \tag{5.17}$$

where F_{ep} and F_{ee} are shown in Fig. 5.11.

Elasto-plastic force F_{ep} in the first branch

+ Spring A is linear: $F_{ep} = K_a u_a$ (5.18)

K_a is the stiffness of spring A.

+ Slider S will be activated and start to slide, if F_{ep} reaches to yield force Q_y.

$$\begin{cases} \dot{u}_s \neq 0 & if \quad |F_{ep}| = Q_y \\ \dot{u}_s = 0 & if \quad |F_{ep}| < Q_y \end{cases} \tag{5.19}$$

Q_y is yield force.

Elastic force F_{ee} in the second branch

$$F_{ee} = K_b u \tag{5.20}$$

K_b is the stiffness of spring B.

The parameters K_a, K_b, and Q_y are calculated by Eq. (5.21)

$$\begin{cases} K_a = \dfrac{A_b}{h} C_1 \\ K_a = A_b \tau_{cr} \\ K_b = \dfrac{A_b}{h} C_2 \end{cases} \tag{3.21}$$

A_b is cross-section area of the bearing, h is the total thickness of rubber.

The bilinear parameters C_1, C_2, and τ_{cr} are determined from the 1st cycle of sinusoidal loading tests in Fig. 5.12 and table 5.1.

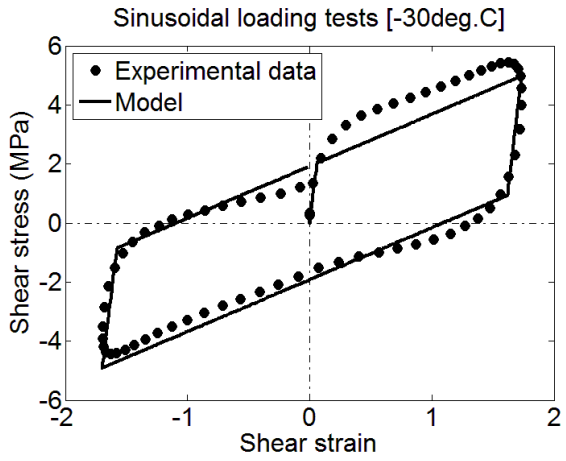

(a)

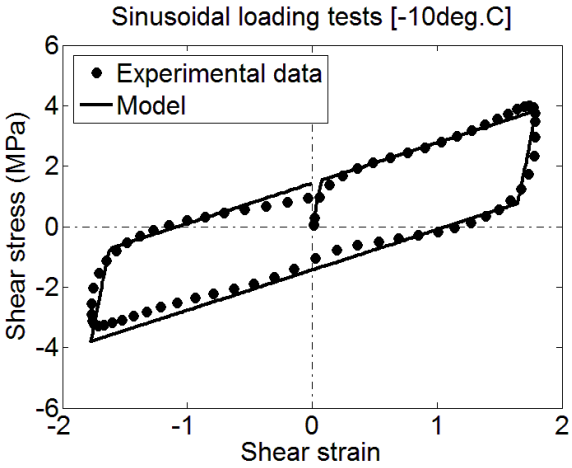

(b)

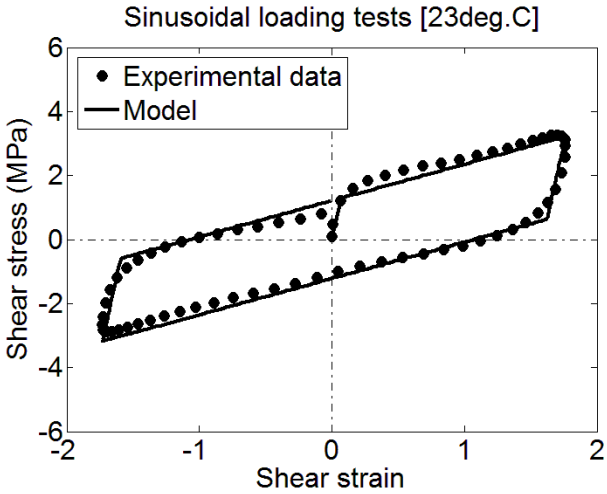

(c)

Fig. 5.12. Identification of bilinear parameters at (a) -30°C (b) -10°C (c) 23°C.

Table 5.1 Bilinear parameters

Temperature	τ_{cr} (MPa)	C_1 (MPa)	C_2 (MPa)
-30^{o}C	1.921	32.58	1.761
-10^{o}C	1.435	19.2	1.335
23^{o}C	1.215	17.29	1.136

5.4.1.3 Input data of seismic analysis

Bearing is the same bearings in Razzaq et al. (2012):

Cross section area of the bearing, A_b=0.65x0.65 m^2.

Total thickness of rubber layers, H=6x0.01354 = 0.08124 m.

Superstructure includes a reinforced concrete slab, covered asphalt, rail, and steel girders:

Mass of the structure is calculated for P1 pier with the span of 35.0 meters.

M= 196928 (kg).

Viscous damping ratio of the superstructure, h=0.05%.

The natural period of the system, T= 2 sec for Type II ground (JRA, 2002).

Damping coefficient of the structure, C

$$C = 2hM\omega = 2hM\frac{2\pi}{T} \qquad \text{(N.s/m)}$$

Time step of integration

$\Delta t = 0.01$ (s); γ=1/2, and β=1/6 (Linear acceleration method).

The tolerance of residual force, ε_R=0.001xQ_y (N).

Earthquake ground motion:

Level 2 Earthquake Ground Motion of Type I and type II (JRA, 2002) is used in this analysis.

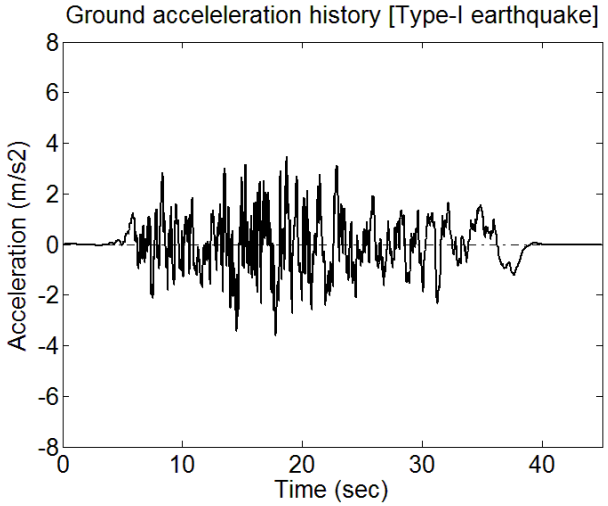

(a)

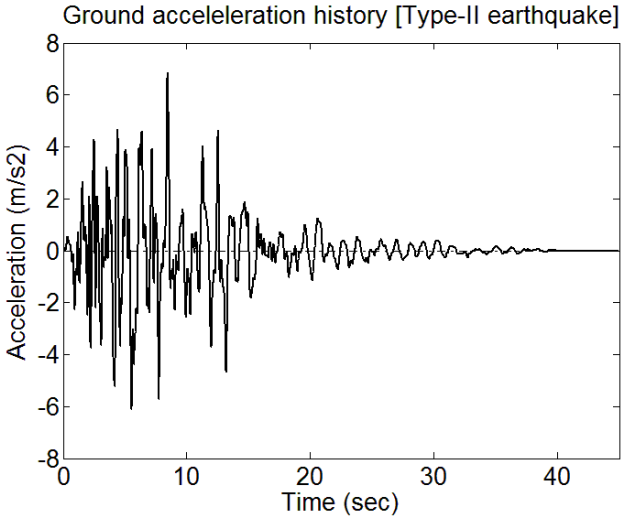

(b)

Fig. 5.13. Ground acceleration histories used in the seismic analysis: (a) type-I earthquake (b) type-II earthquake.

5.4.1.4 Numerical results

Figs. 5.14 to 5.16 show the seismic responses obtained at the top of the bearing at different temperatures under Type-II earthquake. The displacement of the bearing is larger at room temperature and the stress-strain loops presenting the dissipated energy of HBRBs are smaller at low temperatures due to the increase in the stiffness of the bearings at low temperatures.

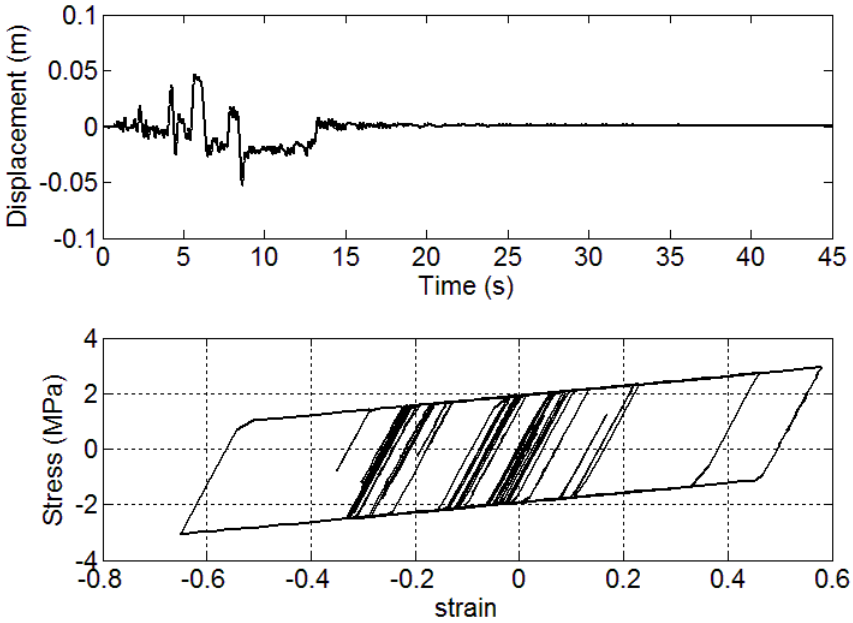

Fig. 5.14. Seismic responses obtained at the top of the bearing at -30°C due to type-II earthquake

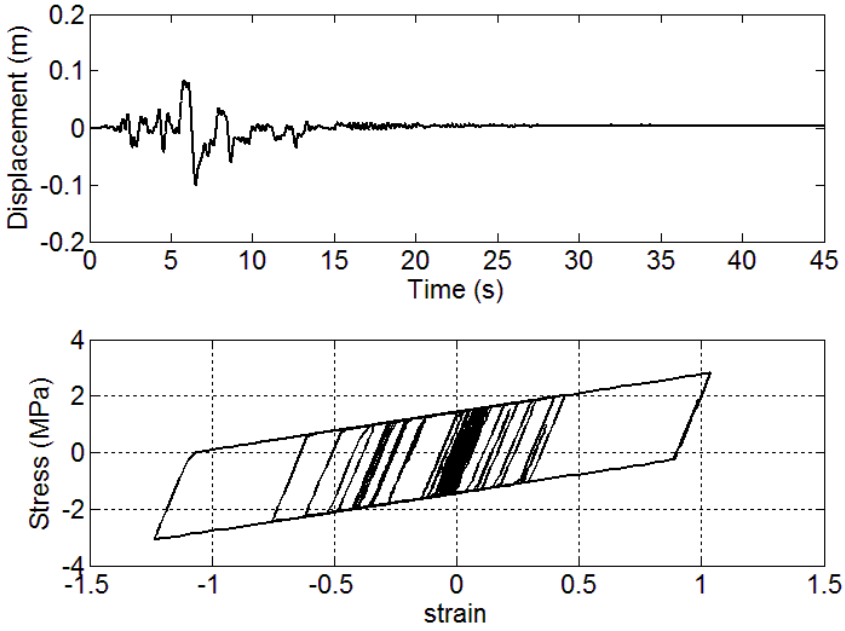

Fig. 5.15. Seismic responses obtained at the top of the bearing at -10°C due to type-II earthquake

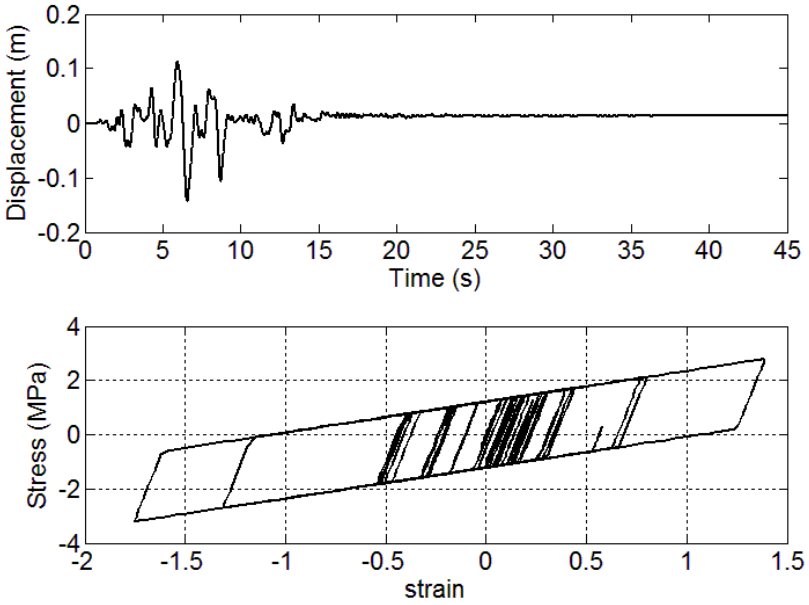

Fig. 5.16. Seismic responses obtained at the top of the bearing at 23^{o}C due to type-II earthquake

5.4.2 Temperature rise inside HDRBs under earthquakes

On the basis of the dissipated energy in numerical results and Eq. (5.3), the temperature rises inside HDRBs under earthquakes are presented in Figs. 5.17. The temperature rise during Type-II earthquake is higher than that during Type-I earthquake. It means that this rise depends on the magnitude of ground acceleration.

The inside temperatures of HDRBs increase about 10^{o}C and 5^{o}C at 23^{o}C and -30^{o}C ambient temperatures, respectively. The temperature rise during an earthquake is much less than that in sinusoidal loading tests at low ambient temperatures. It implies that the effect of self-heating on the design practice is small at low temperatures.

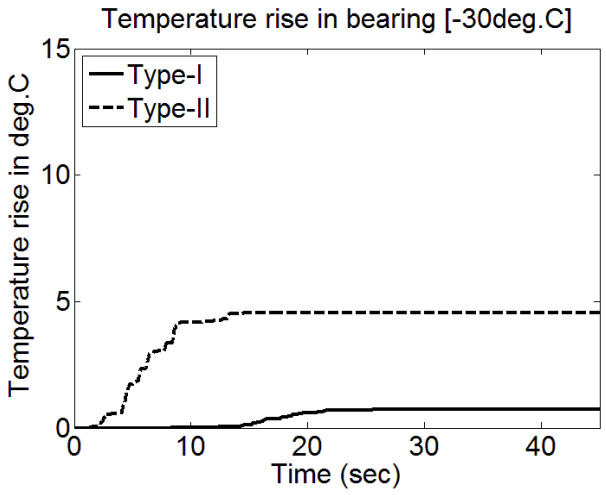

(a)

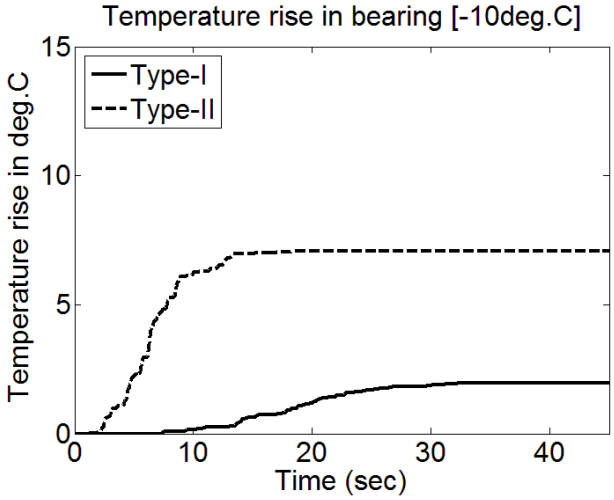

(b)

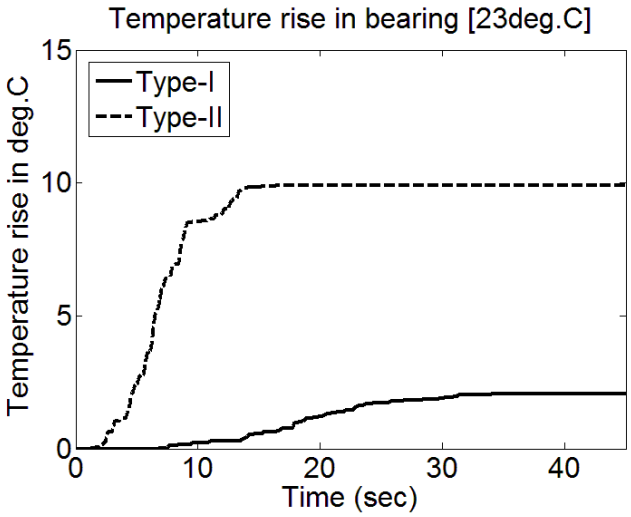

(c)

Fig. 5.17. Temperature rise inside HDRBs under earthquakes at (a) -30^{o}C (b) -10^{o}C (c) 23^{o}C.

5.5 Summary

The inside temperatures of HDRBs increase by sinusoidal loading tests, and the rise in the inside temperature becomes larger at lower ambient temperatures. In addition, it is shown that the stress-strain relationships of HDRBs are governed by the inside temperatures but not by the ambient temperature. The overstress parameters of the proposed model in Chapter 3 should be deteremined based on a stress-strain cycle obtained from sinusoidal loading tests after several cycles of loading to avoid the stress-softening phenomenon appearing in the 1^{st} cycle. Since the temperature increases during an earthquake is considered not so large as that during a cycling loading test, a seismic model for HDRBs at low temperatures should be based on the inside temperatures. The design temperature of the model is chosen to be the inside temperature of the bearings in the selected cycle of the sinusoidal loading tests.

In order to develop an estimation procedure of inside temperature increase of HDRBs during an arbitrary strain history, the temperature increase in a sinusoidal test is estimated from the dissipated energy density under a simple adiabatic assumption. The measured temperatures are lower than the estimated temperatures, because there is a heat transfer in the actual condition.

CHAPTER 6
SUMMARY AND CONCLUSIONS

6.1 Experimental observation at room and low temperatures

A test program was carried out to investigate the mechanical behavior of HDRBs at constant ambient temperatures in an environmental test chamber. All specimens were tested under shear deformation with a constant vertical compressive average stress of 6 MPa. All virgin specimens were first subjected to a preloading sequence before the actual tests to remove Mullins effect.

The stress response of the equilibrium state of HDRBs obtained from multi-step relaxation tests increases with decreasing ambient temperatures. However, this increase is smaller than the increase in the overstress when ambient temperature is reduced.

CS tests were carried out to identify the instantaneous response of HDRBs. The stress response at a strain rate of 5.5/s accords almost with the response at the rate of 8.75/s. It means that the instantaneous response of HDRBs can be obtained at 8.75/s.

Simple relaxation test results show that the overstress responses at the same strain level remarkably increase at low ambient temperatures. This behavior can be attributed to the temperature dependence of the viscosity of HDRBs. In addition, the temperature dependence of overstress is much larger than the dependence of the equilibrium stress at the end of relaxation period.

6.2 Proposed model and parameter identification

The equilibrium state of HDRBs obtained from multi-step relaxation tests presented high strain hardening at high strain level and hysteresis phenomenon. Therefore, a rate-independent model that is constructed by combining a nonlinear spring and an ideal elasto-plastic model (spring-slider) in parallel is proposed to represent these experimental observations.

The instantaneous state obtained from CS tests shown that the initial stiffness is very high and then the second stiffness is lower. These aspects can be simulated by combining a spring and an elasto-plastic element in parallel. Therefore, a structure similar to the rate-independent part is used in the rate-dependent overstress part. This part is connected with a dashpot that can describe the rate-dependent behavior of HDRBs. Moreover, on the basis of the nonlinear viscosity law deduced from the simple relaxation test results, a relationship between the overstress and the strain rate of the dashpot is proposed.

Finally, the equilibrium parameters are identified from MSR tests by a standard nonlinear least square method. The overstress parameters are determined from the first cycle of sinusoidal loading test with an optimizing technique.

6.3 Numerical verification

In order to verify the adequacy of the proposed rheology model, a series of numerical simulations of the experimental tests were carried out. To do this, the model with the identified parameters was used in the simulation. The experimental data were compared with the simulation results for the verification. The simulations of relaxation tests (SR tests and MSR tests) and cyclic shear tests portrayed the adequacy of the proposed model in reproducing the mechanical behavior of HDRBs.

In addition, the numerical simulation results of CS responses at slow and fast strain rates illustrated that model can produce logically the rate-dependent behavior of HDRBs, and its inherent promises at the design desk. However, there are some differences between experimental data and simulation results of the first cycle of Sin tests, especially at low temperatures. These differences may be caused by self-heating or Mullins effect.

6.4 Self-heating of high damping rubber bearings

Self-heating of HDRBs at room and low temperatures is investigated experimentally. The experimental results show that the temperatures in the HDRBs significantly increase under sinusoidal loading tests, especially at low ambient temperatures. In addition, the experimental results also present that stress-strain relationships of HDRBs are governed by

the inside temperatures but not by the ambient temperature. Since the temperature increases during an earthquake is considered not so large as that during a cycling loading test, a seismic model for HDRBs at low temperatures should be based on the inside temperatures. The design temperature of the model is chosen to be the inside temperature of the bearings in the selected cycle of the sinusoidal loading tests.

6.5 Future studies

On the basis of the experimental observations, a rheology model of HDRBs for seismic analysis at room and low temperatures has been proposed in the present study. The rate-dependent overstress parameters are identified from the first cycle of sinusoidal loading tests to minimize self-heating effect. However, the first cycle behavior is quite difference from the following cycles and then it makes some difference between experimental data and numerical results in cyclic loading tests, especially at low temperatures. Therefore, the parameters should be identified from a stress-strain relationship obtained from sinusoidal loading tests after several cycles of loading. Moreover, experimental results also show that the inside temperatures of HDRBs increase by the sinusoidal loading tests, and the stress-strain relationships of HDRBs are governed by the inside temperatures. Therefore, it could be more appealing to put further research works on the improvement of the proposed rheology model by incorporating self-heating effect into the present model.

In addition, all specimens in the current study are preloaded to remove Mullins effect that always appears in virgin specimens. Therefore, the incorporation of Mullins effect into the proposed model would be a good approach to enhance its capability to reproduce the mechanical behavior of HDRBs.

REFERENCES

Abe, M., Fujino, Y., Yoshida, J., 2000. Dynamic behavior and seismic performance of base-isolated bridges in observed seismic records. Proceedings of the 12th world conference on earthquake engineering, Auckland, New Zealand, paper No. 0321.

American association of state highways and transportation officials (AASHTO), 2010. 3rd Edition. Washington DC: Guide Specification for Seismic Isolation Design.

Amin, A.F.M.S., Alam, M.S., Okui, Y., 2002. An improved hyperelasticity relation in modeling viscoelasticity response of natural and high damping rubbers in compression: experiments, parameter identification and numerical verification. Mechanics of Materials, 34, 75-95.

Amin, A.F.M.S., Wiraguna, S.I., Bhuiyan, A.R., Okui, Y., 2006a. Hyperelasticity model for finite element analysis of natural and high damping rubbers in compression and shear. Journal of engineering mechanics, 132(1), 54-64.

Amin, A.F.M.S., Lion. A., Sekita. S., Okui. Y., 2006b. Nonlinear dependence of viscosity in modeling the rate-dependent response of natural and high damping rubbers in compression and shear: experimental identification and numerical verification. International Journal of Plasticity, 22, 1610-1657.

Amin, A.F.M.S., Lion, A., Höfer, P., 2010. Effect of temperature history on the mechanical behaviour of a filler‐reinforced NR/BR blend: literature review and critical experiments. ZAMM‐Journal of Applied Mathematics and Mechanics/Zeitschrift für Angewandte Mathematik und Mechanik, 90(5), 347-369.

Bergström, J.S., Boyce, M.C., 1998. Constitutive modeling of the large strain time-dependent behavior of elastomers. Journal of the Mechanics and Physics of Solids, 46, 931-954

Bhuiyan, A.R., Okui, Y., Mitamura, H., Imai, T., 2009. A rheology model of high damping rubber bearings for seismic analysis : Identification of nonlinear viscosity. International Journal of Solid and Structures 46, 1778-1792.

Cardone, D., Gesualdi, G., Nigro, D., 2011. Effects of air temperature on the cyclic behavior of elastomeric seismic isolators. Bulletin of Earthquake Engineering, 9(4), 1227-1255.

Dall'Asta, A., Ragni, L., 2006. Experimental tests and analytical model of high damping rubber dissipating devices. Engineering Structures 28, 1974-1884.

EC8.,2004. Eurocode 8: Design of structures for earthquake resistance Part 1: General rules, seismic actions and rules for buildings (EN 1998-1:2004). European Committee for Standardization.

Fuller, K.N.G., Gough, J., Thomas, A.G., 2004. The effect of low‐temperature crystallization on the mechanical behavior of rubber. Journal of Polymer Science Part B: Polymer Physics, 42(11), 2181-2190.

Gu, H., Itoh, Y., 2006. Ageing effects on high damping bridge rubber bearing. Proceeding of the 6th asia-pacific structural engineering and construction conference, Kuala Lumpur, Malaysia.

Gent, A.N., Hindi, M., 1988. Heat build-up and blow-out of rubber blocks. Rubber Chemistry Technology, 63, 892.

Huber, N., Tsakmakis, C., 2000. Finite deformation viscoelasticity laws. Mechanics of Materials, 32, 1-18.

Hwang, J.S., 1996. Evaluation of equivalent linear analysis methods of bridge isolation. Journal of structural engineering, 122, 972-976.

Hwang, J.S., Chiou, J.M., 1996. An equivalent linear model of lead-rubber seismic isolation bearings. Engineering structures, 19, 528-536.

Hwang, J.S., Chiou, J.M., Sheng, L.H., Gates, J.H., 1996. A refined model for base isolated bridges with bi-linear hysteretic bearings. Earthquake spectra, 12, 245-273.

Hwang, J.S., Wu, J.D., Pan, T.C., Yang, G., 2002. A mathematical hysteretic model for elastomeric isolation bearings. Earthquake Engineering and Structural Dynamics, 31,771-789.

Igarashi, A., Lemura, H., 1996. Experimental and analytical evaluation of seismic performance of highway bridges with base isolation bearings. Proceedings of the 9th world conference on earthquake engineering, Tokyo, Japam, paper No. 553.

Imai, T., Bhuiyan, A.R., Razzaq, M.K., Okui, Y., Mitamura H., 2010. Experimental studies of rate-dependent mechanical behavior of laminated rubber bearings. Joint conference proceedings 7CUEE&5ICEE, March 3-5, Tokyo Institude of Technology, Tokyo, Japan, 1921-1928.

International organization of standardization (ISO), 2005. Elastomeric seismic protection isolators. Part 1: test methods; 2005.

Japan road association (JRA), 1996. Specifications for highway bridges. Part V: seismic design. Tokyo: Maruzen.

Japan road association (JRA), 2002. Specifications for highway bridges. Part V: seismic design. Tokyo: Maruzen.

Japan road association (JRA), 2012. Bearing support design guide for highway bridges (in Japanese). Tokyo: Maruzen.

Jangid, R.S., 2004. Seismic response of isolated bridges. Journal of bridge engineering, 9, 155-166.

Kelly, J.M., 1997. Earthquake resistant design with rubber. 2nd edition, Springer-Verlag Berlin Heidelberg, New York.

Koo, G., Ohtori, Y., 1998. Loading rate effects of high damping seismic isolation rubber bearing on earthquake response. KSME international journal, 12, 58-66.

Lion A., 1996. A constitutive model for carbon black filled rubber: Experimental investigations and mathematical representation, Continuum Mech. Thermodyn ,8,153-169.

Lion, A., 1997. On the Large deformation behavior of reinforced rubber at different temperatures. *J.* Mech. Phys. Solids 45, 1805-1834.

Marioni, A., 1998. The use of high damping rubber bearings for the protection of the structures from the seismic risk. Jornadas portugesas de engenharia de estruturas, Lisbon, Portugal.

Matsuda T, Igarashi A, Furukawa A, Ouchi H, Uno H, Matsuda H. Effect of inter-component phase difference in bi-directional seismic ground motion input to dynamic response of ICSS (in Japanese). J JSCE, Ser.A1 (Struct Eng & Earthq Eng (SE/EE)) 2013;69(2): 688-702.

Miehe, C., Keck, J., 2000. Superimposed finite elastic-viscoelastic-plastoelastic stress response with damage in filled rubbery polumers. Experiments, modeling and algorithmic implementation. Journal of the Mechanics and Physics of Solids, 48, 323-365.

Mullins L., 1969. Softening of rubber by deformation. Rubber Chemistry and Technology, 42, 339-362.

Nguyen DA, Okui Y, Hasan MD, Mitamura H, Imai T. Mechanical behavior of high damping rubber bearings at low temperatures. In: Proceedings of the 12nd International Symposium on New Technologies for Urban Safety of Mega Cities in Asia, Hanoi Vietnam; 2013, p.1067-74.

Park, D.M., Hong, W.H., Kim, S.G., Kim, H.J., 2000. Heat generation of filled rubber vulcanizates and its relationship with vulcanizate network structures. European polymer journal, 36(11), 2429-2436.

Research committee of isolation structure in road bridges. Collection of examples of isolated bridges in Japan (in Japanese). Tokyo: Public Works Research Center; 2011.

Tsai, C.S., Chiang, T.C., Chen, B.J., Lin S.B., 2003. An advanced analytical model for high damping rubber bearings. Earthquake Engineering and Structural Dynamics, 32, 1373-1387.

Takaoka, E., Takenaka, Y., Kondo, A., Hikita, M., Kitamura, H., 2008. Heat-mechanics interaction behavior of laminated rubber bearings under large and cyclic lateral deformation. The 14th world conference on earthquake engineering, Beijing, China.

Tsopelas, P., Constatinou, M.C., 1997. Study of elasto-plastic bridge seismic isolation system. Journal of structural engineering, 123, 489-498.

Uruta, H., Yamazaki, T., Ohsima, T., Nakamura, M., 2004. Experiments and numerical analysis on response of internal temperature of high damping rubber bridge bearing under low temperature. Proceedings of JSCE (Japan Society of Civil Engineers) Vol. I, 773, 113-123.

Wang, Y.P., Chung, L., Wei, H.L., 1998. Seismic response analysis of bridges isolated with friction pendulum bearings. Earthquake engineering and structural dynamics, 27, 1069-1093.

Wei, Z., Kai, Q., Weihua, z., Zhengxin, F., 1992. Test and analysis of bridge vibration isolation. Proceedings of the 10th world conference on earthquake engineering, Madrid, Spain, 4, 739-752.

Yamamoto, M., Minewaki, S., Yoneda, H., Higashino, M., 2012. Nonlinear behavior of high‐damping rubber bearings under horizontal bidirectional loading: full‐scale tests and analytical modeling. Earthquake Engineering & Structural Dynamics, 41(13), 1845-1860.

Yoshida, J., Abe, M., Fujino, Y., 2004. Constitutive model of high-damping rubber materials. Journal of engineering mechanics, 130(2), 129-141.